MICRO AND NANO COMPOSITES COMPOSED OF A POLYMER MATRIX AND A METAL DISPERSE PHASE

Oscar Fernando Olea Mejía, B.S.

Dissertation Prepared for the Degree of

DOCTOR OF PHILOSOPHY

UNIVERSITY OF NORTH TEXAS

December 2007

APPROVED:

Witold Brostow, Major Professor
Rajarshi Banerjee, Committee Member
Eli Buchman, Committee Member
Brian P Gorman, Committee Member
Richard F. Reidy. Interim Chair of the Department of Materials Science and Engineering
Oscar Garcia, Dean of the College of Engineering
Sandra L. Terrell, Dean of the Robert B. Toulouse School of Graduate Studies

Olea Mejia, Oscar Fernando. Micro and nano composites composed of a polymer matrix and a metal disperse phase. Doctor of Philosophy (Materials Science and Engineering), December 2007, 115 pp., 3 tables, 100 figures, references, 81 titles.

Low density polyethylene (LDPE) and Hytrel (a thermoplastic elastomer) were used as polymeric matrices in polymer + metal composites. The concentration of micrometric (Al, Ag and Ni) as well as nanometric particles (Al and Ag) was varied from 0 to 10 %. Composites were prepared by blending followed by injection molding. The resulting samples were analyzed by scanning electron microscopy (SEM) and focused ion beam (FIB) in order to determine their microstructure. Certain mechanical properties of the composites were also determined. Static and dynamic friction was measured. The scratch resistance of the specimens was determined. A study of the wear mechanisms in the samples was performed. The Al micro- and nanoparticles as well as Ni microparticles are well dispersed throughout the material while Ag micro and nanoparticles tend to form agglomerates. Generally the presence of microcomposites affects negatively the mechanical properties. For the nanoparticles, composites with a higher elastic modulus than that of the neat materials are achievable. For both micro- and nanocomposites it is feasible to lower the friction values with respective to the neat polymers. The addition of metal particles to polymers also improves the scratch resistance of the composites, particularly so for microcomposites. The inclusion of Ag and Ni particles causes an increase in the wear loss volume while Al can reduce the wear for both polymeric matrices.

Copyright 2007

by

Oscar Fernando Olea Mejía

ACKNOWLEDGMENTS

I would like to deeply express my gratitude to my advisors: Prof. Witold Brostow for accepting me with arms wide open to his lab and for his guidance through my studies at UNT and Dr. Eli Buchman for proposing me this project from which I learned many things. Both of them happily shared with me their knowledge and experience.

Many thanks to my committee members Dr. Raj Banerjee and Dr. Brian Gorman for having the time and eagerness to help me making this project a better one. Special thanks to Dr. Brian Gorman for teaching me with patience all I know about electron microscopy.

Thanks to Dorota, Tea, Wunpen, Haley for offering their friendship and making a friendly environment in the lab.

Finally, the greatest gratitude to my family. My parents, Oscar and Lina always caring and supporting me in every aspect. My brothers Alejandro and Angelina for shearing true endless friendship. Jesica for being there with me in every moment.

TABLE OF CONTENTS

LIST OF FIGURES

LIST OF TABLES

1. POLYMER COMPOSITE MATERIALS

1.1 Composite Materials

A composite material can be defined as a material in which two or more distinct structurally complementary substances are combined to produce structural or functional properties not present in either of the individual components. Composites can be produced either naturally (i.e. wood, teeth, etc.) or synthetically (cement, aerospace materials, etc.) [1]. The most commonly used and studied composites are those used in structural applications, such as cement, fiber reinforced polymers, etc. However, as technology develops and more materials with very specific properties are needed to meet the demanding requirements, other functional applications have been studied and developed such as electronic, optical or biomedical. Thus, an efficient way to categorize composite materials is by the application in which they are used. Table 1 shows several types of composites for the most common types of applications and examples of those materials [2].

Other method to divide composite materials is by the type of matrix or majority phase it contains. Considering the nature of the present work, this way to categorize composite materials is more suitable, since results on polymer matrices with metallic dispersed phase composites are presented. Table 2 shows these different categories of composites and some examples and applications for each one [2]. A more detailed discussion of polymer matrix composites is presented in the next section of this Chapter.

Table 1. Types of application and examples of composite materials [2].

Application	Brief description	Examples
Structural	Composites that require high mechanical performance. The material may or not bear the load in the structure. Often a low density is also required.	Steel-reinforced concrete. Race bicycles frames. Tennis rackets. Satellites. Furniture. Missiles. Wheelchairs. Automobiles (body, bumper, brakes, etc)
Electronic	These materials include electrical, optical and magnetic applications.	*Electric*. Resistors, solar cells, heaters, thermocouples, light sensors. *Optical.* Lasers, light sources, optical lenses, optical fibers. *Magnetic*. Magnetic field sensors, shielding, magnetic recording, magnetically levitated trains.
Thermal	Applications that involve heat transfer by conduction, convection or radiation.	High thermal conductivity materials. Thermal interface materials. Thermal insulation materials.
Environmental	Related to the protection of the environment from pollution by reduction of the amount of pollutant generated or removal of pollutant.	Biodegradable polymer composites. Activated carbon fiber composites. Macroporous filtering on absorption materials.
Biomedical	Related to the diagnosis and treatment of conditions, diseases and disabilities, as well as their prevention.	Implants (e.g. hips, teeth, heart, veins) Surgical devices. Pharmaceutical packaging.
Prize reduction	Related to composite materials with low coat inert filler	Materials as: talk powder and CaCO3

Table 2. Composite materials divided by the type of matrix or majority phase.

Composite matrix	Examples	Applications
Cement	Concrete (cement, sand and gravel). Carbon fiber reinforced concrete.	Structural, prize reduction
Carbon	Carbon fiber reinforced graphite (also called Carbon-carbon composites). Carbon-metal nanocomposites.	Structural. Thermal. Electronic. Biomedical. Environmental
Metal	Carbon fiber metal-matrix composites.	Structural. Electronic. Thermal.
Ceramic	Silicon carbide, silicon nitride, alumina composites.	Structural. Thermal.
Polymer	Polymer-clay composites. Polymer-carbon composites. Polymer-metal composites. Polymer glass	Structural. Electronic. Thermal. Biomedical. Environmental.

1.2 Polymer Matrix Composites

Polymers have both advantages (low cost, low density, ease of process) and disadvantages (poor mechanical properties) compared with other types of materials like metals and ceramics. One way to eliminate or mitigate these disadvantages is by producing polymer-matrix composite materials. Polymer matrix composites are much easier to produce than other composites (metal-matrix, ceramic-matrix or carbon-matrix composites) independently of the type of polymer (thermoplastic or thermoset). The reason is the relatively low temperatures needed to process the polymers. Normal processing temperatures for epoxy resins range from

room temperature to 200°C; for thermoplastics such as polyethersulfone (PES) and polyimide (PI) the respective temperatures range from 300°C to 400°C [2].

Thermosets composites have long been used and they remain as the majority of polymer-matrix composites so far. A good example is provided by car tires where carbon black is added to vulcanized natural rubber to give the structural properties needed to bear the load of the vehicle. The main use for thermoset composites are circuit boards and structural boards for ships. However, thermoplastic composites are growing in importance and production and they are under rapid development because of their inherent advantages over thermoset polymers such as:

- No cure needed
- Unlimited shelf life
- Higher processing speed
- Reprocessability (for recycling and repair)
- Reduced risks due to chemicals during processing
- Thermal shaping possible
- Recently, also high temperature thermoplastics

Polymer composites can also be classified from the point of view of the dispersed phase they contain. By far, the most common types of polymer composites are the ones with added carbon, whether in the form of fibers, laminates or particulates; they are so popular that entire books are devoted only to the study of carbon polymer composites [3]. The use of ceramic and clay composites is growing rapidly because of properties achievable with the different types of additives available [4]. More recently, metallic additives have been used to produce metal polymer composites - precisely the materials we shall be concerned in this work; a separate section on this type of materials is presented in this chapter.

The shape and morphology of the dispersed phase dictates to a significant degree the properties of the final composite. This is why it is important to know and understand types of internal structures that can be achieved. Fiber composites can give good mechanical properties or conductivity if the fibers are conductors, such as carbon fibers or metal fibers; however, the properties achieved are highly anisotropic [3]. Short fibers and rod-like particles can give more isotropic properties depending on their alignment. Spherical particles, flakes and irregular shaped particles give highly isotropic materials; the low degree of anisotropy is due to the directionality of the polymer chains imposed by the process used to produce the material (i.e injection molding or extrusion). Figure 1 shows schematically several types of composites with different shapes of the dispersed phase.

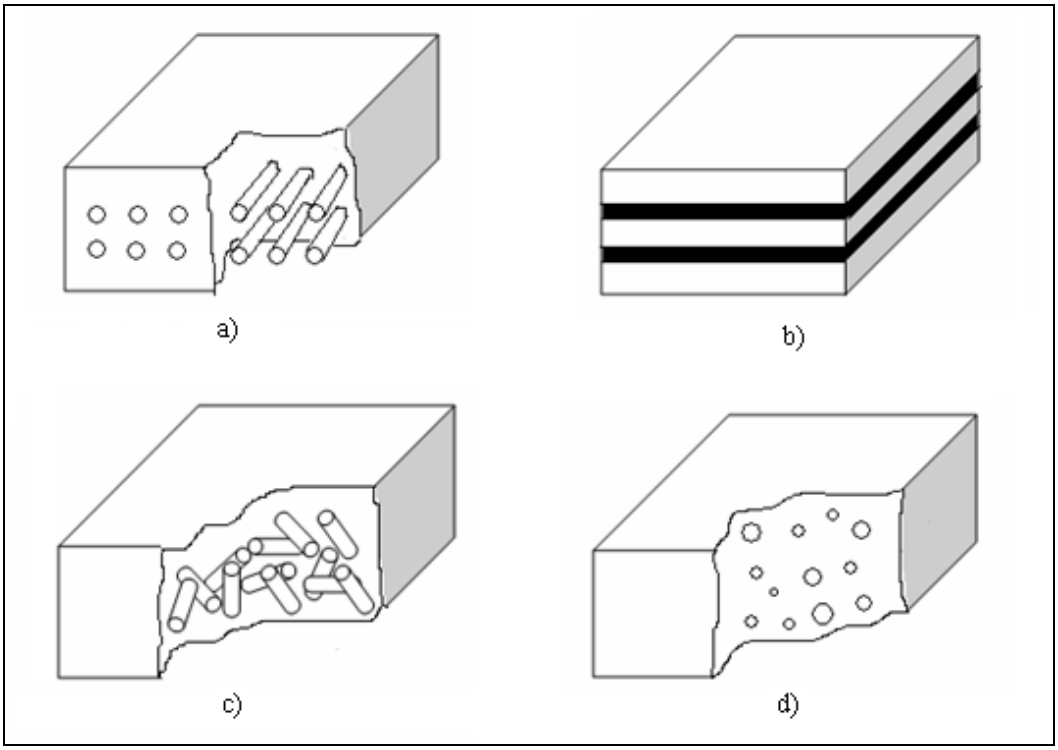

Figure 1. Composite materials with several types of dispersed phase. a) Long fiber composite. b) Laminate composite. c) Short fiber or rod-like particle composite. d) Spherical particle composite.

1.3 Nanotechnology

So far we have described polymer matrix composites with a dispersed phase in the micron size particle region or even larger (as in the case of long fibers and laminates). However, in recent years there has been a whole new area of research called nanotechnology. It includes nanocomposite materials which in turn include polymer + metal nanoparticles. We shall review some work done on polymer nanocomposite materials when we discuss results on nanoclay, carbon nanotubes and evidently on nano-sized metal composites. However before starting with these systems it is helpful to give a brief introduction of nanotechnology and why it is a popular topic nowadays.

Nanotechnology is multidisciplinary and its goal is the control and behavior fundamental structure and of the matter at a scale in the nanometer range. It finds applications in many fields of engineering and it is expected to develop much more in the next decade. Table 3 shows several of the main applications where nanotechnology can be used [5, 6].

1.4 Polymer Matrix Nanocomposites

When additives are nano-scaled, there are certain advantages to filled polymers and composites that lead to a better performance of the materials. This is a result of the filler size reduction and the consequent increase in surface area available. The concentration of the additive can be decreased by up to three orders of magnitude relative to the conventional fillers assuming an ideal mixture and dispersion. Moreover, many fields of engineering associated with electrical or optical properties benefit from quantum confinement effects induced by the nanoscale dimensions of the material.

Table 3. Application of nanotechnology on several fields [6].

Field	Application
Pharmacy	It can be possible to create nanoparticles that because of the very small size can be solubilized and carried in the blood. These particles can deliver the necessary drug for certain deseases.
Computer science	Nanoparticles are being used in video and audio discs that depend on the magnetic and optical properties of the ultrafine particles.
Ceramics and insulators	The compression efficiency of nanoscale ceramic particles allows creating more flexible solids due apparently to the large amount of existing grains. Non-porous high density materials can be also developed that can serve as metal replacements.
Metallurgy	When some nanoparticles are compressed into solid objects, they show a stronger surface, frequently five times more than the normal polycrystalline metals
Environmental chemistry	Semiconducting nanoparticles can be used in a more efficient way to generate power via solar cells. Photoexcitation of nanoparticles produces oxidation and reduction of polluting agents, so that decontamination of water can be achieved.
Catalysis	Different nanoparticles have been tested for catalytic reactions. However, such reactions will depend on the type of material used, its size and its shape, all these parameters change the net surface area available for reaction.
Gas sensors	Materials with high superficial area whose electric conductivity changes when they absorb certain gases.
Electrodes	Magnetic metals such as iron can form dense magnetic materials with soft mechanical properties; thus, these materials can be used to create electric transformers.
Polymers	There are several effects produced when nanoparticles are added to polymers such as an increase in electric and thermal conductivity, mechanical reinforcement, fracture toughness, etc.

Table 3. Continues

Paints	It has been demonstrated that when paintings are doped with nanoparticles such as TiO_2 there is no need for cleaning the painting. This is related to the photo-oxidation of the contaminants by the TiO_2 particles in water.

For instance, compare a microcomposite and a nanocomposite with the same volume fraction of a dispersed phase, where the spherical particles have volumes of 1 μm^3 and 1 nm^3 per particle, respectively. The mean separation between particles is smaller by three orders of magnitude; the total internal interfacial area increases by six orders of magnitude; and the number density of particles increases in nine orders of magnitude. Although these numbers are impressive by themselves, the filler size must be observed relatively to the size of the polymer chains - to capture the full potential impact of nanoscale fillers on composite materials properties. According to this idea we see that a typical radius of gyration of a polymer chain (approximately its size) is in the range of 3 to 30 nm. Depending on the strength of interaction between the filler surface and the matrix, the polymer chains in close proximity to the filler will be perturbed with respect to those in the bulk [7].

As with traditional filled plastics, an enormous variety of polymer + nanoparticle combinations is possible. Thus, given the diversity of possible properties and tolerable costs, there is no “best universal” nanoparticle filler for polymer nanocomposites. The best nano-sized filler will be determined by meeting both a specific set of physical properties and a price associated with a particular product.

In the following Section we shall review some existing results on polymer composites with dispersed phases such as carbon, ceramic and clay. Some of this review has to do with

polymer nanocomposites. Later on, we will continue with a review on polymer metal composites with a separate section devoted to polymer metal nanocomposites.

Polymer Matrix Composites

As mentioned before, polymer carbon composites have been around for a long time; the use of these materials is growing considerably. They can be suitable for electronic applications especially because specific values of their electric conductivity can be attained [3, 8], as well as provide new suitable materials in the battery industry [9]. They find use also in thermal applications as both heat conductors or insulators because of their thermal conductivity and thermal expansivity that can be varied and even oriented (as in the case of fibers) in a preferred direction [2, 10]. However, structural applications are by far the most studied and applied for this type of composites; the importance of understanding and prediction of their mechanical properties of polymer carbon composites is reflected in the many studies carried on so far. This is true for a variety of structures of the carbon dispersed phase, from macro laminates to the recent carbon nanotubes (single and multi walled) which have very interesting properties and their development is growing notably [2, 3, 11 - 13]. An interesting idea is that polymer carbon composites can also be the dispersed phase in other composites as in the case of concrete-matrix composites [14].

Polymer ceramic composites find application in the energy storage, electric, electronic, biomedical and structural fields. Alumina and zirconia are often selected additives to fabricate high performance electrolyte composites to be used in batteries [15, 16]. Other electronic applications are piezoelectric and dielectric materials where CdO, borium strontium titanate (BST), strontium cesium titanate (SCT) are used as the dispersed phase [17 - 20]. In some cases the dielectric constant of the composite equals that of a pure ceramic material, such is the case of CdO + polymer composites which show a dielectric constant of 2200 while for pure $BaTiO_3$ the value is around 2000 [20]. Among thermal materials we find those composed of

Al_2O_3, SiO_2 and TiO_3 compounds where low isobaric expansivities are desired in high performance chips, wiring and electronic packaging [21, 22].

Biomaterials have become in recent years an area of research that is growing rapidly because of the technology achievements that allow producing materials with outstanding properties used in implants, drug delivery substance, medical equipment, etc. In this field, polymer ceramic composites find wide acceptance because of their potential suitable mechanical properties, wear resistance and - more importantly - the biocompatibility which is a key property for any biomaterial. Among other biocompatible materials, hydroxyapatite is one of the most used materials that are combined with polymers to produce bone replacements and implants [23-28] while calcium phosphate is used to fabricate scaffolds for tissue generation and gene delivery [29, 30].

Polymer clay composites have received significant attention, especially in recent years with the availability of nano-sized clays that give very large amount of surface area per unit of mass. Thus small quantities of clay are needed in order to change the composite properties drastically [9]. High elastic modulus [31, 32], increased strength and heat resistance [33], decreased gas permeability [34], low flammability [35, 36] and increased biodegradability of degradable polymers [37] can be attained at low concentrations of clay while lowering the production costs in some cases.

1.5 Polymer Metal Composites (PMC)

We have reviewed so far several types of polymer composites including those with carbon, ceramic and clay as the dispersed phase. However, because of the objective of this work, this Section will be entirely devoted to polymer matrix composites with metallic particles as the dispersed phase.

Polymer composites with metal fillers are of great interest for many fields of engineering. As already mentioned, PMs possess intrinsic advantages including low cost and ease of

processing among others. On the other hand, metallic materials also have useful properties and characteristics that are crucial for many applications; among them, high electric conductivity, paramagnetism, high thermal conductivity as well as good mechanical properties are the most important ones. The interest in polymer + metal composites arises from the fact that the electric and magnetic characteristics of such materials are close to those of metals; there can be also significant improvement in the thermal properties of the pure polymers and a mechanical reinforcement effect might also be achieved, whereas the processability is the same as for the neat polymer, a great advantage for speed of production and processing costs.

A review of some specific applications and recent work in polymer + metal composites (PMCs) is presented in the following.

As already noted, the electric conductivity of PMCs is one of the main properties of interest and a good amount of information is available on the subject. For example, poly(ethylene oxide) with added aluminum particles was studied in terms of electric conductivity by Muszynska and her colleagues [38]. They have found that only 1 - 2 wt.% is needed in order to increase the conductivity of the pure polymer by over one order of magnitude, reaching a value of 5×10^{-6} S cm^{-1}. There is a big advantage of using aluminum instead of a ceramic as the filler: in order to get the maximum conductivity with the ceramic, a concentration of around 40 wt. % is needed; this of course is reflected in the cost of production of the material. Mamunya et al. [39] used copper and nickel powders as fillers in an epoxy resin and in poly(vinyl chloride) and studied the concentration dependence of the electric and thermal conductivity of the resulting composites. They have found that less than 1 vol. % was sufficient in order to reach the percolation concentration and achieve a big jump in electric conductivity (around 12 orders of magnitude). On the other hand, the thermal conductivity increases linearly with the metal powders concentration. Arshak et al. [40] added a soft Al-Fe-Si magnetic powder to a polymeric matrix to produce magnetic films to be used for shielding of electromagnetic waves. It was found

that the level of shielding is mostly dependent of the film thickness and density and related to an increase of magnetic permeability and electric conductivity.

As noted before, metallic particles are also added to polymers to improve their mechanical properties. Brito and Sanchez [41] used Zn, Cu and Al as fillers in thermosets systems composed by epoxy and amino resins at several concentrations up to 30 wt % and they studied the mechanical properties as well as the thermal decomposition of the composites. The temperature of decomposition decreases when metal is added to the epoxy + amino resins, this is true for all metals and all epoxy:amino ratios. The breaking strength tendency is a more complex one; for the ratio of 1:1 epoxy/amino the effect on this mechanical property is a negative one for all metals; in the case of 1.5:1 and 2:1 ratios copper and aluminum act as reinforcement agents increasing the breaking strength while zinc lowers the value of this property.

Gosh and Maiti [42] prepared polypropylene composites with silver powder (several tens of microns) as filler and studied their mechanical properties. Tensile modulus, strength and elongation at break decrease initially when adding the Ag particles and then start increasing when adding more powder. Impact strength also decreased with Ag powder content. This negative effect on the composites properties is attributed to a discontinuity in the structure as well as poor interaction between the two phases. However, flexural modulus and strength increased with filler content due to an increase in rigidity.

A different way of improving mechanical properties of PMCs is irradiating the material. Bare et al. [43] irradiated high density polyethylene (HDPE) reinforced with steel and copper particles with a Co^{60} source at doses between 10 and 70 kGy. There was a positive effect on the mechanical properties when the composites were irradiated at low doses (around 10 kGy). For the pure HDPE the elastic modulus increases up to 100 %, while for the polymer containing the metallic particles, the modulus increases 200 % approximately. Furthermore, the impact resistance increased up to 600% when metallic powder was added. This improvement is

attributed to a crosslinking effect of the polymer chains due to the irradiation making the material stronger.

Metal particles can also help in the processability of the plastics. Kubat and Rigdahl [44] used several thermoplastics (low density polyethylene (LDPE), polypropylene (PP), polystyrene (PS) and acrylonitrile-butadiene-styerene (ABS)) with iron, copper and magnesium as fillers and studied the internal stresses of the composites generated during injection molding as well as their mechanical properties. The elastic modulus for LDPE increased when the metal concentration was increased, while for the other polymers it remained constant. It was determined by means of flow rate measurements that the internal stress decreased for all materials.

As shown in the last few paragraphs the mechanical properties of PMCs are complex and depend on type of metal, shape and size of the metallic particles, the type of polymer used as matrix and also the process used in the production of such materials and dispersion.

An interest in PMCs is increasing because of their potential to be used as sensor and actuators, especially for biomedical and biological applications. Punning et al [45] developed a new type of sensor/actuactor that responds to mechanical bending of the composite. Inversely, when a voltage is applied to the composite in a circuit, there is a mechanical response depending of the voltage value. This kind of materials can be used potentially as sensors for active noise damping and biosensors. Their large actuation strain and flexibility make them suitable for artificial muscles and other bio-inspired devices [46, 47].

PMCs are not only restricted to be used as actuators in the biomedical field. For example Zhao et al. [48] studied bacterial adhesion on metal + polymer composite coatings. Bacterial adhesion in medical devices, food processing equipment and heat exchangers is a known problem. Bacterial adhesion on the composite coatings was investigated in terms of the surface energy of the coatings. They used Ag + Teflon and Ni + Cu + P + Teflon composites

tested at different surface energies. They have found that in general there is an optimal surface energy where the bacterial adhesion is minimal - what can be quite important for reducing biofouling in medical devices and industrial equipment.

Polymer + Metal Nanocomposites (PMNs)

The fundamental knowledge on the preparation and nature of metal + polymer nanocomposites has a long history. The oldest technique for the preparation of such materials can be found in an abstract that appeared in 1835. A gold salt was reduced in the presence of arabic gum in an aqueous solution; subsequently a nanocomposite material was obtained in the form of a purple solid by coprecipitation with ethanol [49].

Metals undergo considerable property changes by size reduction and their composites with polymers are very interesting for functional applications. Some new properties observed in nano-sized metals are produced by quantum-size effects, such as electron confinement. These quantum effects arise from the fact that there are a big number of surface atoms compared to a normal bulk metal. These properties are size-dependent and can be tuned by changing the dimension; thus, the same material may show different sets of properties by changing its size. Particularly interesting are: dependence on the size of ferromagnetism and the superparamagnetism characterizing all metals; chromatism observed with silver, gold and copper metals due to plasmon absorption; the photo and thermoluminescence; and the supercatalytic effect due to the very large superficial area of very fine particles. These materials are highly chemically reactive, highly absorbent, and show very different thermodynamic parameters. For example, they melt at much lower temperatures. Many of these unique chemical and physical characteristics of nano-sized metals remain unmodified after embedding in polymers (i.e. optical, magnetic, dielectric and thermal transport properties), and therefore they can be used to provide special functionalities to polymers.

Polymer + metal nanocomposites can be obtained by two approaches, namely in situ and ex situ techniques. In the in situ methods, metal particles are generated inside a polymer matrix of a metallic precursor dissolved in the polymer. In the ex situ approach, nanoparticles are first produced by soft-chemistry routes and then dispersed into the polymeric matrix. Usually the preparative method allows us to obtain metal nanoparticles whose surfaces has been passivated. Surface passivation has a fundamental role since it avoids aggregation and surface oxidation and contamination phenomena. In addition, passivated metal particles are hydrophobic and therefore can be easily mixed with polymers. However, the oxide layer diminishes the interaction between polymer and metal, thus reducing especially the mechanical properties. One way to overcome this poor interaction is by adding a primer.

As mentioned before, the optical properties of polymer + metal nanocomposites (PMNs) are of interest since different size of different metals can give a wide range of values of absorption, chromatism, etc. The main contribution for these properties to occur is the plasmon absorption. Significant efforts have been put into understanding and predicting the plasmon behavior on nano-sized metals [50]. For this type of optical application, unpassivaded particles are preferred since the oxide layer of passivated particles quench different surface plamsons.

Barcikowski and Chichkov [51] elaborated a technique to create PMNs by using ultrashort pulsed laser ablation (USPLD). They focused the laser beam into a submerged metal target with an energy density high enough to provoke an explosion of the metal, generating the nanoparticles that remained dispersed inside the monomer. Afterwards the target was removed and the polymerization of the monomer took place. There is an advantage to this technique, mainly the absence of chemical in the formation of the nanocomposites, with the exception of the monomer and the initiator. The technique also proved to be suitable to produce stoichiometric nanoparticles such as shape memory alloys (NiTi) generated from the bulk

material. The nanocomposites produced find application in the biomedical field, in medical devices (implants) and bionic clamping devices for micro-parts.

Casting of a solution containing the dissolved polymer with metallic nanoparticles is also a suitable approach to produce PMNs. Tilaki et al. [52] prepared silver nanoparticles + polystyrene nanocomposites via casting the polystyrene solution in a mixture of carbon tetrachloride and acetone containing silver nanoparticles. Ag nanoparticles were synthesized by pulsed laser ablation of pure bulk silver. The mean size of the particles was 3 nm. Ag particles in acetone exhibit single maximum of optical extinction at 399 nm, which is related to surface plasmon resonance. After casting they obtained a transparent polymeric sheet in light yellow color. This film shows an optical extinction at 428 and exhibites a red shift due to change of refractive index of the medium. Apparently laser ablation in liquids with casting method provides a simple, applicable and flexible technique to fabricate PMN.

As mentioned, polymer metal nanocomposites also find application in electronics. Dostenko et al. [53] prepared a polyethylene matrix with iron nanoparticles composite and varied the filler concentration from 0 to 30 %. Their main goal was to determine the influence of the metal concentration on the electrophysical properties for the composites. Besides characterization by TEM and SRD, they measured magnetic and dielectric properties.

1.6 Fabrication of polymer composites

In the case of particulates or short fibers, composites are obtained by mechanically mixing the fibers or particles with an unpolymerized liquid (in the case of a thermoset) or with a molten polymer (in the case of thermoplastics) and then molded to form the composite. Thermoplastic composites can be fabricated by using the conventional methods for neat polymers. These methods include compression molding (applying high pressure and temperature to melt polymer and then cool it down), calendaring (pouring the slurry into a set of rollers with an aperture between them to form a film), thermoforming (heating above the

softening temperature of the thermoplastic and forming over a die) extrusion (forcing the melt through a die opening by using a screw mechanism) and injection molding which will be treated separately next.

Injection Molding

Injection molding is one of several thermoplastic manufacturing processes. It has its roots in the work of John Wesley Hyatt who first injected cellulose into a mold to produce billiard balls back in 1868 [54]. In this process, molten plastic is injected at high pressures by means of a plunger or a screw into a closed two-piece mold which is the inverse of the part shape. Once inside the mold, the melt is cooled down until solidification, the mold opens, the part is ejected and the cycle is repeated [55]. Injection molding is used in a wide variety of parts from small parts to entire panels and furniture pieces. It is the most common production method for thermoplastics and thermosets. Figure 2 shows a schematic diagram of the injection molding equipment.

In the industry, it is very common to use the injection molder also as a blender. For example, when colorants have to be added to polymers the color pellets and the polymer pellets are mechanically blended. While they both pass through the screw they are mixed and the final product inside the mold has already the desired color. However, for the purpose of this work, another step is needed to ensure a good dispersion of the particles since micrometric and nanometric powders are used. That is the reason of using a blender specifically designed to prepare polymer blends. The specific characteristics of the injection molding machine and the blender used in this work will be presented in detail in the experimental section.

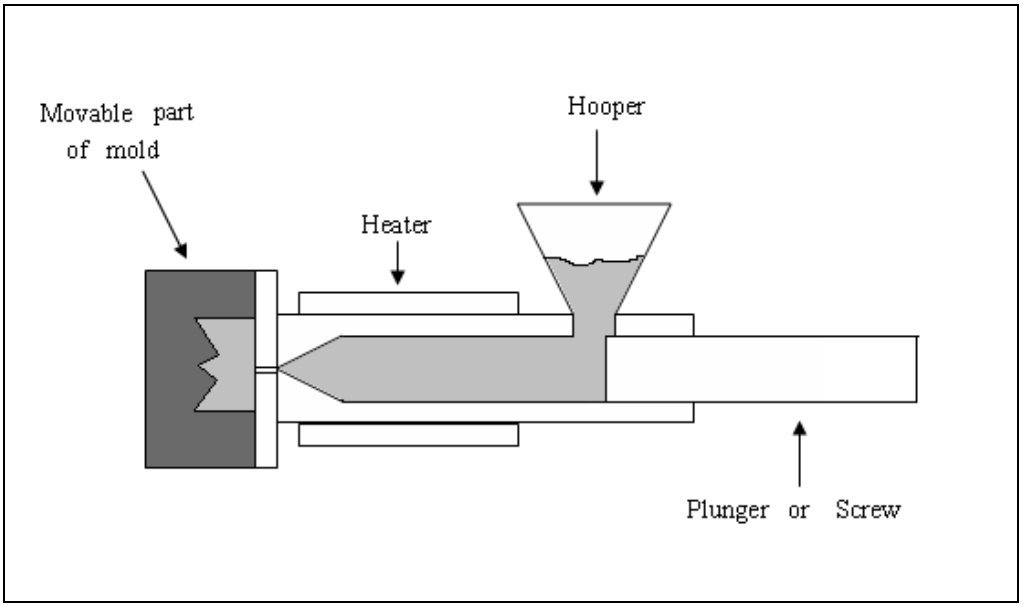

Figure 2. Schematic diagram of Injection molding equipment.

2. CHARACTERIZATION OF POLYMER COMPOSITES

Chapter 1 was devoted to composite materials, including ceramic, metal and polymer composites. This chapter deals with some theoretical aspects of the characterization techniques that will be used to study the polymer composites created for this project.

2.1 Tribological Tests

Perhaps as much as one third of our global energy consumption is consumed wastefully in friction: at a time when energy resources are at premium, the contribution that can be made to their efficient utilization, as well as to the reduction of pollution, by making use of the best tribological practices is obvious. In 1966 an important landmark in the development of the subject was carried on by the Peter Jost report, which indicated that 500 million British pounds could be saved if the best techniques in machine design and operation were utilized [56, 57].

The purpose of research in tribology is understandably the minimization and elimination of losses resulting from friction and wear at all levels of technology where the rubbing of surfaces is involved. Research in tribology leads to greater plant efficiency, better performance, fewer breakdowns, and significant savings in materials and expenses.

Friction

Friction is the resistance to motion during sliding or rolling that is experienced when one solid body moves tangentially over another with which it is in contact. The force that is resisting tangentially and in opposite direction of motion is called the friction force and there are two types: static and dynamic (see Figure 3). Static friction is the force that is required to initiate motion. It may take a few milliseconds before relative motion is initiated at the interface. Kinetic or dynamic friction is the tangential force required to maintain relative motion. The static friction is either higher than or equal to the kinetic friction force. Both types of friction are usually

measured as the ratio of F and W from Figure 3 and are denoted by μ (often called “coefficient of friction”)

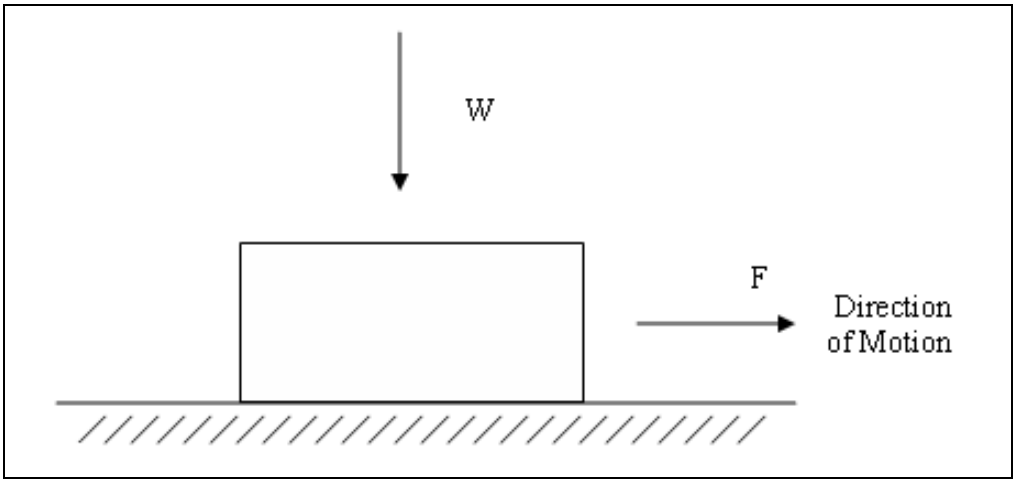

Figure 3. Schematic illustration of a body sliding on a surface with a free body diagram.

It is highly important to recognize and remember that friction is not a material property; it is a system property (including environment). The same material can show different friction values according to the system conditions. Such affecting conditions include temperature, materials roughness, surface cleaning procedure, atmosphere (air, nitrogen, vacuum), presence of a lubricant, speed of motion, among others. That is why it is useless to compare friction results of material pairs that have been tested in different conditions. However, by comparing different material pairs in the same conditions, we can have an idea of how a material pair behaves with respect to other such pairs.

Though the measurement of friction is carried on a macroscopic scale, it has to be understood that the main phenomena occur at a microscopic level. In reality, there are no perfectly flat surfaces; there is always a degree of roughness and asperities inherent to all surfaces. The contact between the asperities of the materials is the responsible of the frictional

behavior of the system. The real contact area is the sum of the contact area of the asperities, and it is much smaller than the apparent contact area (see Figure 4)

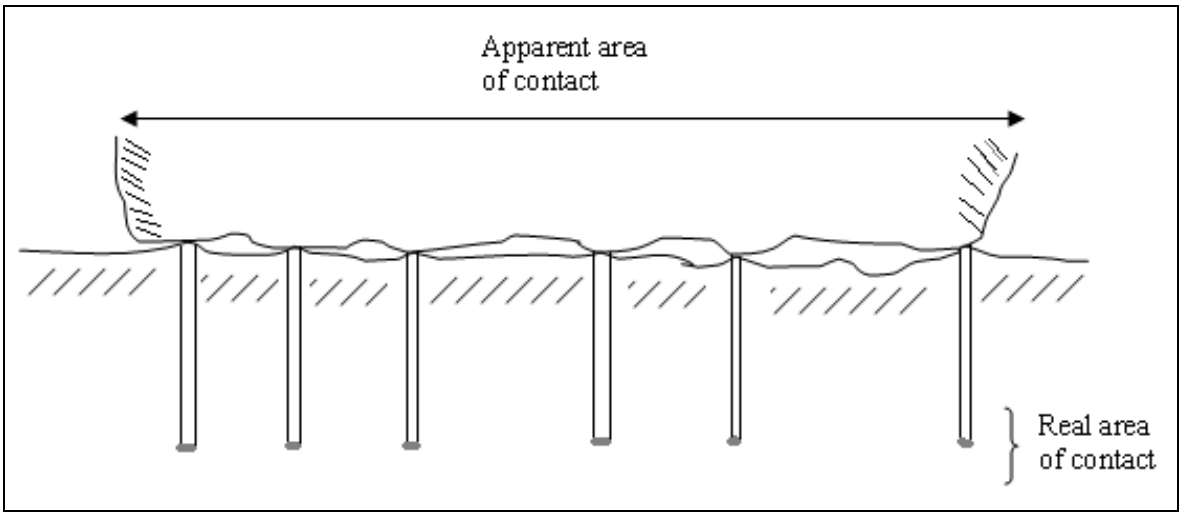

Figure 4. Schematic representation of an interface, showing the real and apparent area.

Friction Tests

There are several methods to determine friction on materials, the most popular ones are pin-on-disc testing and linear sliding friction determination which are used in this work. There are other methods such as rolling friction determination cylinder-on-a-plane or cylinder-on-cylinder usually for metallic contacts. However for the sake of this project, these methods are not covered

Sliding Friction Determination

The experimental set up for this method is very simple and a tensile machine such as the one depicted in Figure 5 can be used for this purpose [58, 59]. A flat sample (at least in one of their sides) is placed in a flat sliding surface (it can be made of a polymer, a metal, a glass, etc. depending on the goal of study). The weight of the sample is determined previously since

this will be the normal force as shown in Figure 8, it is very common to use small samples and an external known weight is attached to the sample. By means of a load cell the required force to move the specimen is recorded using a frictionless pulley. In this manner, it is common to measure static and dynamic frictions. Figure 5 shows schematically the experimental set up for sliding friction determination.

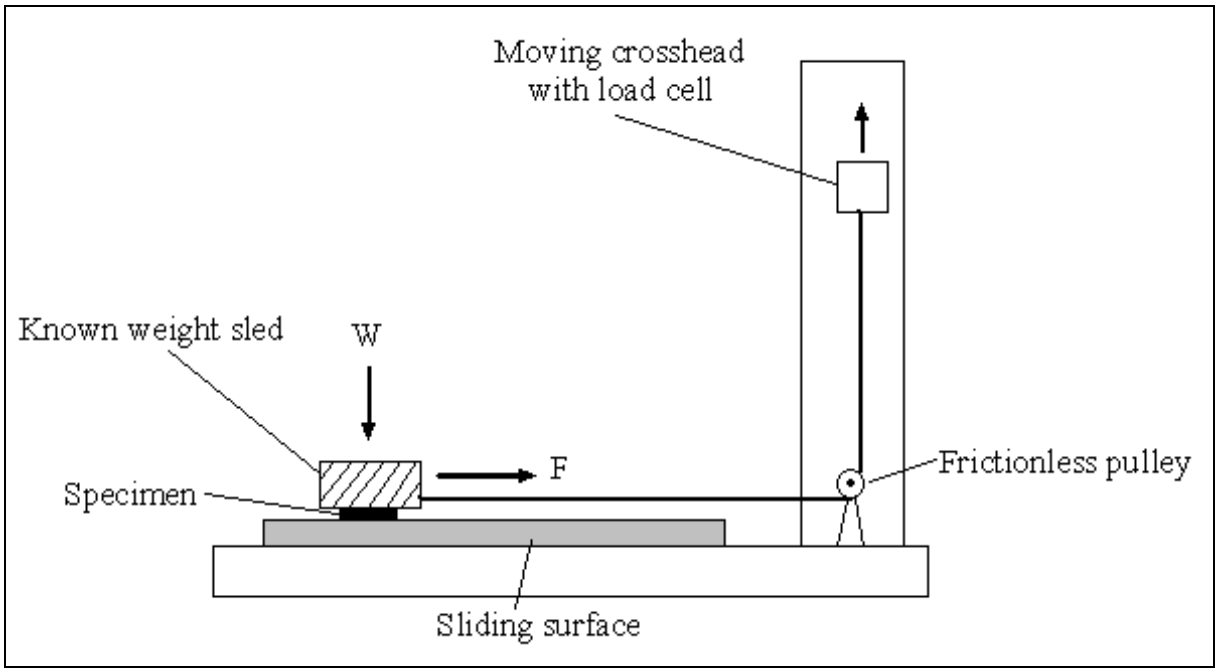

Figure 5. Scheme of the sliding friction determination set up.

Pin-On-Disc Test

This is the most often used technique to determine friction on materials, not only for polymer based materials but it is the choice for films (thin films, electronic materials, etc.). A flat specimen is placed in a spinning disc and a pin is placed off-centered from the spinning axis. The pin carries a known constant load and the resulting frictional force is measured. The load, angular speed of the disc and sliding track radius are usually the controlled parameters. Also,

the pin can be polymeric, metallic or ceramic. A schematic representation of this technique is shown in Figure 6.

There are various advantages of this technique over the sliding friction determination; the contact area is much smaller and by means of Hertzian contact theory parameters such as area of true contact and contact stresses can be calculated relatively easy. It is also easier to change and control certain parameters such as temperature, environmental gasses (air, nitrogen, oxygen, etc). It is usually possible to introduce a lubricant, what is especially useful for metallic and ceramic materials.

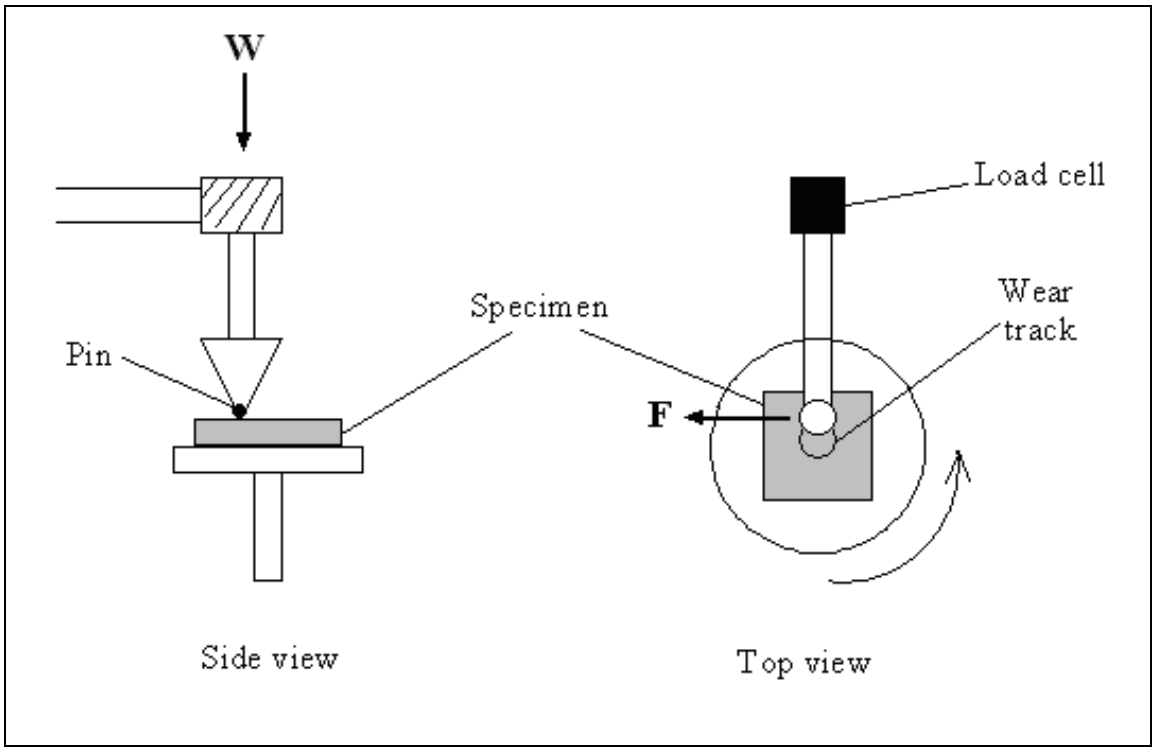

Figure 6. Schematics of the pin-on-disc method.

Wear

As friction, wear is not a material property; it is a system property and will depend on the operating conditions. It often believed that high-friction pairs exhibit high wear rates. Although

this holds true often, it is definitely not the case for all interfaces. For example, interfaces with solid lubricants and polymers exhibit relatively low friction and relatively high wear, whereas ceramics exhibit moderate friction but extremely low wear.

Wear Determination Tests

Wear determination can be done in a variety of ways. Many industries have their own systems to determine wear according to the characteristics of their products. Thus, in this section only the most frequently used methods are presented - including the ones performed on the polymer + metal composites studied in this work.

Pin-On-Disc Test

The experiment set up is the same shown in Figure 6 for friction determination. However what we measure in this case is the height of the pin on the sample. The longer the experiment the deeper the pin penetrates the sample. This change in the pin height is measured by means of a linear voltage differential transduction device (LVDT). The pin depth can be monitored during the test at any time.

A second way to determine wear using the pin-on-disc tribometer is by measuring the dimensions of the groove produced by the pin. This is done with a profilometer and although it is more accurate than the LVDT, it is more costly and more difficult to operate.

A third way is mass loss measurement. The specimen weight is determined prior the experiment. After the test, the specimen is weighted and the difference in mass is recorded. It is common to report the mass loss as a function of the distance traveled by the pin.

All the three measurements listed above are required for a complete wear test. Also it is pertinent to study the wear debris particles by optical or electron microscopy to determine the wear mechanism present in the process.

Scratch Test Using an Indenter

In this test, a hard tip (usually a diamond) with a constant normal load moves along the sample as shown in Figure 7 [60 - 62]. A scratch test involves scratching the surface of the specimen and measuring the depth of the groove while the scratch is in progress. This can be done under either a constant load, a progressively increasing load or else under a stepwise increasing load. It is possible also to change the length of the groove and the linear speed of the indenter. The resulting values are called the penetration (instantaneous) depth and the residual (healing) depth. Since polymers are viscoelastic materials, they should recover or heal after the scratch, with the bottom of the groove going up and settling at a final level which is the residual depth.

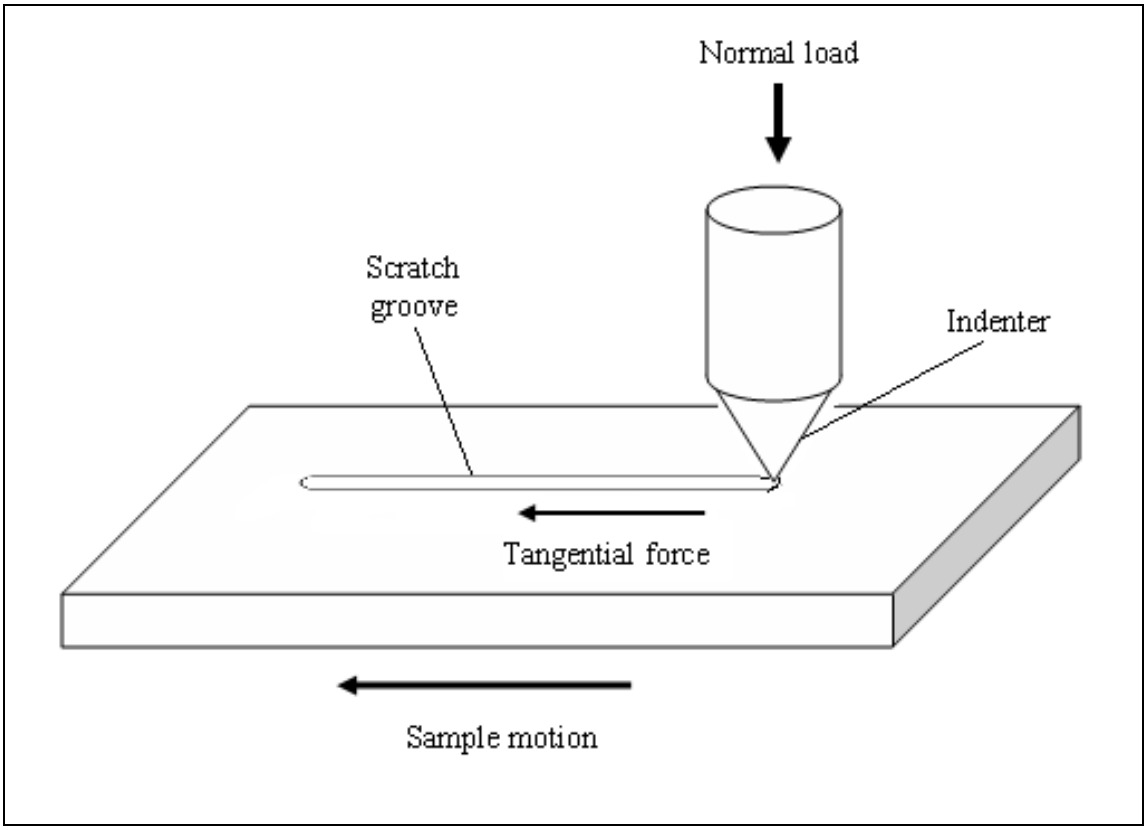

Figure 7. Schematics of the scratch test machine.

2.2 Mechanical Properties

Evidently, mechanical properties are the most important ones not only for polymer composites but constitute the bottom line in Materials Science and Engineering as eloquently argued by Brostow [63]. The majority of materials are created to withstand different levels of loads among other requirements; Brostow states that performance and reliability of polymer based materials are of interest to everybody – polymer scientists, polymer engineers, and all laymen including those who do not even know the meaning of the word “polymer” but who ultimately are the ones using the products.

To understand the mechanical properties of polymer based materials it is imperious to know that they are all viscoelastic. The behavior observed (elastic, viscous flow or a combination of the two) depends on the rate and duration of the applied force as well on the nature of the material and external conditions such as temperature. Viscous flow is observed when force is applied over an extended period of time and relatively slow rates, the polymer chains react to that force and flow in its direction. When the force applied has a short duration the chains are not capable to flow, and entanglements and/or crosslinks are responsible for the elastic response. Following the idea of the time-dependent mechanical properties of polymers, different tests have been created. There are several types of mechanical testing for PBMs such as: quasistatic tests, transient tests, impact tests and dynamic mechanical tests.

Quasistatic Testing

Tensile Test

Tensile testing is the most used method to characterize a material strength. The machine used should provide a constant-rate-of-crosshead-movement type, consisting of one fixed and one movable member, both carrying self-aligning grips. The movable member shall move with a uniform controlled velocity with respect to the stationary one; see Figure 8. Speed

of test is defined as the relative rate of motion of the grips or test fixtures. It is specified for different types of specimens, varying typically from 1 to 500 mm/min. The specimens are dumbbell-shaped or straight sided under defined pretreatment conditions such as temperature, humidity and deformation rate.

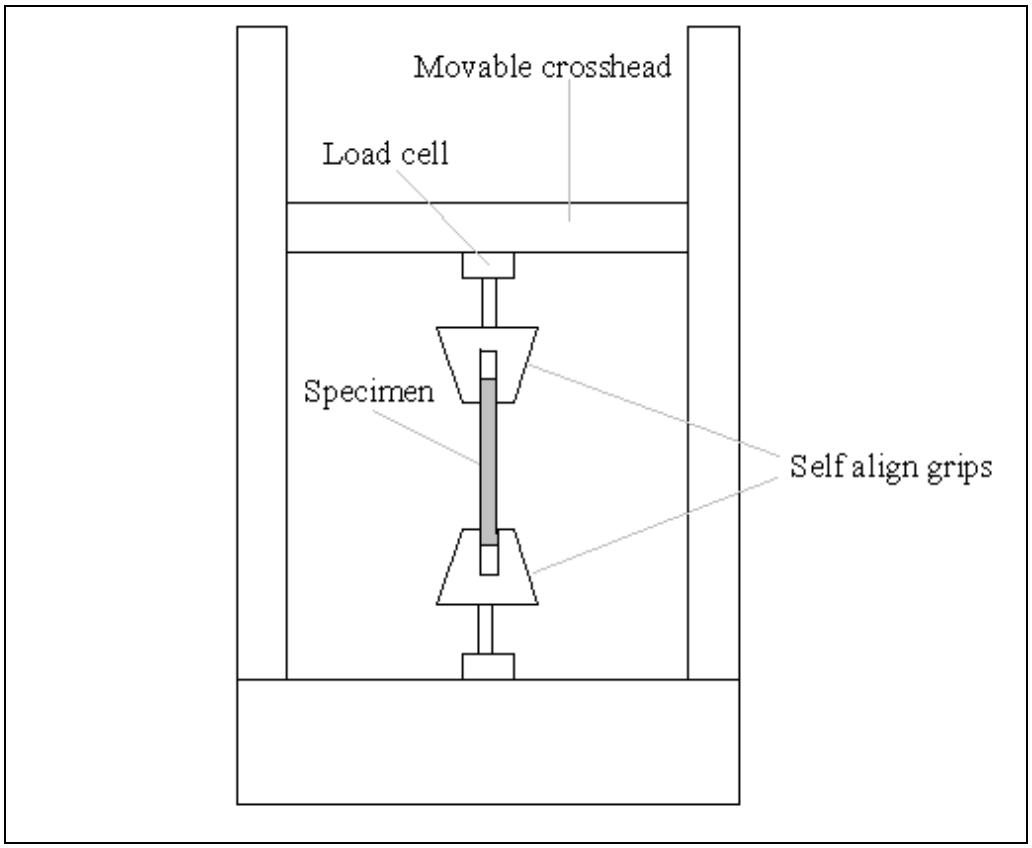

Figure 8. Schematic diagram of the machines used for quasistatic testing including, tensile, compression, 3 point bending and 4 point bending.

There are two essential properties determined each time. One is the engineering stress which is defined as:

$$\sigma = \frac{F}{A_o} \tag{2.12}$$

where F is the applied force and A_o is

the initial cross sectional area. The other key property is the engineering strain (also known as nominal tensile strain) defined as:

$$\varepsilon = \frac{(l - l_o)}{l_o} = \frac{\Delta l}{l_o} \tag{2.13}$$

where l is the current length of the specimen while l_o is the original length.

The quantities obtained most often from tensile testing are:

Tensile strength: The maximum load divided by A_o

Percent elongation: If the specimen gives a yield load larger than the load at break

W_b, we calculate *percent elongation at yield*. Otherwise, *percent elongation at break* $\in_b$ is reported.

Modulus of elasticity: it is the proportionality factor E appearing in Hooke's law:

$$\sigma = E\varepsilon \tag{2.14}$$

and is also called Young's modulus. *E* is calculated from the initial linear portion of the load vs. extension curve in the stress vs. strain coordinates. Several types of behavior seen in tensile testing for polymers are shown in Figure 9.

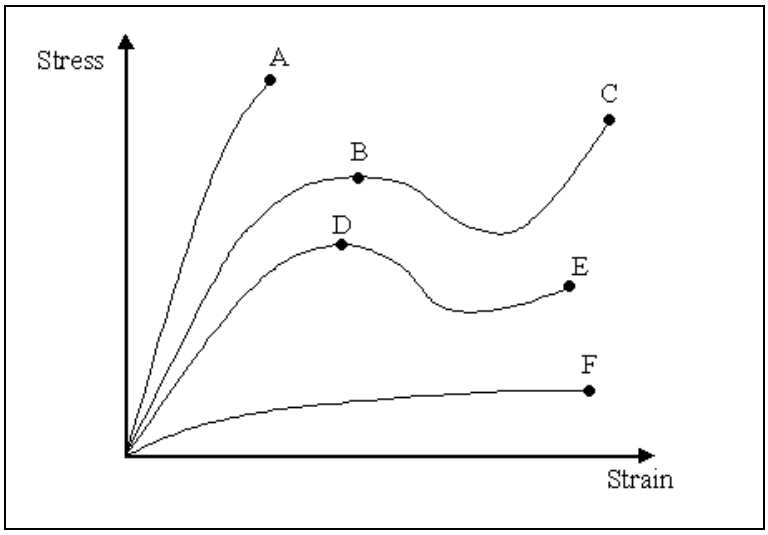

Figure 9. Typical engineering tensile stress vs. engineering strain curves. Points A, C, E and F correspond to the tensile strength and elongation at break, D and B at yield. The A curve is the

one for a brittle material, C and E are tough materials with a yield point, while F is a tough material without a yield point.

2.3 Scanning Electron Microscopy (SEM) and Focused Ion Beam (FIB) Techniques

Scanning electron microscopy (SEM) allows the observation and characterization of the surface of heterogeneous organic and inorganic materials on a nanometer to micrometer scale. The popularity of SEM stems from its capability of obtaining three-dimensional-like images of the surfaces of a very wide range of materials. It can be used for a wide variety of materials such as metals, ceramics, polymers and biomaterials [64].

In SEM, the area to be examined is irradiated with a finely focused electron beam, which may be swept in a raster across the surface of the specimen to form images or may be static to obtain an analysis at one position. The types of signals produced from the interaction of the electron beam with the sample include secondary electrons, backscattered electrons, characteristic x-rays, and other photons of various energies. These signals are obtained from specific emission volumes within the sample and can be used to examine several characteristics of the sample such as surface topography, composition (up to few microns of depth), crystallography, etc.

During de last 25 years, focused ion beam (FIB) instrumentation has become an important technology for a wide range of materials, from circuit editing and transmission electron microscopy (TEM) sample preparation to microstructural analysis and prototype nanomachining. Most modern FIB systems come in conjunction with a SEM column so that the instrument becomes a versatile dual-beam platform for imaging, material removal and deposition at scales ranging from micrometers to nanometers. Io order to understand why FIB has such applications it is important to understand the physical phenomena involved in this technique [66]. A review of

the most relevant aspects of the bombardment of matter with an ion beam is presented in the following. A review of the FIB equipment is presented in the next chapter.

FIB Applications

One of the products of the interaction between the ions and the sample is the generation of low energy electrons called ion-induced secondary electrons (ISE). These electrons can be used to for an image the same way secondary electrons (SE) are used in SEM since the ion beam is also focused and rastered over a surface. Ion beams are not as finely focused as electron beams, thus the resolution achievable by them is not as good as in SEM. However, the contrast mechanisms for ISE are different than for SE and can offer complementary information about the sample, such as grain structure [65].

Because of the sputtering action of the ion beam, FIB can be used to locally remove or mill away material. It is becoming more and more common to use FIB to prepare transmission electron microscopy (TEM) samples. The reason for this appears from the following arguments: No other technique can select the target area as precisely as FIB, lamellae can be prepared with a spatial accuracy of around 20 nm; it is fast and reliable, 20 minutes to 4 hours are needed to prepare specimens of a wide range of materials. However, the main disadvantage of FIB is caused by the nature of the milling process: the ion collisions initiating sputter removal can also lead to ion implantation and cause severe damage to the remaining bulk of the material. Many studies in the literature can be found regarding the use of FIB for different types of materials [66 - 68].

Although FIB has been around for over two decades, it has been primarily used for the semiconductor and metallurgical areas. Little work on polymeric materials has been reported. Our group is one of the pioneers in the application of FIB to polymer based materials. We have studied polymer + metal composites to determine the degree of dispersion of the micrometric and nanometric metallic particles inside the material by creating a milled “pool” and investigate

the cross section of that pool [69]. The details on the experiment are presented in a subsequent chapter.

3. MATERIALS AND EXPERIMENTAL PROCEDURE

3.1 Materials

Polymer matrices

Low density polyethylene (LDPE) which is a branched polymer was obtained as pellets from Huntsman (Polyethylene 1065). PE is one of the most used polymers because its low cost and availability. Figure 10 shows the chemical structure of this polymer.

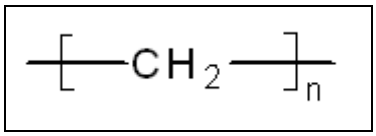

Figure 10. Chemical structure of polyethylene (PE).

In order to compare a low performance polymer, such as LDPE with an engineering polymer Hytrel® was chosen. Hytrel® was provided by Du Pont . It is a block copolymer thermoplastic elastomer composed by a rigid phase of poly(buthylene-therephtalate) (PBT) and a flexible phase of poly(tetramethylene oxide) (PTMO). Figure 11 shows the chemical structure of the two segments that form Hytrel®.

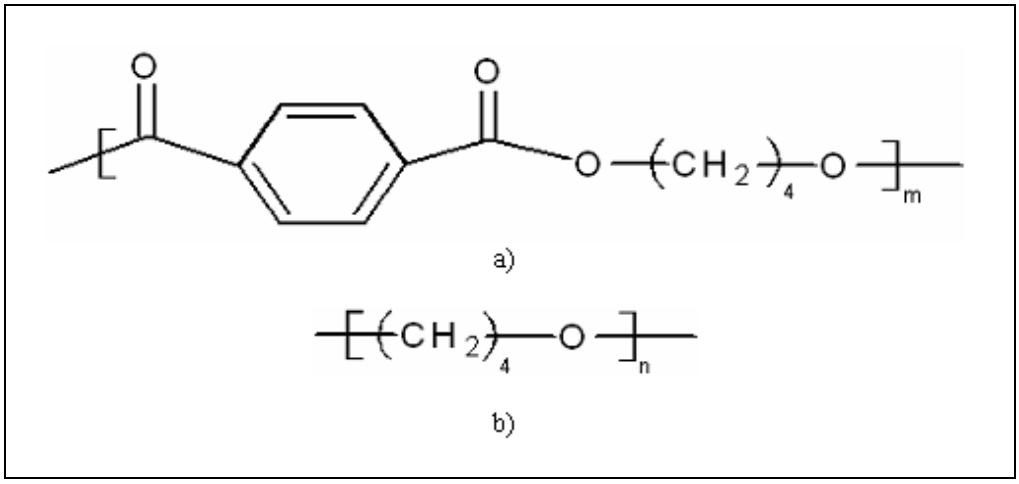

Figure 11. Components of Hytrel®. a) Poly (butylene therephtalate) (PBT). b) Poly(tetramethylene oxide) (PTMO).

Metallic Particle Fillers

Three different metals were selected according to their properties. Al was selected mainly because of the low density compared to other materials, thus it can be used where the weight of the material is critical. Ag was used because of its high electrical conductivity taking in account that the polymer + metal composites can have potential electrical applications. Finally, Ni was used because tribological and mechanical properties can have a dependence of hardness and Ni is the hardest of the three materials used in this project.

Metallic particles in the micron size region were obtained from Atlantic Equipment Engineers, a division of Micron Metals, Inc. The powders used are: Al spheres (1 micron average size), Ag irregular shape particles (8 microns average size) and Ni spheres (7 microns average size). Figure 12 - 14 show the SEM images of the Al , Ag and Ni microparticles respectively.

Metallic particles in the nanometer size region were provided by Nanostructurated and amorphous materials. The powders used are: Al flakes with a particle size of 125 nanometers and Ag particles with a size of 65 nanometers. Figures 15 and 16 show these particles respectively. The Aluminum nanoparticles where surface-passivated while the silver particles were not.

In order to determine the average particle size in number of all the fillers the software Image J was used. The digital images studied are in high resolution tiff format (1024x1024 pixels). The software allows assigning a value of length to each pixel by relating the amount of pixels contained in the micrometric bar of each image. Once the scale is set, measurement of each particle in pixels can be performed, which is directly converted into length units. A histogram of particle size distribution was calculated by measuring at least 200 particles of each micropowder and not less than 250 particles for the nanometric particles. This is an approximation in the determination of particle size. There are other techniques more suitable for

the purpose, such as broadening of peaks in X-ray diffraction or gas adsorption. However the digital approximation is suitable for the purpose of this project.

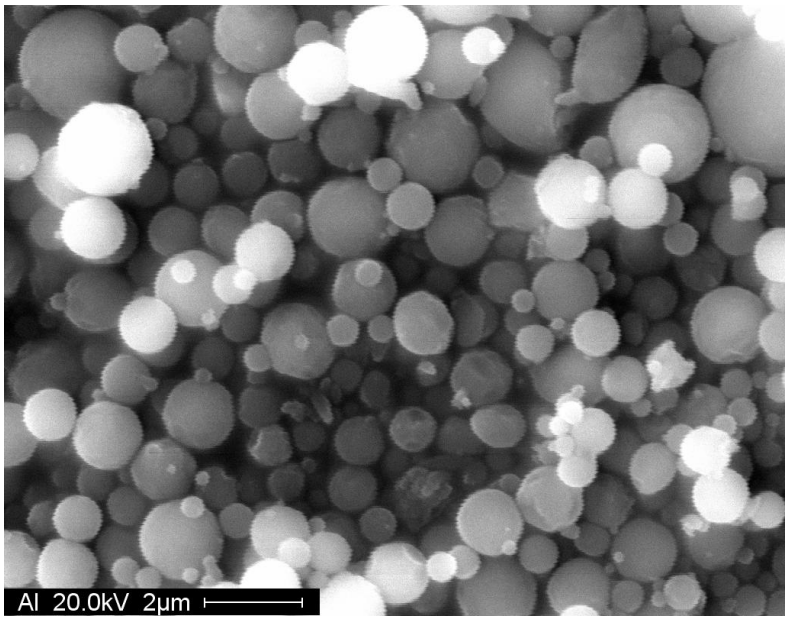

Figure 12. Micrometric Al particles.

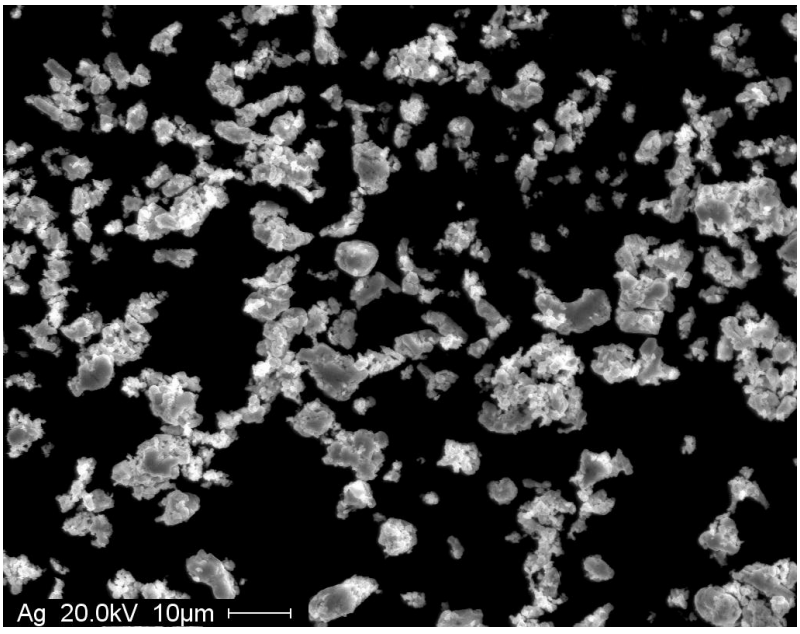

Figure 13. Micrometric Ag particles.

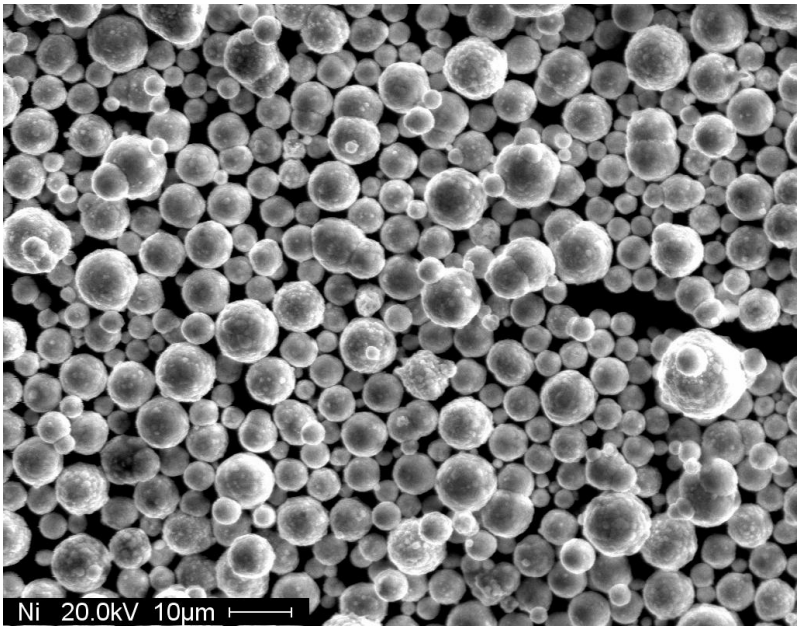

Figure 14. Micrometric Ni particles.

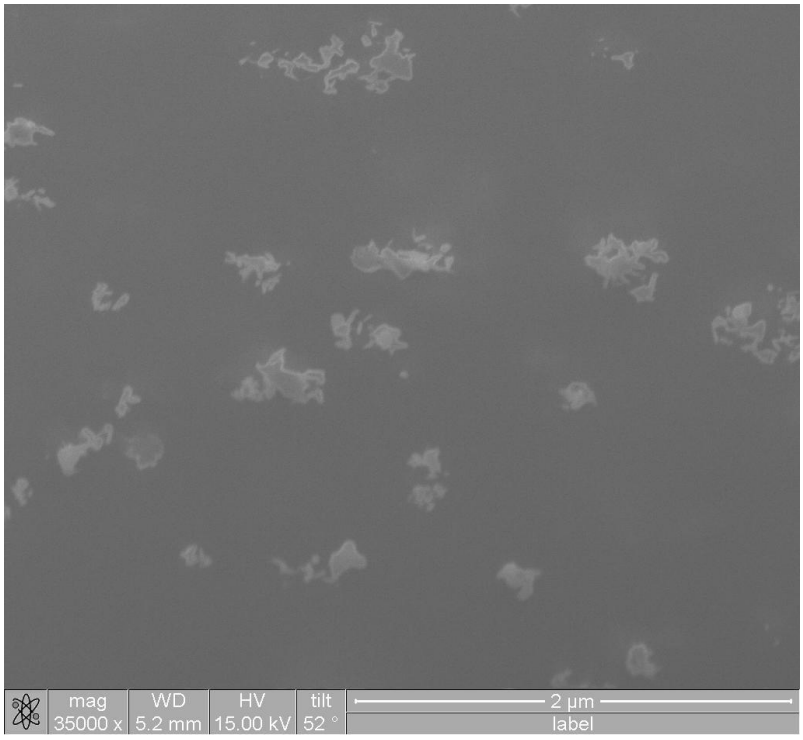

Figure 15. Nanometric Al particles.

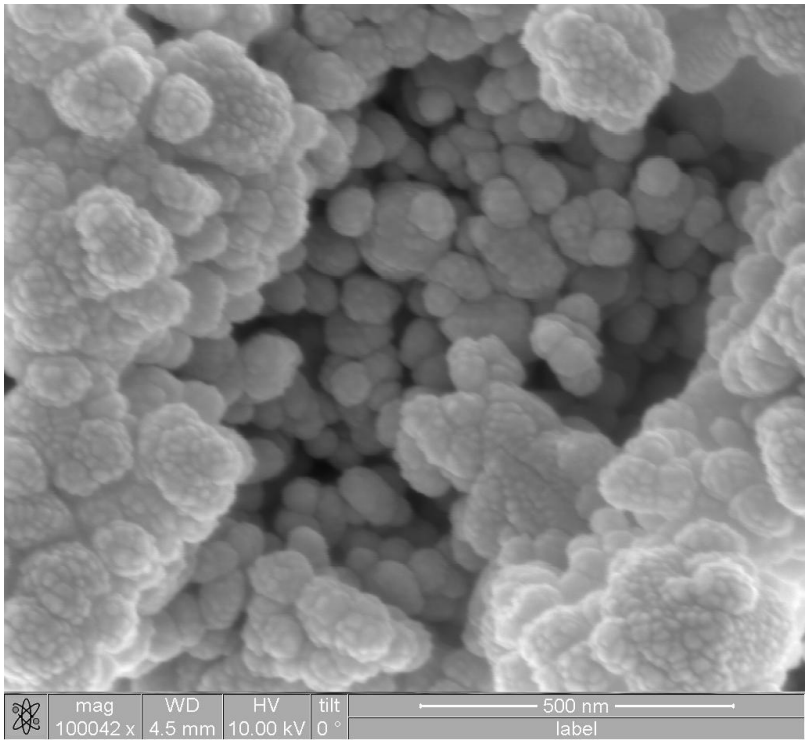

Figure 16. Nanometric Ag particles.

Primer agent

A primer agent was used in the micro composites in order to achieve a chemical interaction between the metal and the polymer matrix. The primer used is 3-metacryloxypropyl-trimethoxysilane from Dow Chemical (product ID: Silane Z-1630). The chemical structure is shown in figure 17.

The metallic micrometer particles were dispersed in a 80/20 ethanol + primer solution. The amount of primer was 5 % in mass respect to each metallic filler. The mixture was ultrasonicated for 2 hours and then mechanically stirred at 50°C for the chemical compatibilization to take place. Only LDPE was primed since the primer was specifically chosen for vinyl polymers.

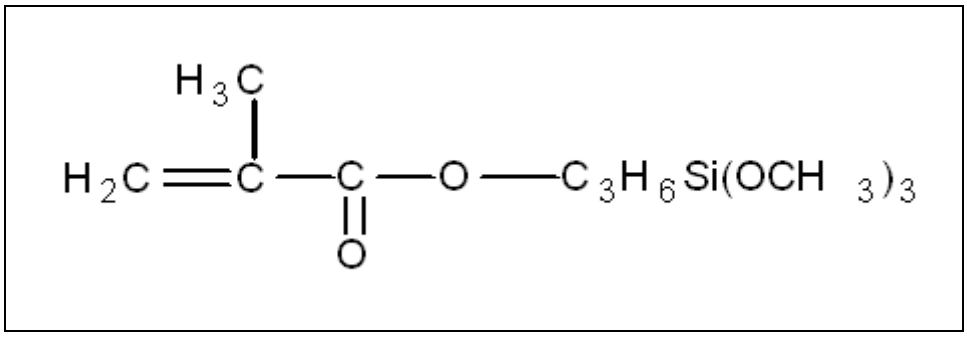

Figure 17. The 3-metacryloxypropyl-trimethoxysilane chemical structure.

3.2 Composites Preparation

All the composites were prepared according to the following steps: after mixing the components the blends were pelletized and finally injection molded into the final shapes. For the sake of comparison, even the neat polymers were treated the same way as the composites. The composition of the metallic powders ranged from 0 to 10 wt. %. We now shall describe each of these techniques.

Blend Mixture

A Brabender type 6 mixer was used to blend all the components of the composites. Figure 18 shows the mixer. It has a 120 mL total volume. The blades rotate in opposite directions and at slightly different speeds to ensure good mixing. The volume with the blades inside is 60 mL and it is desirable to fill 70% of this volume to prepare the blends. Thus, each run has approximately 45 g of material.

For all the LDPE composites including those with the primer, the conditions were:

- Speed of the blades: 80 rpm
- Temperature of processing: 150 °C
- Time of mixing: 5 minutes

For all the Hytrel composites, the conditions were:

- Speed of the blades: 80 rpm
- Temperature processing: 210 °C
- Time of mixing: 5 minutes

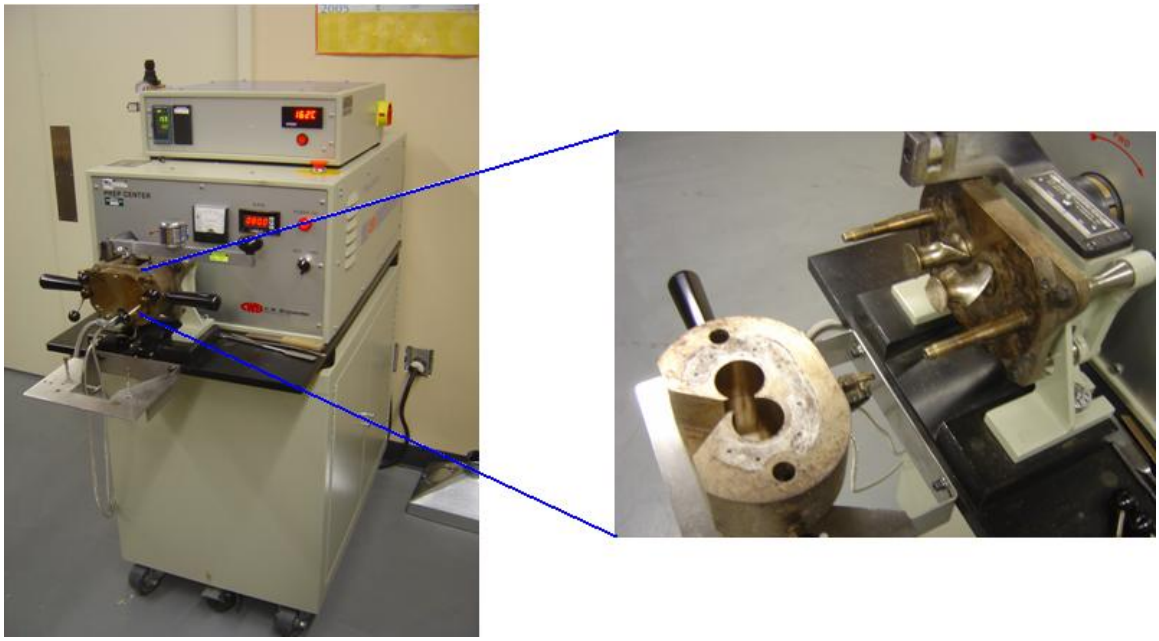

Figure 18. The Brabender type 6 mixer.

Pelletizer

A milling machine (model LC-124) from Gilson Company, INC. was used to pelletize the blends obtained in the blender. All samples including the neat polymers were pelletized for consistency in the processing history. Figure 19 shows the pelletizer used.

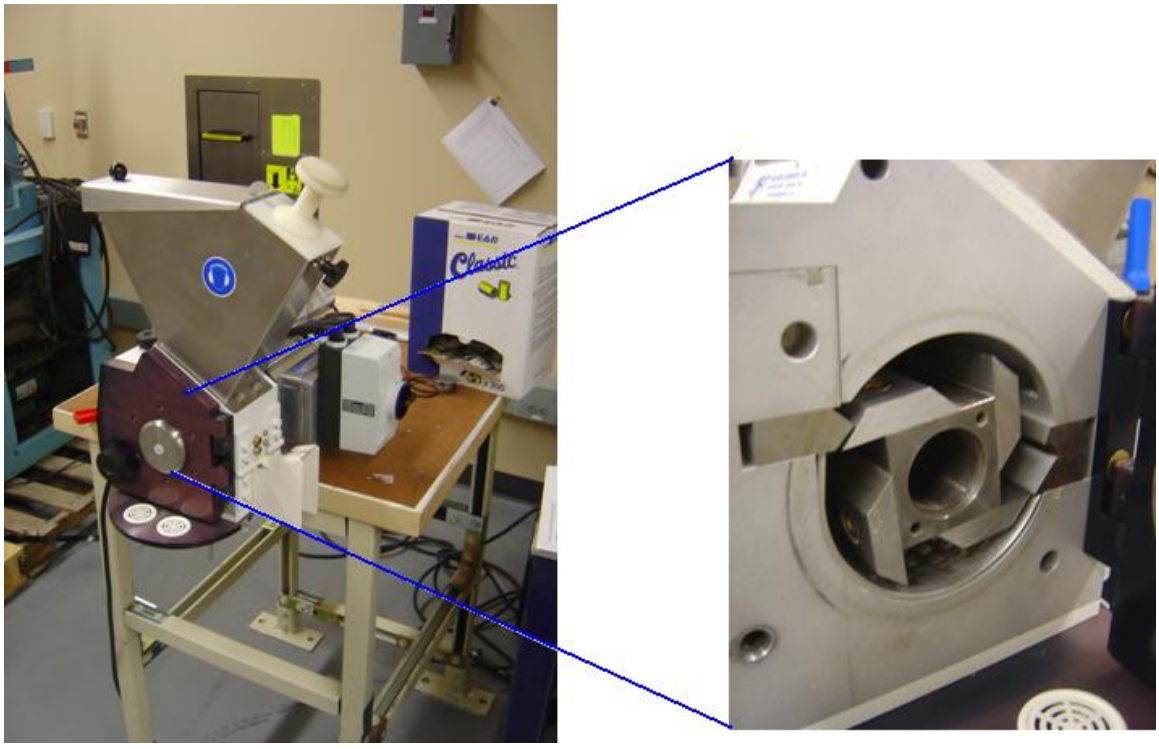

Figure 19. The Pelletizer.

Injection Molding

An injector molding machine (model AB-100 from AB Machinery) was used to produce the final specimens of all composites. The injection temperature for LDPE and Hytrel was 170 °C and 240°C respectively. The pressure was 60 psi in all cases. Figure 20 shows the injection molding machine. The final shapes of the specimens for the different tests were obtained using different molds during the injection. Squares of 40x40x2 mm, dogbones according to ASTM 630 D standard size, and rectangles of 20x5x2 mm were prepared.

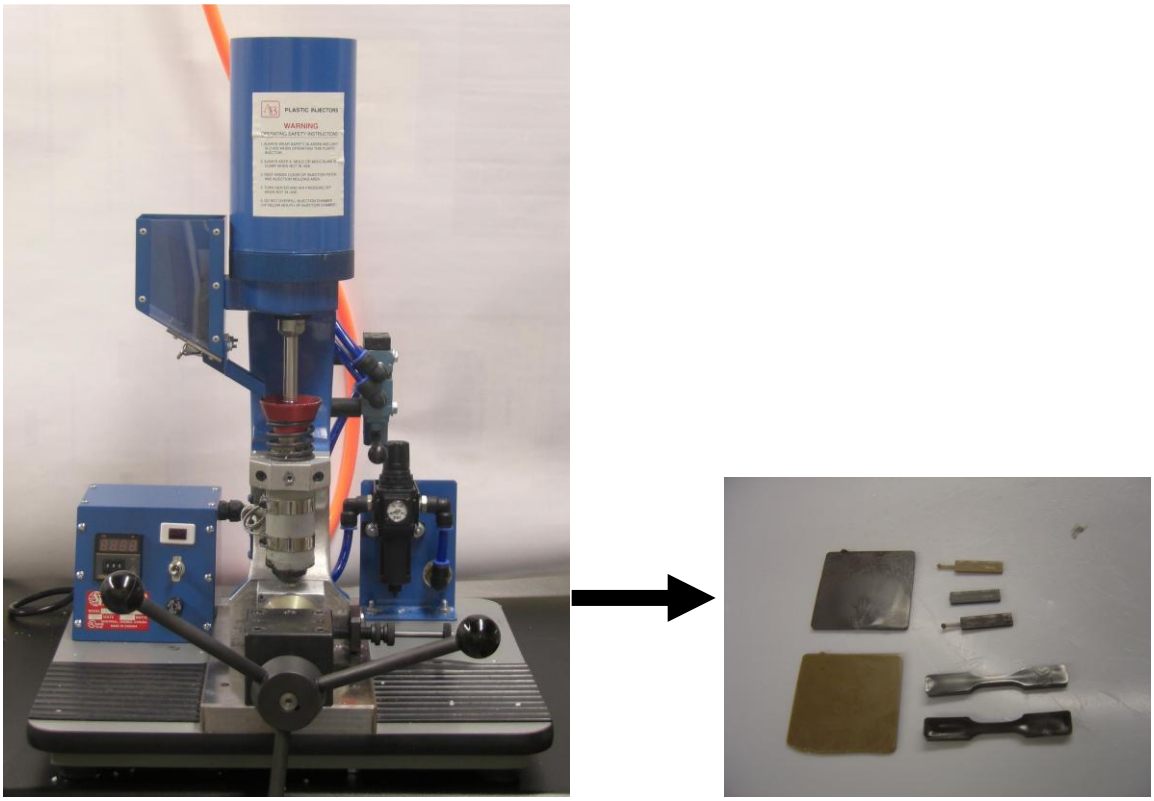

Figure 20. The injection molding machine.

3.3 Composites Characterization

Scanning Electron Microscopy (SEM) and Focused Ion Beam (FIB)

Two scanning electron microscopes were used in order to study the morphology of all the composites. A JEOL JSM-5800 with a thermionic gun was used to obtain images in the secondary electron (SE) and backscattered electron (BSE) modes. The acceleration voltage was 20 kV.

The second SEM is a FEI Analytical Dual Beam FIB. It is equipped with a field emission electron gun. For high resolution SEM images a through lens (TTL) detector was used. The acceleration voltage was set at 15 kV. Figure 21 shows this dual beam microscope.

For the focused ion beam cross section imaging, the following milling parameters were used:

- Ion beam acceleration voltage: 20 kV
- Ion beam size: 7 nA
- Overlap of x and y (discussed in the next chapter): 0 %
- For cleaning the surface cross section after milling the ion beam current was 3 nA
- The average milling rate was approximately 300 μm^3/min

For investigating the fractured cross section, the composites where cooled down to liquid nitrogen temperatures and then broken in the glassy state (brittle materials). All the samples were gold-coated prior the experiments to avoid excessive charging of the material.

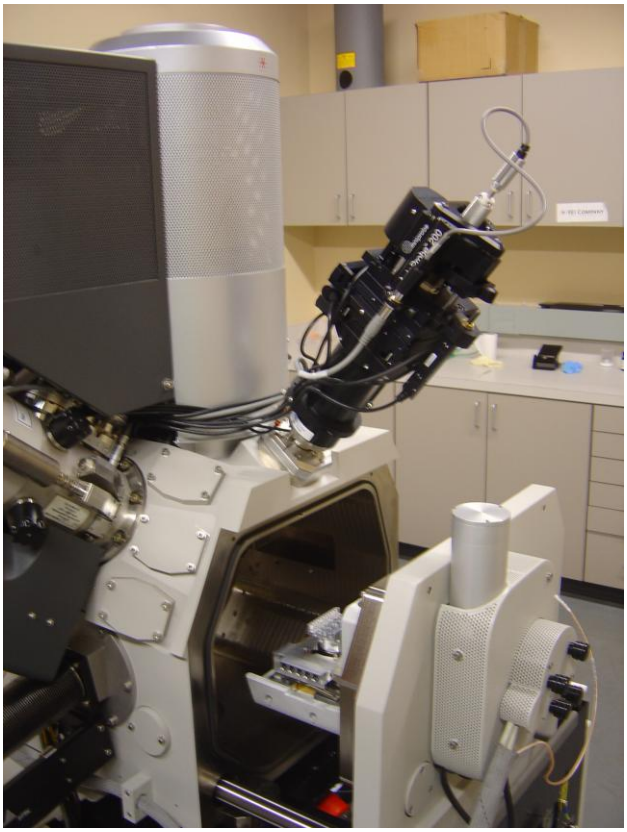

Figure 21. The FEI Analytical Dual Beam FIB.

Mechanical Properties

To determine several mechanical properties such as elastic modulus of the composites a MTS QTEST/5 universal machine was used (see Figure 22). The load cell used has a capacity of 2000 lb. The cross head speed was set at 200 mm / min and the acquisition data rate was 10 Hz. All the tests were performed at ambient temperature. The specimens used are those of the Type IV according to the ASTM D 638 Standard. At least 5 specimens were tested for each sample.

Figure 22. The QTEST/5 universal machine.

Friction Determination

The same QTEST/5 universal machine from MTS was used to determine friction of the composites. In this case different fixtures and accessories than for tensile test and a load cell with a capacity of 22.5 lb were used. Static and dynamic frictions were determined. Steel was selected as the sliding surface because of the difference in hardness. It can be expected that the deformation suffered by the steel asperities is much less than the asperities in the composites. The experimental conditions were:

- Sliding speed: 150 mm / min
- Sled weight: 431 g
- Friction surface: Stainless steel
- Ambient temperature

Scratch Resistance Determination

A micro-scratch tester (MST) from CSM instruments was used to determine the scratch resistance of the composites (see Figure 23). The tester is equipped with a Rockwell (conical) type diamond tip with a tip radius of 200 μm. The penetration (instantaneous) depth was measured as well as the residual (after viscoelastic recovery) depth. The conditions of the experiments were the following:

- Scratch velocity: 10 mm / min
- Groove length: 5 mm
- Applied load: 5 – 25 N
- Ambient temperature

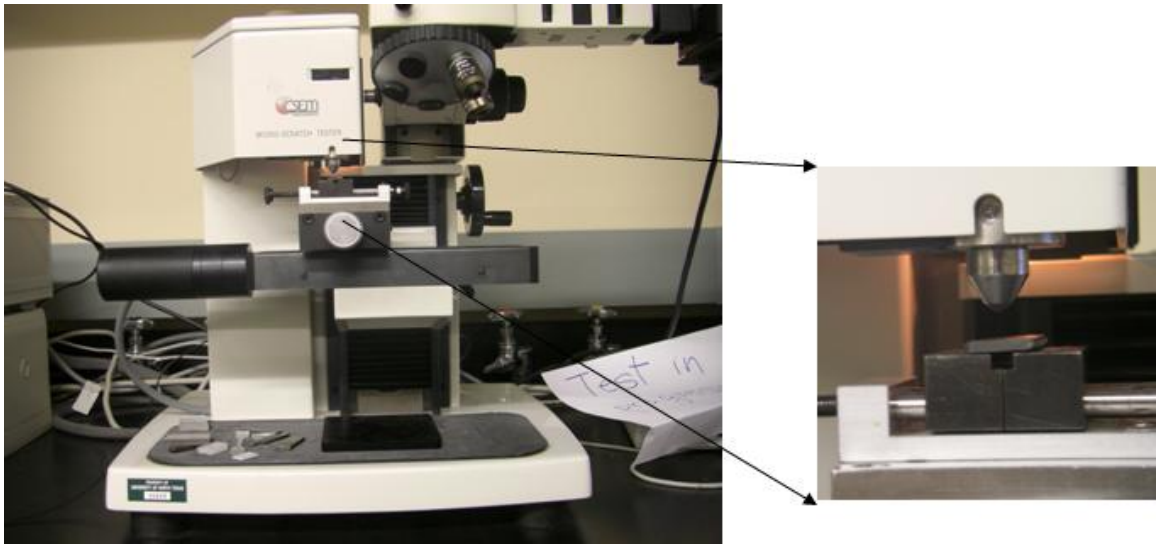

Figure 23. The CSM micro-scratch tester.

Pin On Disc Tribometer

In order to determine wear and wear mechanisms of the composites, a pin-on-disc tribometer (Nanovea series from Microphotonics, see Figure 24) was used. For these experiments only the highest concentration of metal particles of the different composites were tested. Carbon nitride was selected as the pin ball because of its exceptionally high hardness (1580 kg/mm^2) compared with the composites. Thus, we can safely assume that practically, there is no deformation of the ball. The experimental conditions were:

- Ball material: Carbon nitride
- Ball diameter: 3.12 mm
- Track radius: 2 mm
- Disc rotational speed: 200 rpm
- Total revolutions: 2000
- Applied load: 3 and 7 N

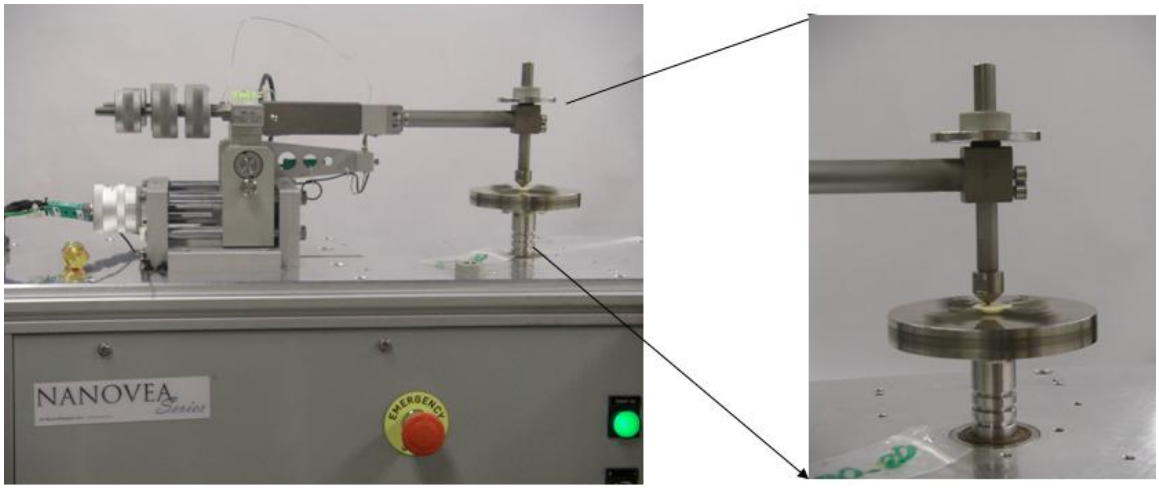

Figure 24. The pin-on-disc tribometer.

4. RESULTS AND DISCUSSION

This chapter will be divided in sections according to the technique used. Furthermore, in each section results for micro and nanocomposites will be presented and compared for both polymeric matrices: low density polyethylene (LDPE) and Hytrel.

4.1 Scanning Electron Microscopy (SEM) And Focus Ion Beam (FIB)

In order to understand the changes in the properties of the polymeric matrices used, it is pertinent to study the morphology of our composites. Since mechanical properties depend on the bulk material while tribological properties depend on the contacting surfaces it is important to know where the particles are located in the material and their dispersion. This is why, the surface of the samples as well as the fracture and (in some cases) FIB cross sections of the specimens were studied.

Among the signals that can be collected in SEM there are the secondary electrons (SEs) and the backscattered electrons (BSEs). As mentioned in chapter 1, the backscattered coefficient η depends on the atomic number of the specimen. η is higher at higher atomic numbers. According to this, it is reasonable to expect a fair amount of contrast in BSE imaging mode between materials with a relative high atomic number difference. This is the case in polymer + metal composites, where there are two separate phases with a relatively high atomic number difference (metal particles vs. organic polymer).

Microcomposites

The first SEM images are from the surface of the composites (Figures 25 - 30) while Figures 31 – 36 are from the fractured cross section of the same composites. Figure 25a shows a secondary electron SEM image of the surface of the PE composite containing 7.5 % aluminum micropowder. We can observe clearly the surface morphology in the micron scale, but more important is the determination of spatial distribution of the particles in the material. As

discussed above, BSEs can help in differentiating the two phases. Figure 25b shows a backscattered image of the same area as 25a. Now we can see very clearly where the particles are located; the bright spheres are the Al particles. This is also true for nickel and silver composites as shown in figures 26 and 27 respectively. It is important to note that some particles appear brighter than others. The reason is that there is always a defined interaction volume where the signals (SEs and BSE) come from. There are less backscattered electrons (signals) coming from the metallic particles deeper into the interaction volume. On the contrary, the number of electrons coming from the particles sitting closest to the surface is bigger and they appear brighter.

From figures 25 - 27 it is clear that for Al and Ni we achieve a good dispersion of the metallic phase, since individual particles can be recognized. However, in the case of silver, the irregular shaped particles tend to form agglomerates. The same is true for Hytrel + Al, Ag and Ni microcomposites as shown in figures 28, 29 and 30 respectively.

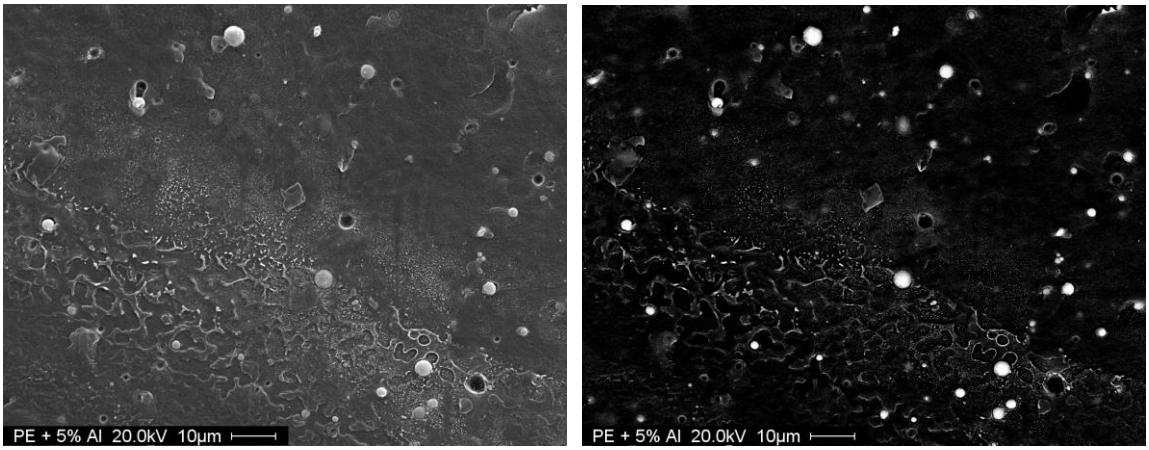

a) *b)*

Figure 25. a) Secondary electron image of the surface of PE + 7.5 wt % Al microcomposite. b) Backscattered electron image of the surface of PE + 7.5 wt % Al microcomposite.

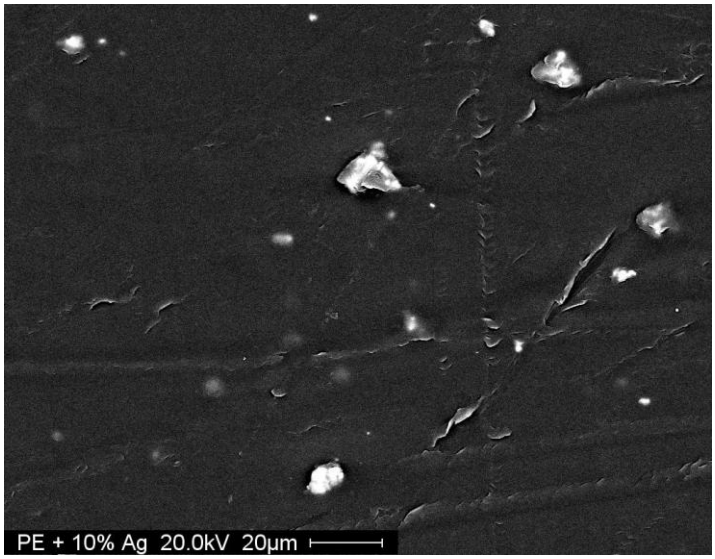

Figure 26. Backscattered electron image of the surface of PE + 10 wt % Ag microcomposite.

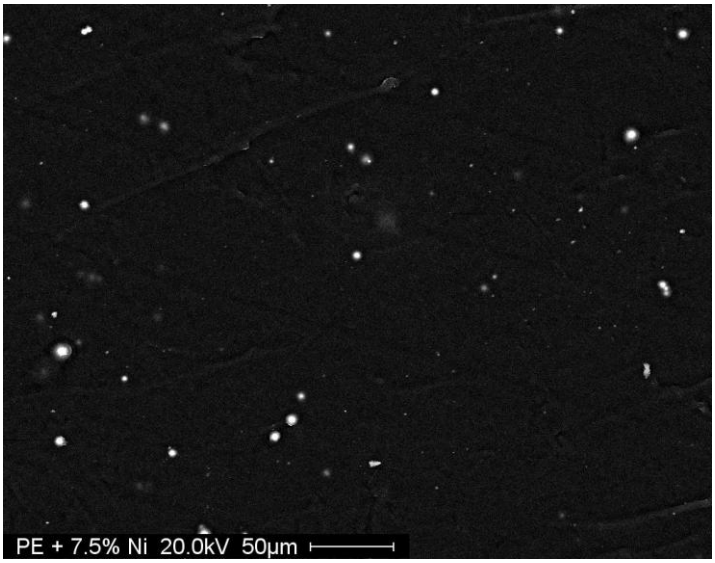

Figure 27. Backscattered electron image of the surface of PE + 7.5 wt % Ni microcomposite.

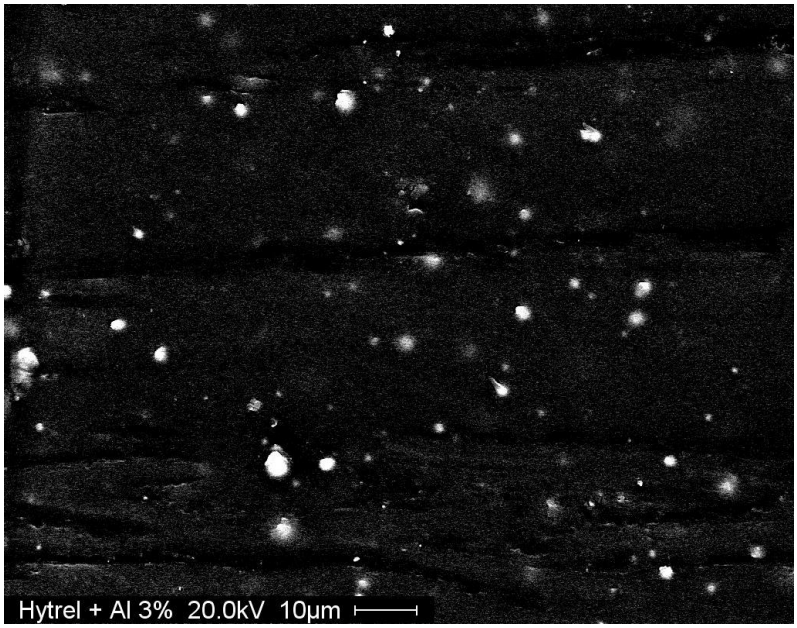

Figure 28. Backscattered electron image of the surface of Hytrel + 3 wt % Al microcomposite.

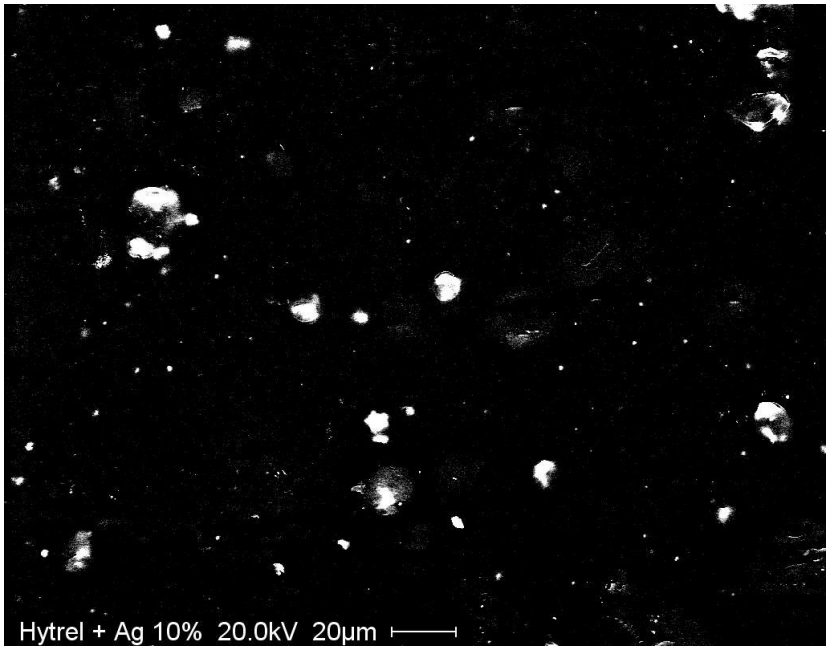

Figure 29. Backscattered electron image of the surface of Hytrel + 10 wt % Ag microcomposite.

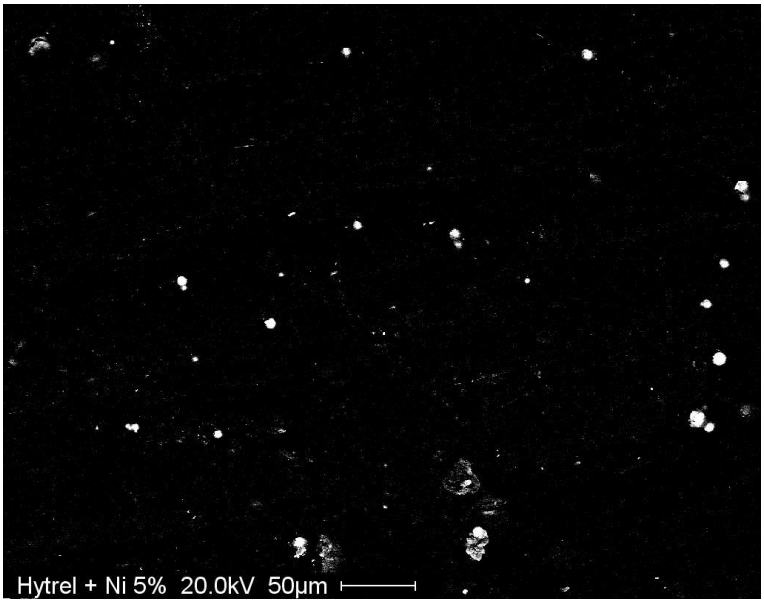

Figure 30. Backscattered electron image of the surface of Hytrel + 5 wt % Ni microcomposite.

So far, we have been studied the morphology of the composites on the surface. However, as mentioned before, mechanical properties depend on the bulk. For this reason, fractured surfaces were prepared by breaking the specimens at liquid nitrogen temperature and analyzing the fracture cross section. Figures 31 - 33 show the BSE images of the fracture cross section of PE + Al, Ag and Ni microcomposites. It is clear that the dispersion inside the material is as good as in the surface for Al and Ni, and the same tendency to form agglomerates is observed for Ag composites. This is also true for Hytrel microcomposites as seen in figures 34 - 36.

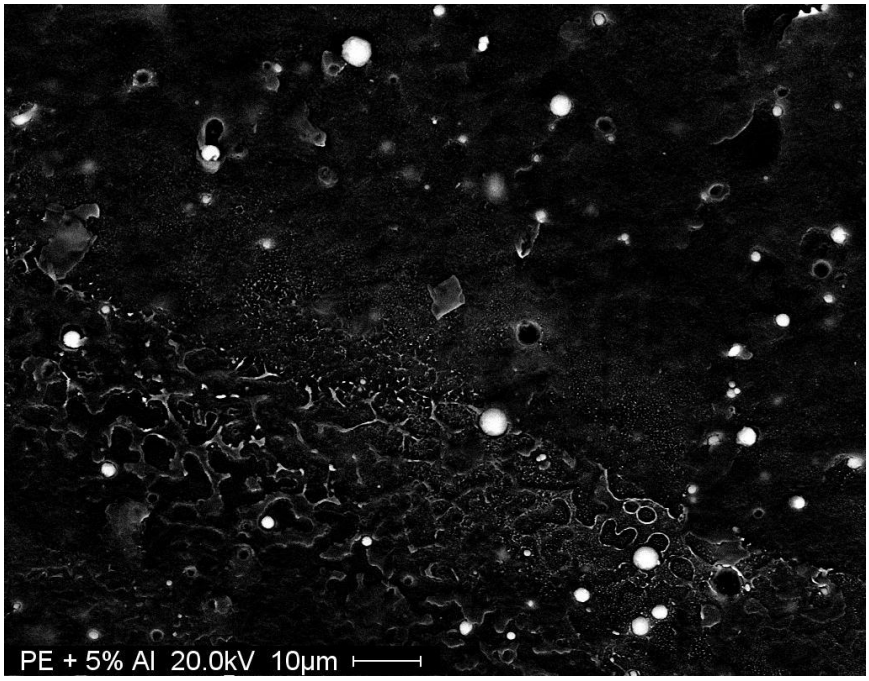

Figure 31. Backscattered electron image of the fracture cross section of PE + 5 wt % Al microcomposite.

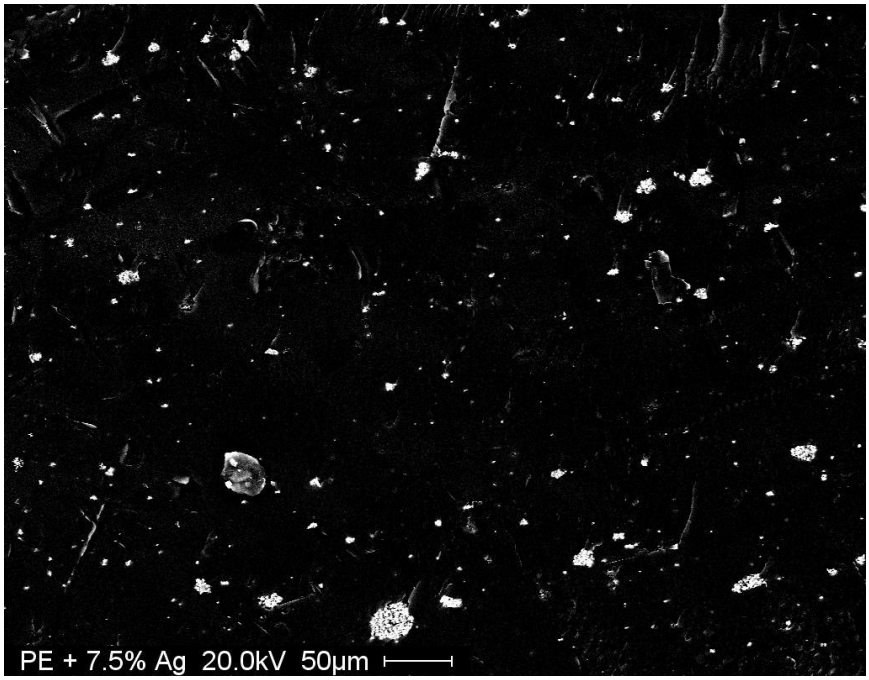

Figure 32. Backscattered electron image of the fracture cross section of PE + 7.5 wt % Ag microcomposite.

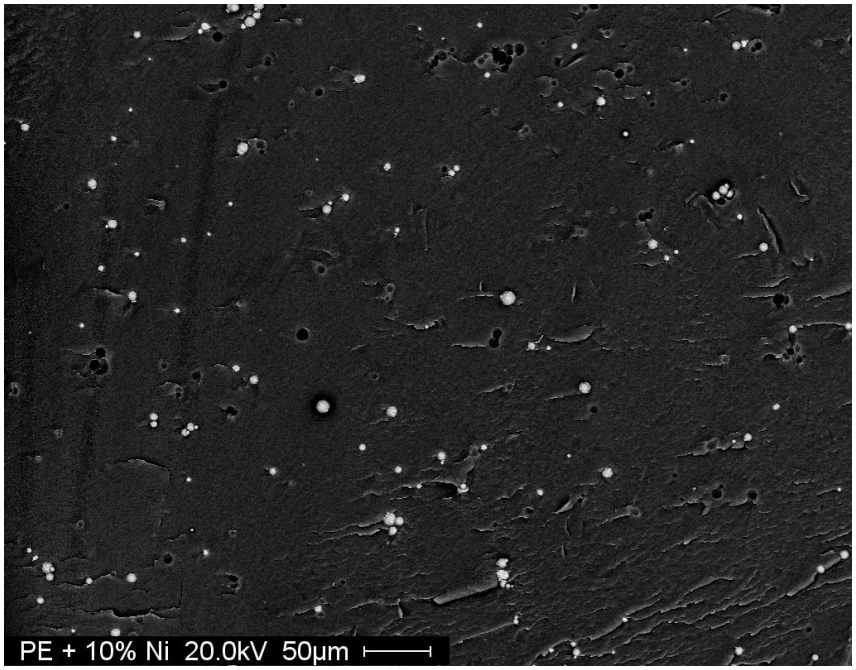

Figure 33. Backscattered electron image of the fracture cross section of PE + 10 wt % Ni microcomposite.

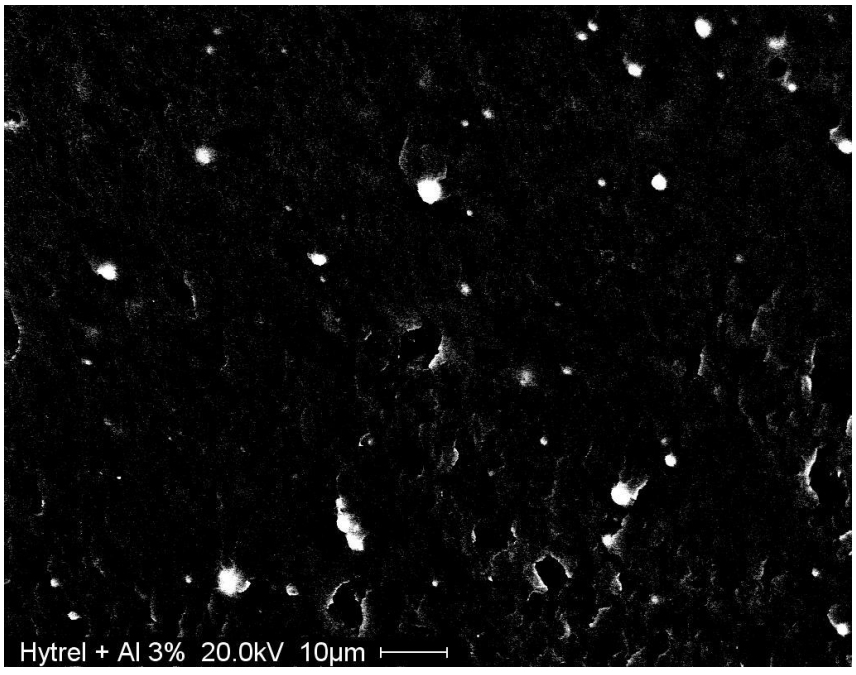

Figure 34. Backscattered electron image of the fracture cross section of Hytrel + 3 wt % Al microcomposite.

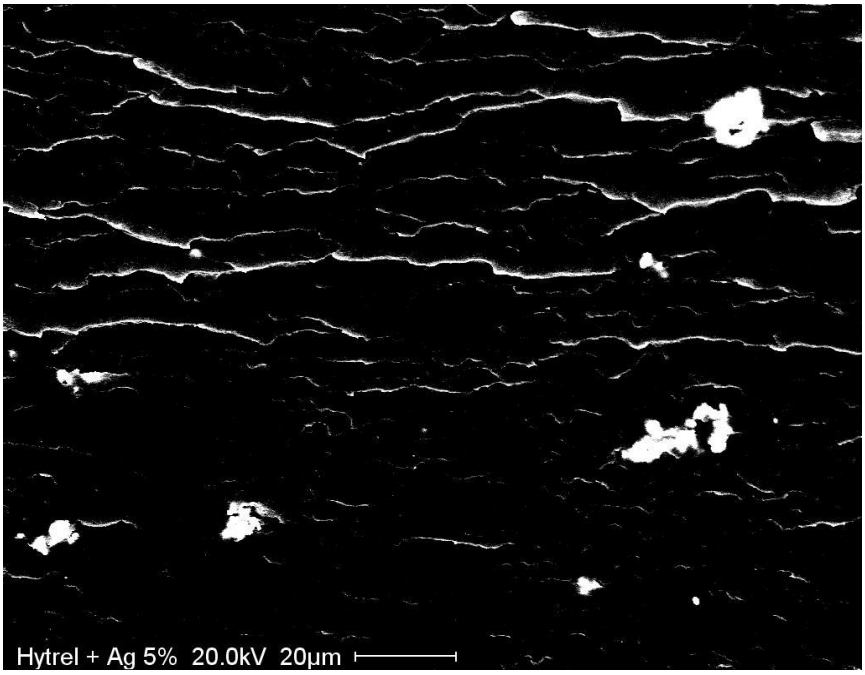

Figure 35. Backscattered electron image of the fracture cross section of Hytrel + 5 wt % Ag microcomposite.

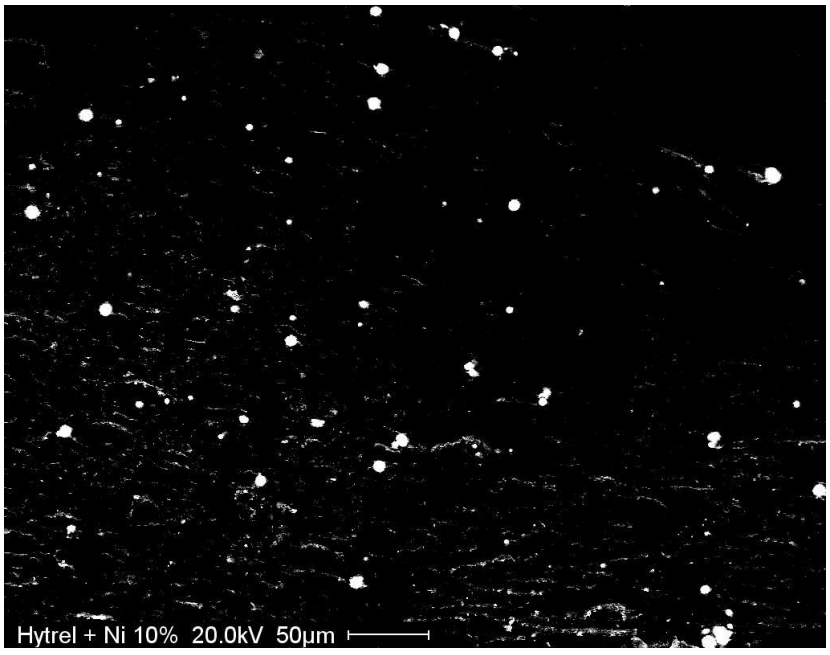

Figure 36. Backscattered electron image of the fracture cross section of Hytrel + 10 wt % Ni microcomposite.

So far, fractured cross sections have been presented. This is a destructive method that requires the breaking of the specimens. Focus ion beam (FIB) in the other hand, is a non-destructive method that allows studying a cross section of a material with only micrometric-scale damage. PE + 10 wt % Al was chosen for FIB since there is a sufficient concentration of particles per volume to be studied by this technique.

Figure 37 shows a FIB cross section of the composite. It is possible to observe the Al particles well distributed inside the material. Another interesting phenomenon is the cracking of the edges of the milled box. This cracking is due to the rapid changes of temperature provoked by the Ga^+ beam. This problem was overcome by changing the overlapping in the passes that the beam does from 50 % to 0 %.

In order to understand the concept of beam overlap it is pertinent to understand how the ion milling works (see Figure 38). The focused ion beam has a defined spot size or diameter *d*. The beam is swept from side to side (x axis) over the length that is to be removed. Once the first pass is completed the beam moves down (y axis) and the second pass in the x axis occurs. These steps continue until the area of interest is covered and the area is swept again and again until the determined volume is removed. As seen in Figure 45a there is an area of overlapping between two consecutive passes. This overlap area is exposed to the beam twice in a short period of time causing local heating. Local heating produces local expansion of the composite and local compressive stresses are produced. The stresses (and thus deformation) are high enough to provoke cracking of the material. On the other hand when we set the overlap of the beam to 0% the overlap area is eliminated. The material heated in each pass has now time to cool down until the whole area of interest is swept and the beam returns to that spot. This way cracking of the material is prevented. It is also important to note that the total time of milling is not affected since the area of interest need to be swept more times but each scan takes shorter time to be completed.

Figure 39 shows images taken at 5, 15 and 30 min during the ion milling process. During the process there is a phenomenon of redeposition of the material being milled away on the cross-sectioned wall. A cleaning of the cross section with a lower ion beam current is necessary. Figure 40 shows the FIB cross section of the composite after the cross section cleaning. It is evident that the Al particles were “hidden” under the redeposited layer.

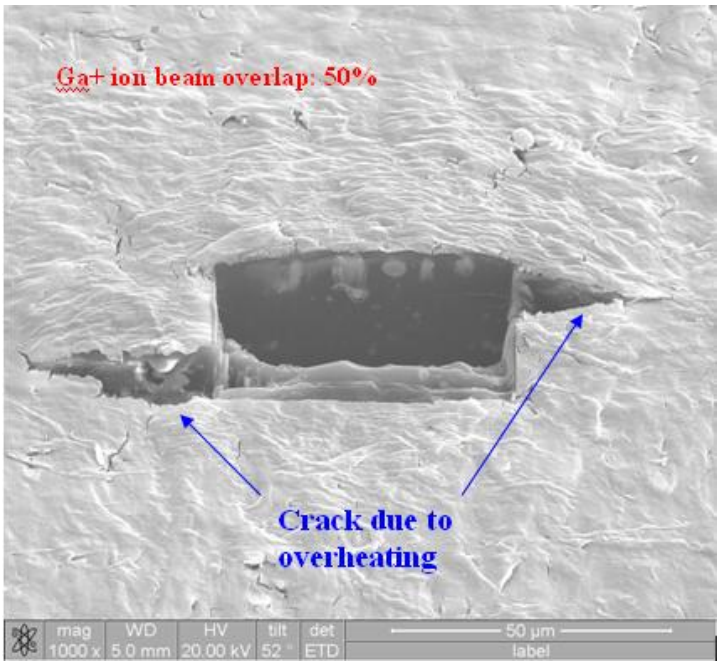

Figure 37. FIB cross section of PE + Al 10 wt. % showing overheating cracking.

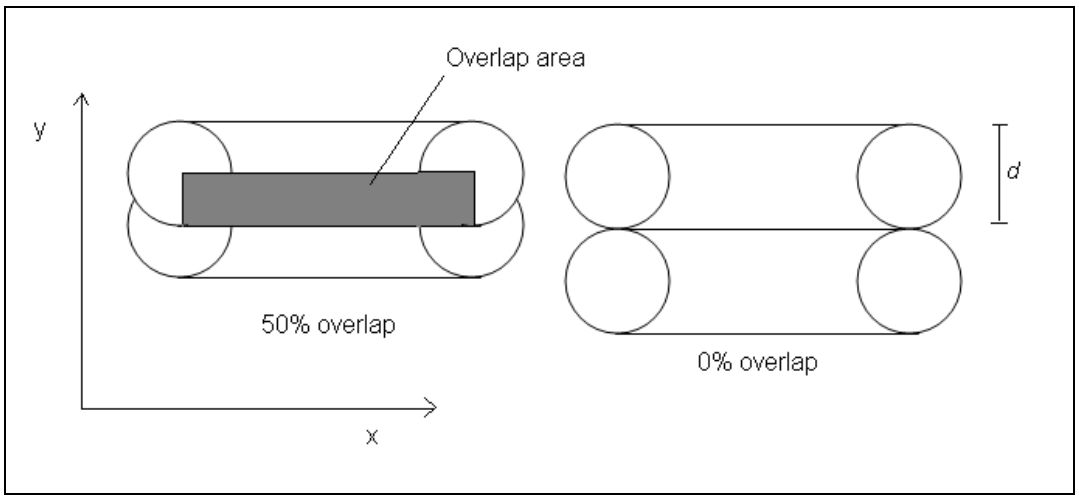

Figure 38. Overlap of the ion beam.

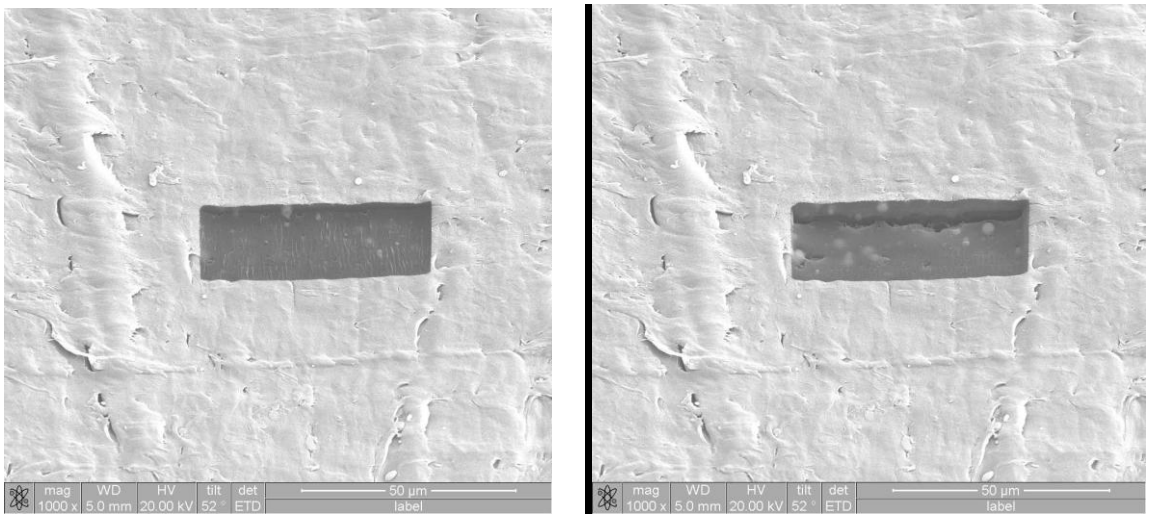

a) b)

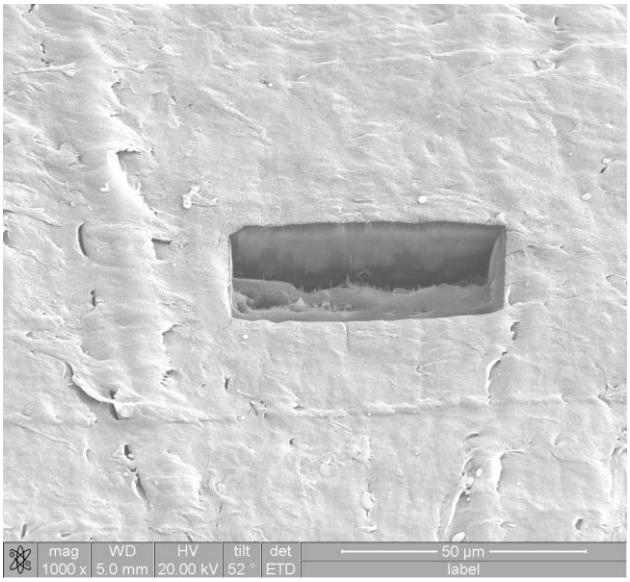

c)

Figure 39. FIB milling process of PE + Al 10 wt. %. a) 5 min b) 15min c)30 min.

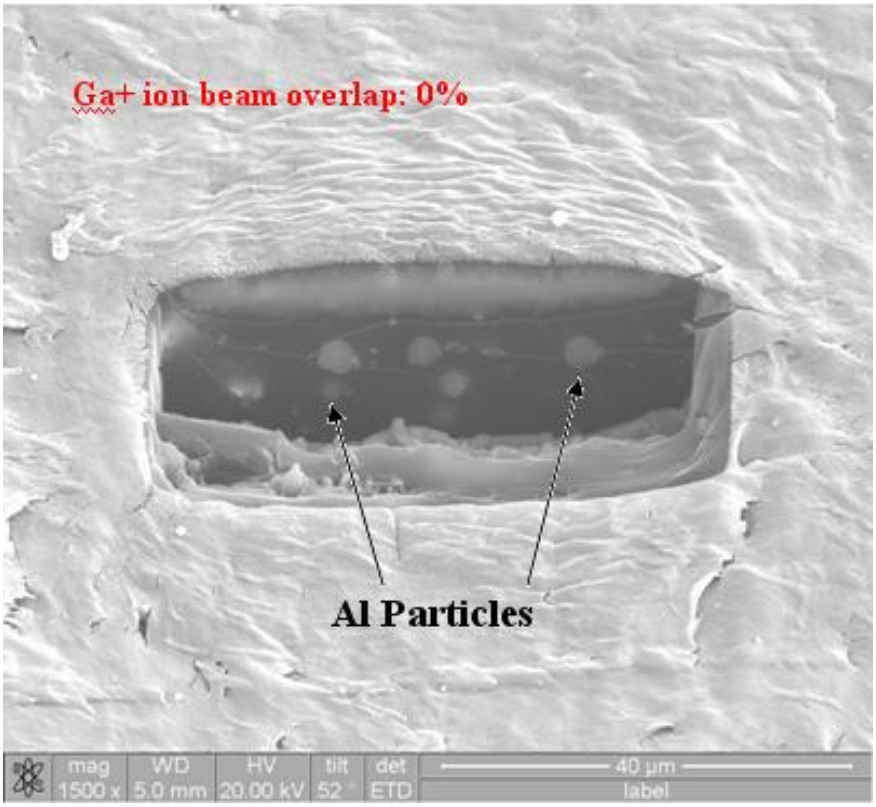

Figure 40. FIB cross section of PE + Al 10 wt % after low beam current surface cleaning and 0 % beam overlap.

Nanocomposites

Figure 41 and 42 shows the SE image of the fracture cross section of PE + Ag 5 wt % and PE + Ag 10 wt % nanopowder respectively. It is clear that there is a high degree of agglomeration and we can find clusters as big as 40 μm. The same happened in the case of Hytrel. Figure 43 shows the SE image of the fracture cross section of Hytrel + Ag 10 wt % nanopowder.

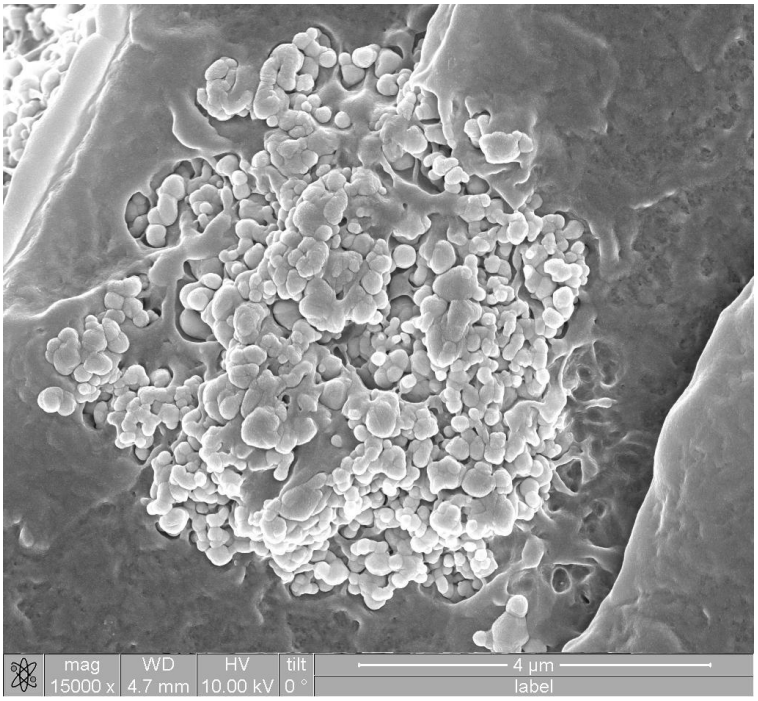

Figure 41. Secondary electron image of the fracture cross section of PE + 5 wt % Ag nanocomposite.

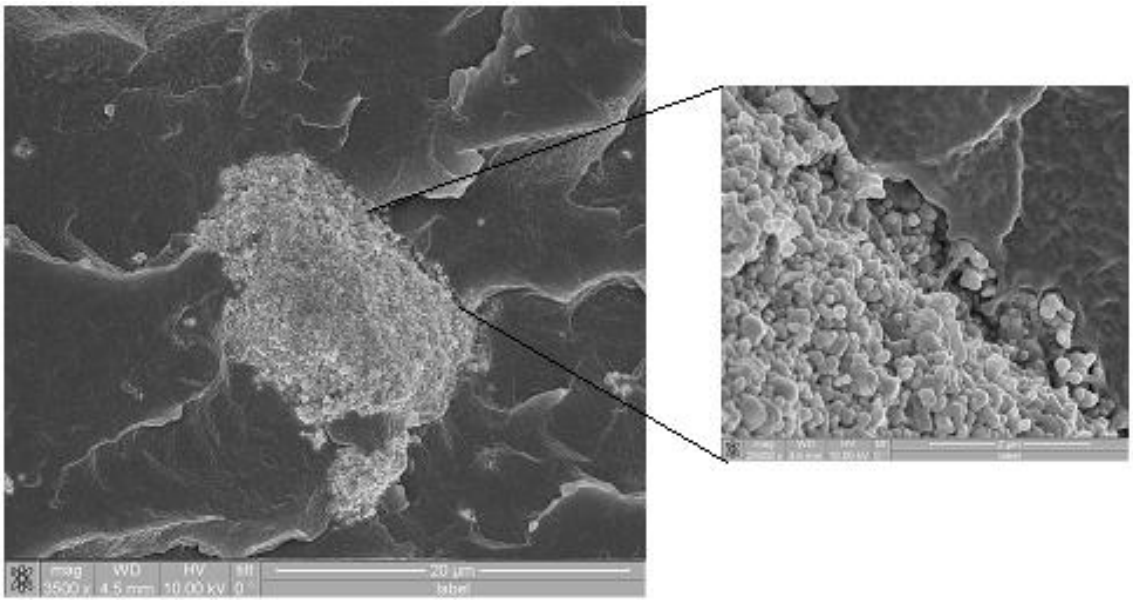

Figure 42. Secondary electron image of the fracture cross section of PE + 10 wt % Ag nanocomposite.

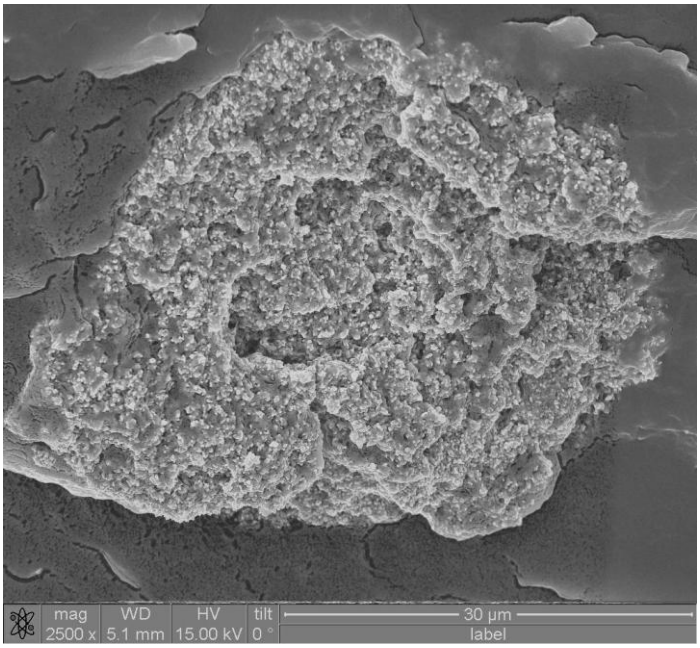

Figure 43. Secondary electron image of the fracture cross section of Hytrel + 10 wt % Ag nanocomposite.

The case of Al nanocomposites is a different one. Figure 44 shows a SE fracture cross section image of PE + 10 wt % Al nanocomposite. It is difficult to be sure that there are particles on the image and it appears that the polymer does not have metal inside. Since we suspect that the particles are in the nanometric range, it is possible that the gold coating act as a “mask” that hides the particles. The specimen was subjected to FIB to prove this hypothesis. Figure 45 shows a FIB cross section of the same material of figure 44. The milling process was the same as for the microcomposites. After the cross section cleaning it is clear that there is a big amount of small Al particles inside the polymer. Although we can still see several agglomerated particles the dispersion is dramatically better than in the case of Ag. It is possible to see that only by removing the gold coating with the ion beam the Al particles can be appreciated. This is shown in figure 46; this is an image of the milling process during the first minute, where only the gold coating was removed. This proves our hypothesis that the gold coating can hide small particles causing an erroneous interpretation of the images.

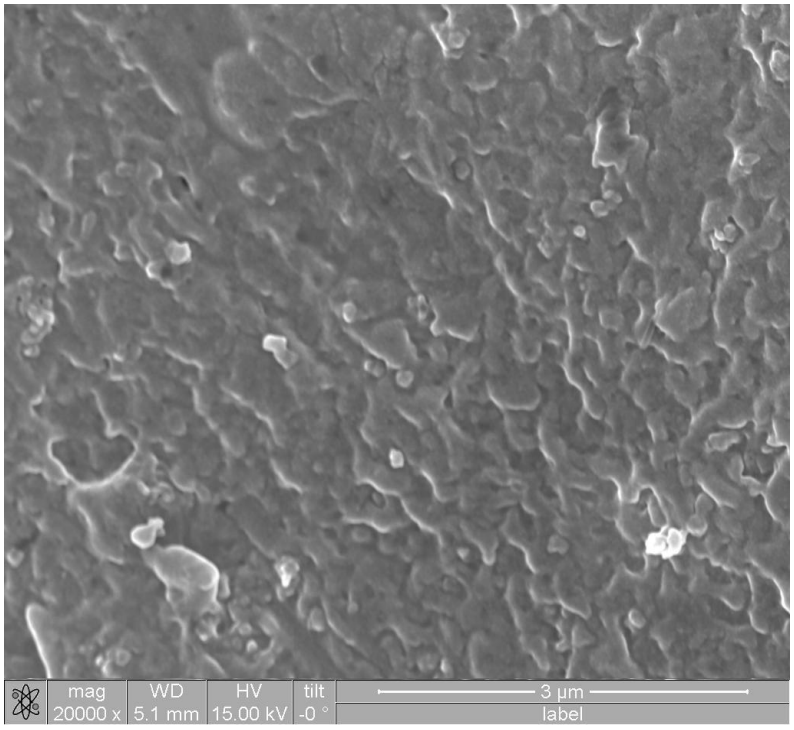

Figure 44. Secondary electron image of the fracture cross section of PE + 10 wt % Al nanocomposite.

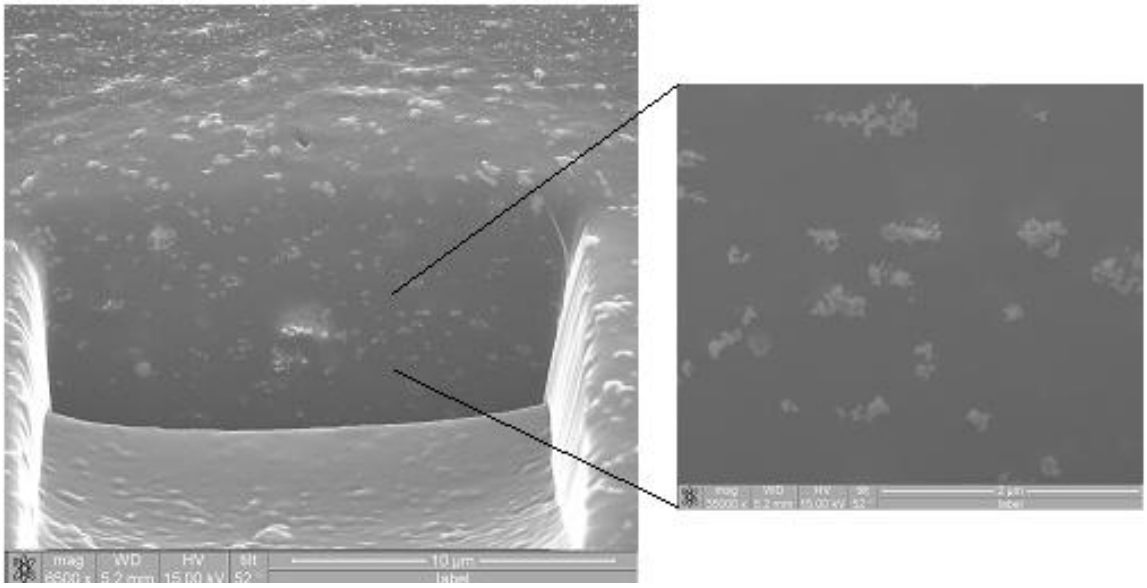

Figure 45. Secondary electron image of the FIB cross section of PE + 10 wt % Al nanocomposite.

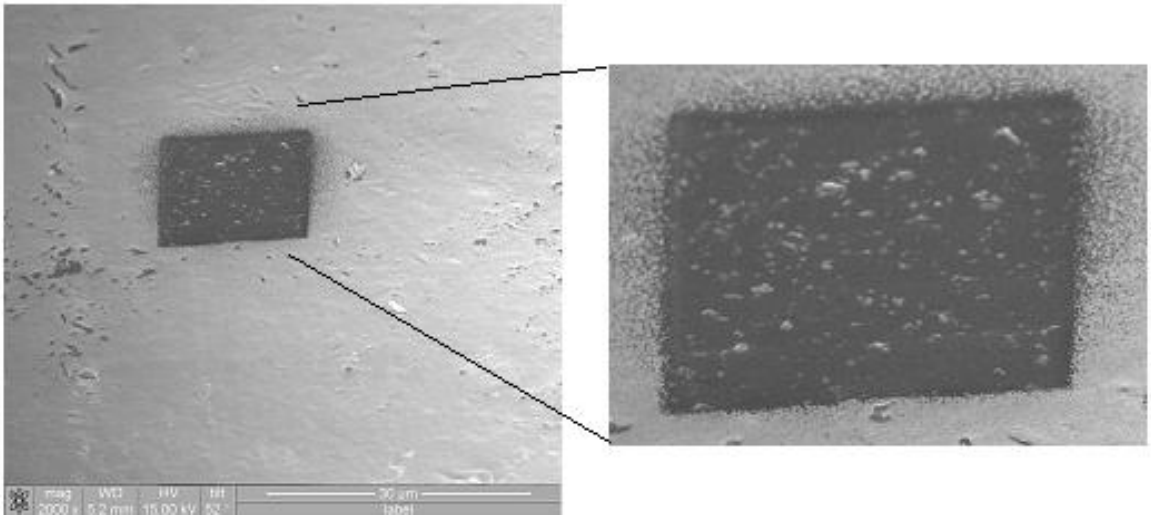

Figure 46. Secondary electron image of the FIB cross section of PE + 10 wt % Al nanocomposite after 1 minute of ion milling.

Microcomposites and nanocomposites comparison

Observing the SEM images for the microcomposites and the nanocomposites, similarities between them can be found. First, the aluminum particles are well dispersed in both cases, while the silver ones tend to form agglomerates in the micrometer and the nanometer sizes. In all cases, the filler is found in the surface of the material as well as in the bulk. According to this, changes in tribological and mechanical properties on the composites are expectable.

4.2 Tensile Testing

The tensile testing was carried on following the ASTM standard D638. The experimental parameters and the dimensions of the specimen were taken from this standard. At least 5 specimens were used in order to obtain one average value of the elastic modulus. Typically, the error bars obtained in this test were about ±7 MPa which represent an error of less than 5% of

the modulus values. Thus, the differences observed in the results obtained can be effectively attributed to the different properties of the composites.

Microcomposites

Figure 47 shows the elastic modulus of the Hytrel microcomposites. The three fillers show the same trend: an initial decrease of the modulus reaching a minimum (at about 1 wt %), followed by a continuous increase. The initial lower modulus probably is due to the filler particles perturbing the polymer matrix since no coupling agent was added. The increase in modulus further on can be explained by the fact that at higher concentrations more filler particles hamper the chain mobility. Our model is reinforced also by the fact that for the smallest particles (Al) we obtain a modulus higher than that of the pure material starting at 3 wt %, while for the two other metals this occurs at a much higher concentration. Apparently, the small Al particles are more effective in limiting the chain mobility and enhancing the modulus earlier.

Figure 48 shows the elastic modulus of the LDPE microcomposites. As seen in the case of Hytrel, there is an initial reduction of the modulus, followed by a continuous increase at higher concentrations. The minimum values occur at different concentrations for the three metals. The different size and shape of the metals is speculated to be the reason for this behavior, although which parameter affect the most (size or shape) is uncertain. The difference is that even at 10 wt %, for any of the metals, the modulus is still lower than for the pure material. This is because LDPE is an uncrosslinked branched material; the metal particles can still limit the chain mobility and affect the modulus, although not to the same extent as for Hytrel.

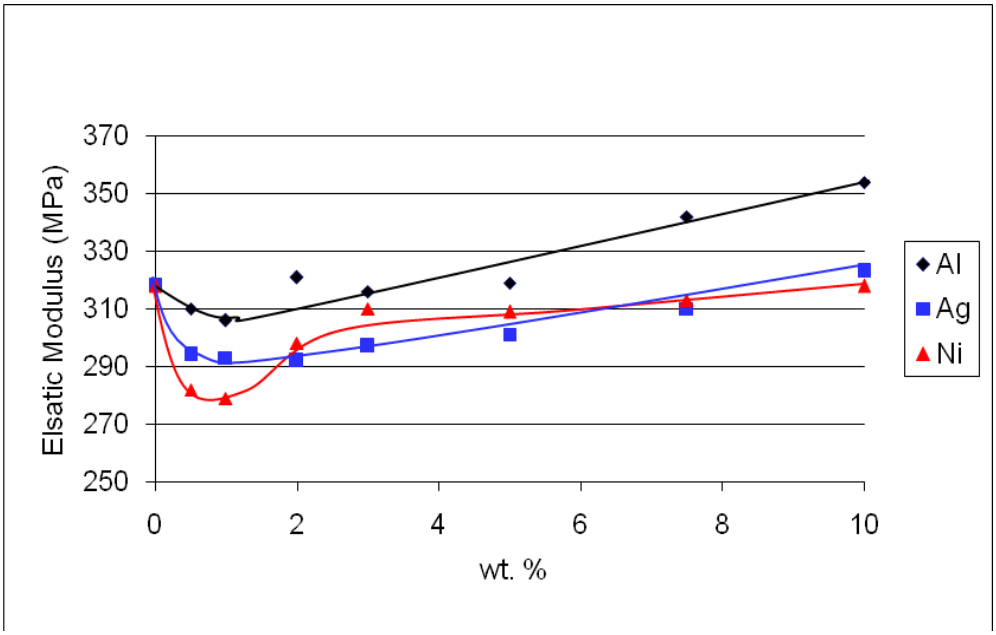

Figure 47. Elastic modulus for Hytrel microcomposites.

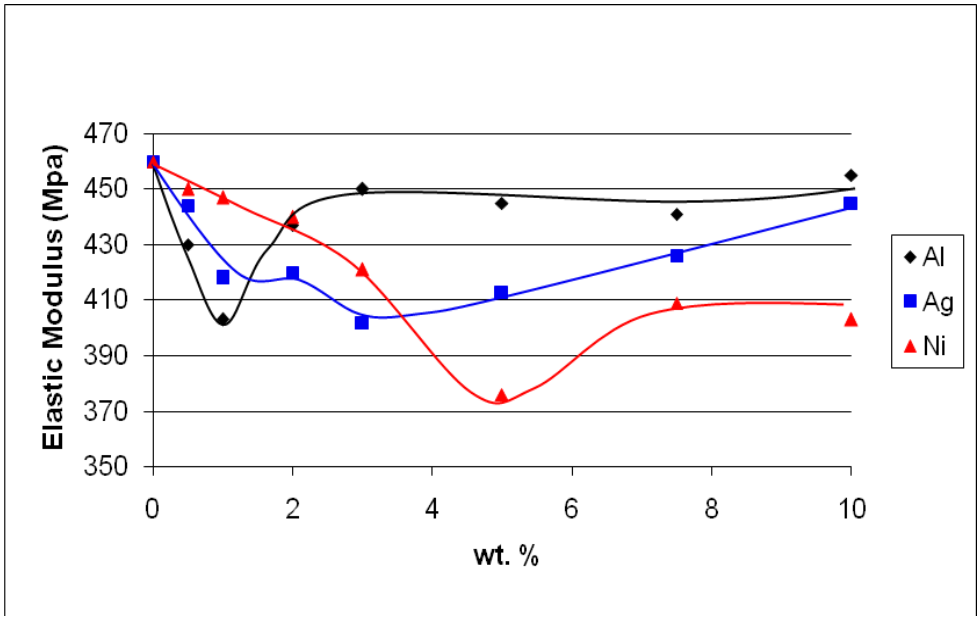

Figure 48. Elastic modulus for LDPE microcomposites.

In order to improve the polymer-metal interaction at the interphase, a silane primer was added to the blends. The way the primer works is explain in the following. The primer (described in Chapter 3) has a double C=C bond in one side and a silane group in the other. When the primer is added to ethanol at 50°C and stirred, CH3-OH groups (methoxy) are formed in the Si

side as well as in the organic part (double C=C bonds can be broken). When the metallic particles are introduced to the ethanol + primer solution a layer of OH groups is formed (if not already existing) on the surface of the metal particles. This OH groups are then hydrolyzed by the OH groups of the primer, thus the primer is attached to the surface of the metal. When the primed particles are added to the molten LDPE matrix two things can happen: one is the reaction between the vinyl groups of the polymer and the primer forming a “chemical bridge” between the polymer and the metal; the second thing is the reaction between the OH groups of the primer attached to the metal with other primer molecules (since both sides of the primer can have OH groups) thus forming a network between the metal particles with the chains of primer molecules as the connecting links. Either way, reinforcement can be expected from these two phenomena.

Figure 49 shows the elastic modulus of the LDPE microcomposites with the silane primer added. As seen in the previous cases, there is a minimum followed by a continuous increase in the modulus. However, for Ag and Al micropowders, a modulus *higher* than the pure LDPE was obtained - in contrast to the microcomposites without primer. This is more clearly seen in Figures 50 - 52 that show comparatively the modulus for each metal with and without the primer.

It is clear that the primer worked best for Ag. The degree of compatibilization of the primer is dependent of the chemical structure of both polymer and metal surface. Thus, there are primers that work better for some inorganic particles and polymers than others. In this case, apparently the chemical affinity of the primer used is higher for Ag than for the other two metals.

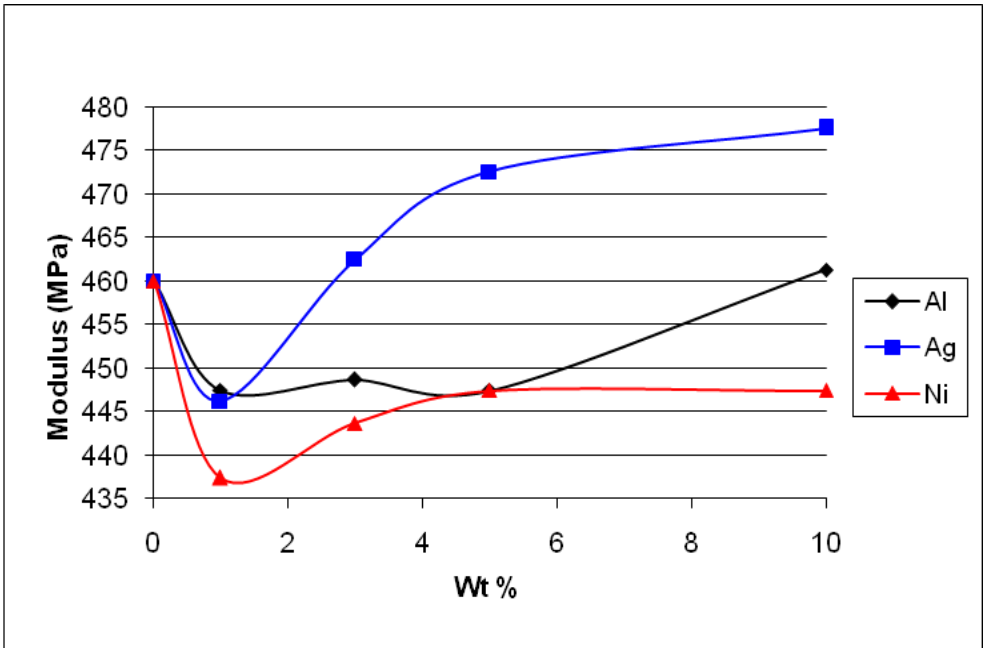

Figure 49. Elastic modulus for LDPE + primer microcomposites.

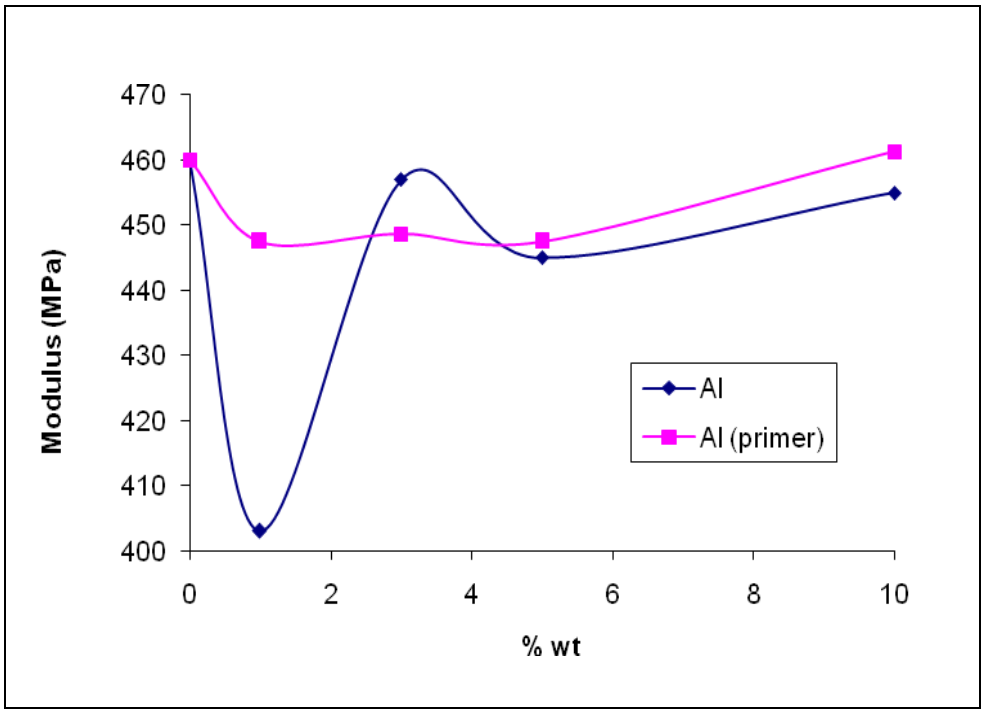

Figure 50. Elastic modulus for LDPE + Al microcomposites.

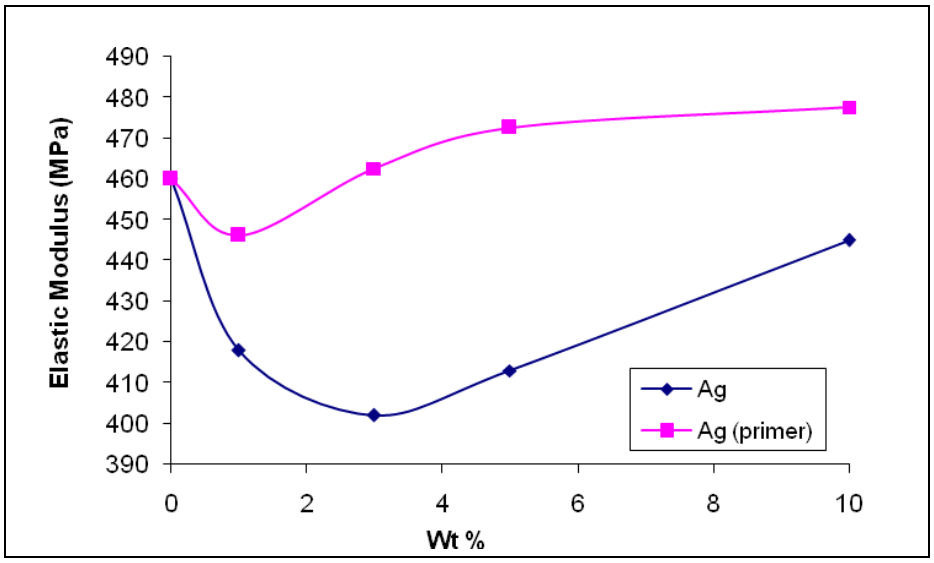

Figure 51. Elastic modulus for LDPE + Ag microcomposites.

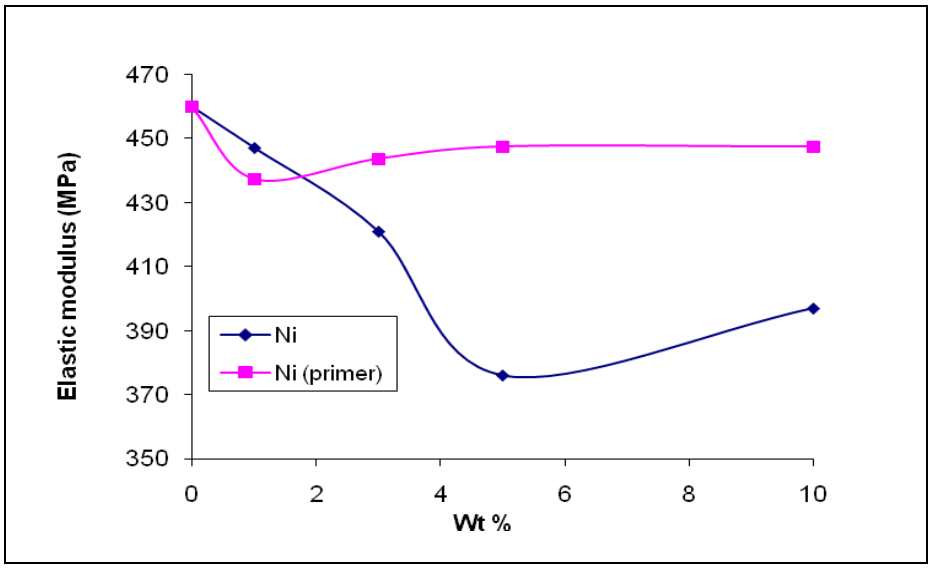

Figure 52. Elastic modulus for LDPE + Ni microcomposites.

The higher modulus in the case of the microcomposites with primer means that there is effectively a reinforcement effect in the polymer-metal interaction. This is also proven by observing the microstructures in the two cases. Figure 53a shows a SEM image of the fracture cross section of the LDPE + Al microcomposite without the primer; it can be seen that there is

no wetting of the particles by the polymer. On the other hand, it is possible to find wetted particles in LDPE + Al microcomposite with the primer added - as seen in 53b.

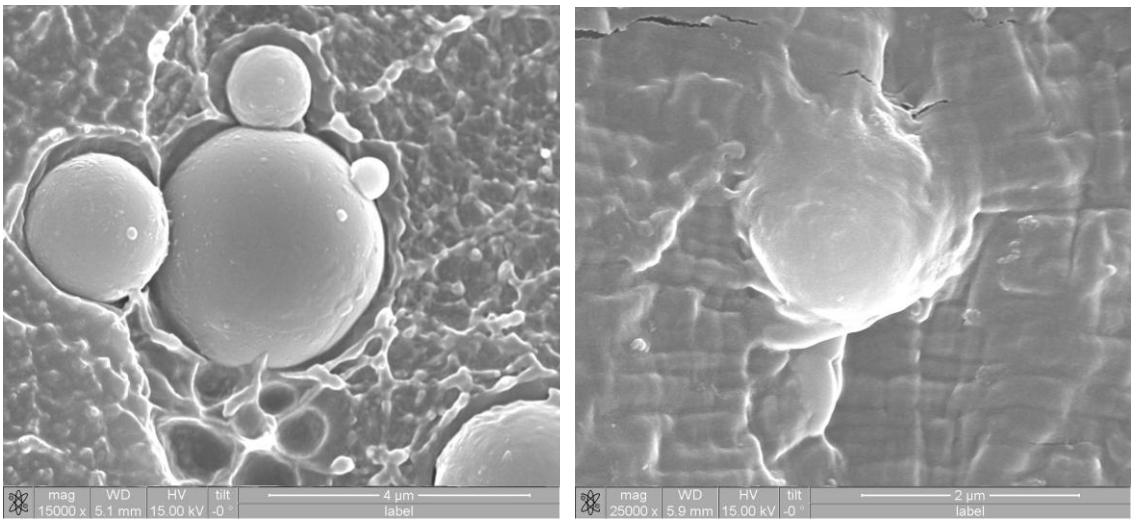

Figure 53. LDPE + Al microcomposites. a) without primer, b) with primer.

Nanocomposites

Figure 54 shows the elastic modulus for LDPE nanocomposites. Similar to the case of microcomposites, there is a minimum value followed by a continuous increase at higher concentrations. Again, at low concentrations there is a disruption of the structure of the polymeric matrix. After the minimum value, the increase in metal particles content hampers the chain mobility causing a reinforcement effect. However, in the case of the nanoparticles we can obtain a higher modulus than the pure LDPE starting at 3 wt % for Al and at 5 wt % for Ag.

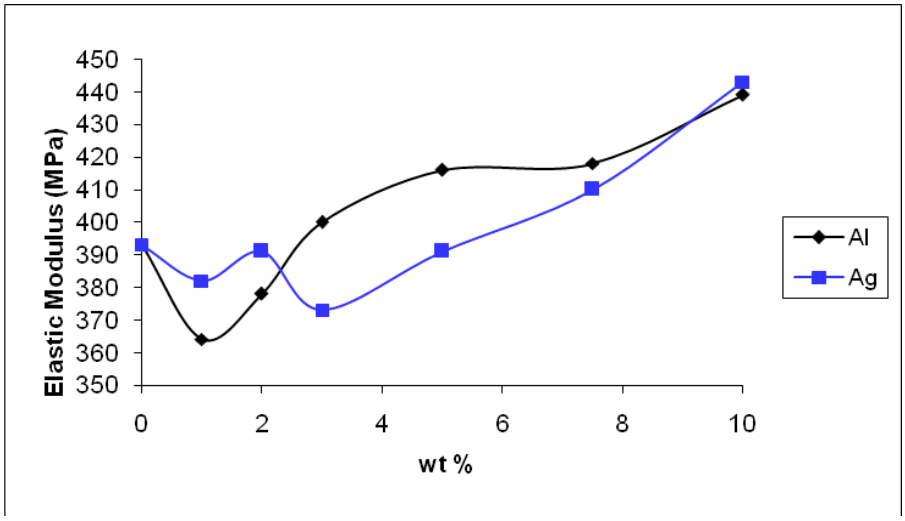

Figure 54. Elastic modulus for LDPE nanocomposites.

Figure 55 shows the elastic modulus for Hytrel nanocomposites. In the case of Ag, we observe the same tendency as for the Hytrel + Ag microcomposite; an initial modulus decrease followed by a continuous increase. However, the decrease in modulus is very small in this case; at only 3 wt % we already have a higher modulus than for the neat polymer. On the other hand, for Al we observe a reinforcement effect as soon as the metallic particles are incorporated into the matrix; this means that the Al nanoparticles hamper the chain mobility even at low concentrations.

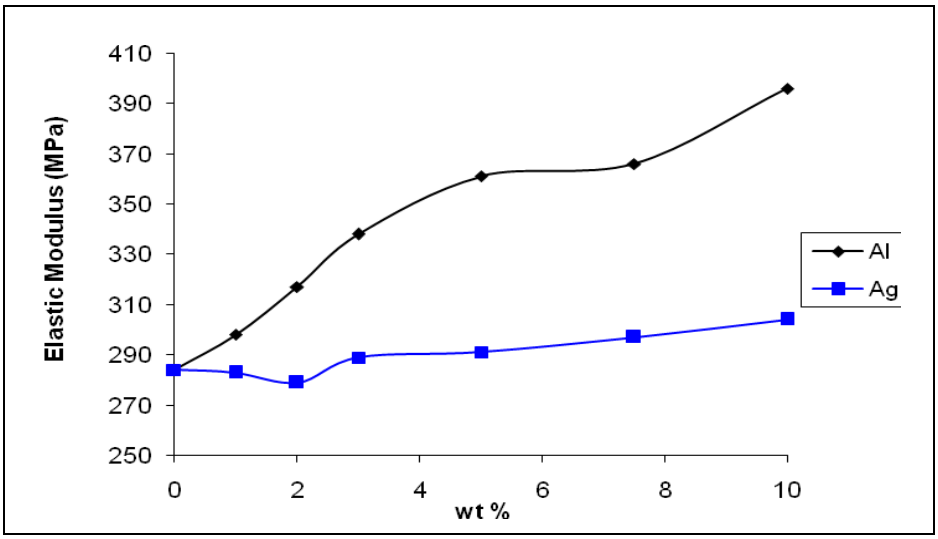

Figure 55. Elastic modulus for Hytrel nanocomposites.

There is an interesting phenomena in the case of Hytrel nanocomposites, namely a loss of elasticity of the material as we increase the amount of filler. Figure 56 shows the percent elongation at break for the Hytrel nanocomposites. This parameter is used only for study the materials since in real practice we never want to reach this point. It is clear that the more particles inside the matrix, the lower percentage elongation at break. This is understandable since by hampering the chain mobility the metal nanoparticles also prevent the polymer to elongate as much as if they were not present.

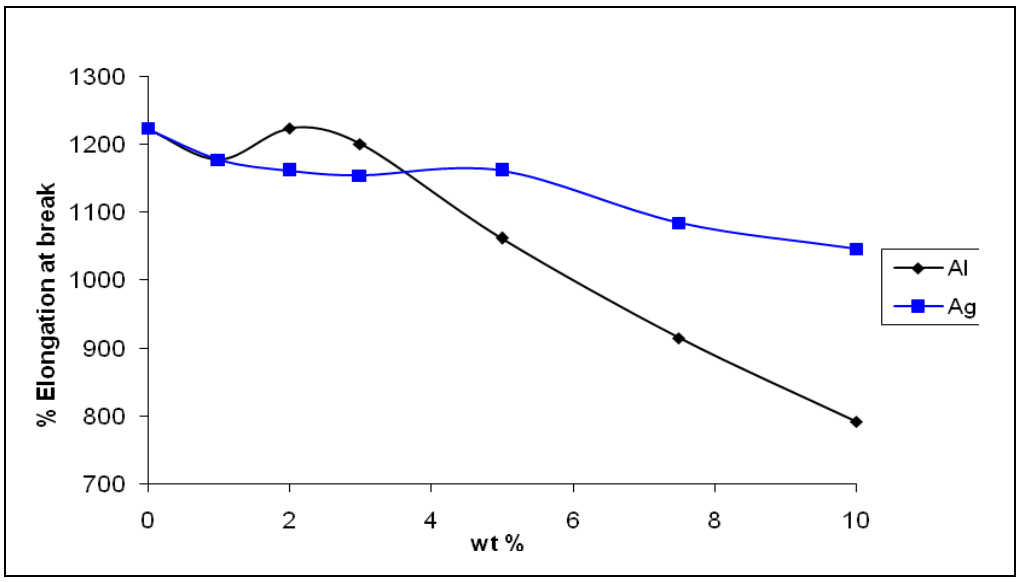

Figure 56. Percent elongation at break for Hytrel nanocomposites.

Microcomposites and Nanocomposites Comparison

Figures 57 and 58 show the modulus for the LDPE micro and nanocomposites for Ag and Al respectively. In the case of Ag the tendency is very similar; however, the modulus of the nanocomposites is higher at all concentrations. Even though both micro and nano Ag particles tend to form agglomerates, the nanoparticles act as a stronger reinforcement. For Al the situation is different. Both micro and nanoparticles are well dispersed through the material. The greater reinforcement of the nanoparticles is due to their size. Even though the weight

percentage may be the same, there is a much bigger number of nanoparticles for a given volume; also the distance between the particles is greatly reduced. Thus, the chain mobility is hampered to a higher degree in the case of Al nanoparticles.

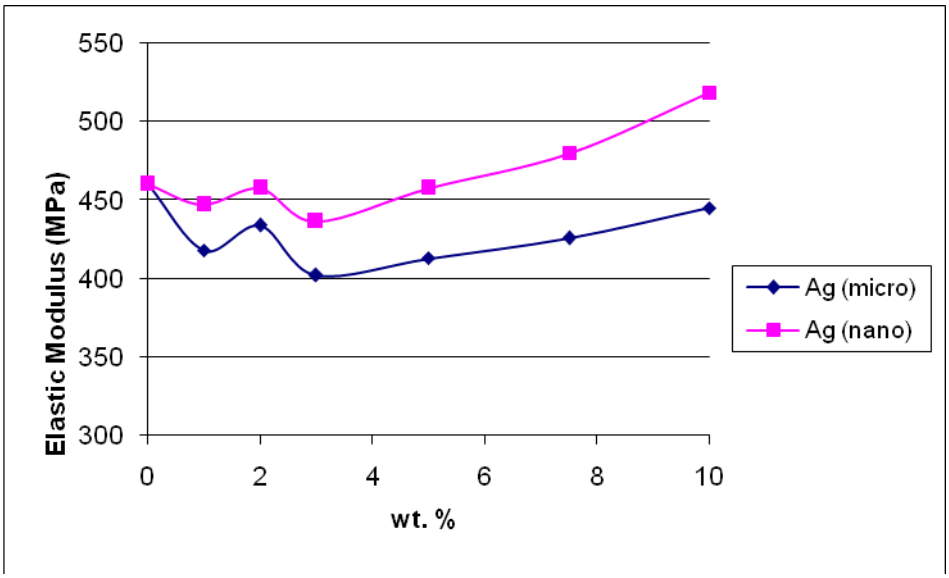

Figure 57. Elastic modulus of LDPE + Ag micro and nanocomposites.

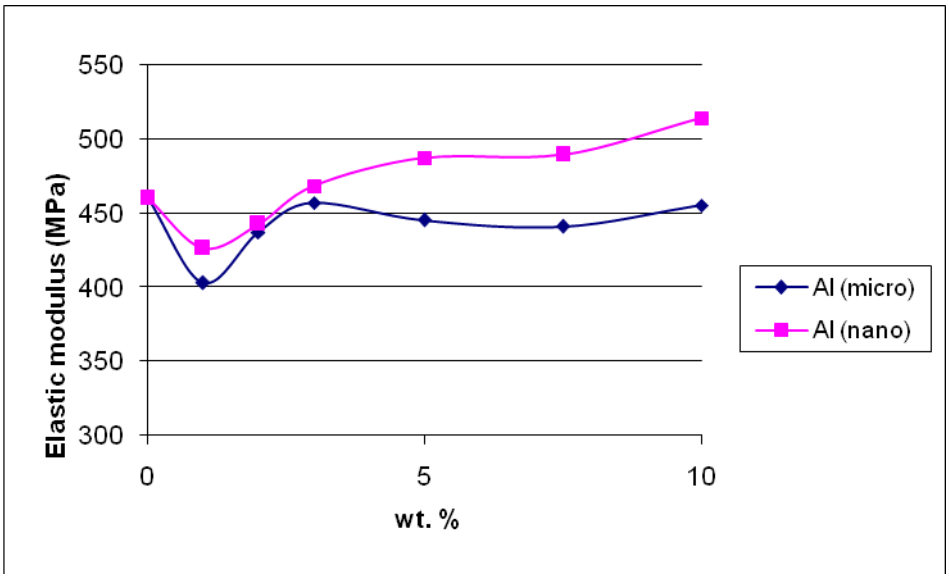

Figure 58. Elastic modulus of LDPE + Al micro and nanocomposites.

Figure 59 and 60 show the modulus for the Hytrel micro and nanocomposites for Ag and Al respectively. A reinforcement effect is observed at all concentrations for the two metals. The same explanation for LDPE composites apply for Hytrel composites. However, the

reinforcement is higher in Hytrel; this is due to the crosslinks present that in the presence of the filler hamper even more the chain mobility.

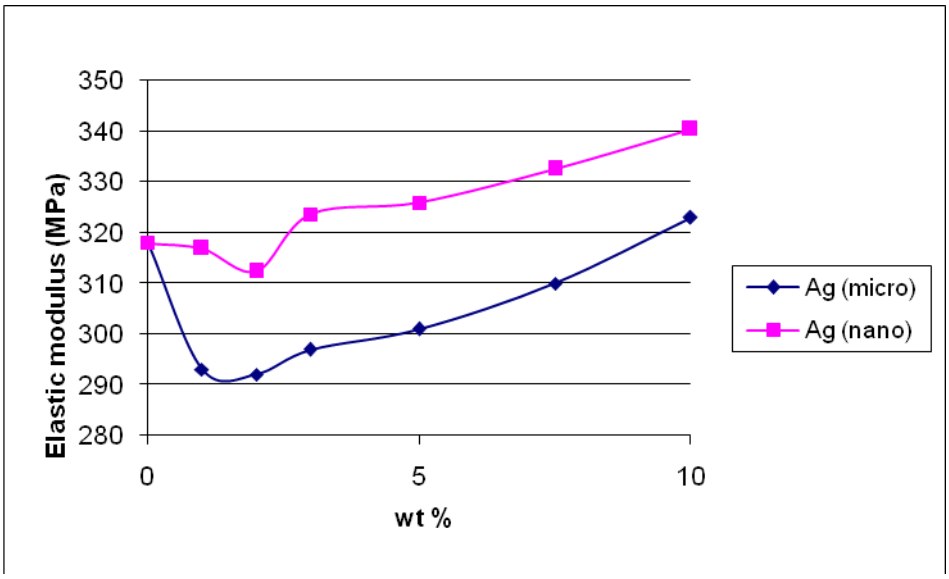

Figure 59. Elastic modulus of Hytrel + Ag micro and nanoparticles.

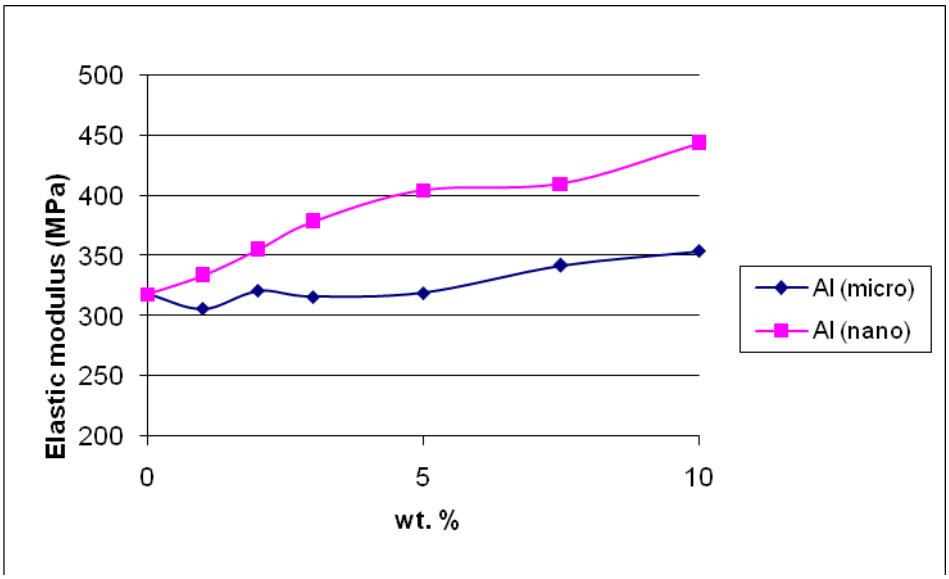

Figure 60. Elastic modulus of Hytrel + Al micro and nanocomposites.

Summarizing, in all cases (except for Hytrel + Al nanocomposites) there is an initial decrease of elastic modulus and it is attributed to a disruption of the polymer matrix by the filler. It is pertinent to note that in tension, polymers are deformed because the chains flow in a

viscoelastic way. The idea of disruption is illustrated in Figure 61. Figure 61a shows the composite without any applied tension, the particles are sitting inside the matrix. In Figure 61b, tension is applied; it can be seen that there is some space separating the metallic particles from the polymer matrix. This space acts in a similar way voids act in a foamed material, weakening the composites. At the same time, there is also the phenomenon of hampering the chain mobility. Since particles are sitting inside the material the polymeric chains have to go around the particles in order to move in the direction of the tension - this is a reinforcement effect. However, at lower concentrations the disruption phenomenon dominates the chain mobility reduction.

The disruption of the matrix can be mitigated by adding a primer. In this case, the space between phases under tension is smaller and the detrimental effect is less pronounced. The chain mobility hampering is also increased as the chemical interaction between the phases presents an extra resistance to flow.

As we increase the concentration or particles, the total sum of spaces created between the phases is the same but it is now distributed among a higher number of particles. However, the total hampering of chain mobility is higher now, since there are more particles that the chains have to go around in order to deform in the tension direction. This is the reason why, after a certain point (the minimum in elastic modulus) a reinforcement effect starts to appear. In some cases this reinforcement is enough to reach or to exceed the elastic modulus of the neat polymer, in other cases (especially for LDPE microcomposites) the reinforcement from the chain mobility is not enough - at least for the concentration range studied.

Finally, in the case of Hytrel + Al nanocomposites the disruption phenomenon is less pronounced than the hampering in chain mobility even at the lowest concentrations; this results in reinforcement even at the lowest concentration studied.

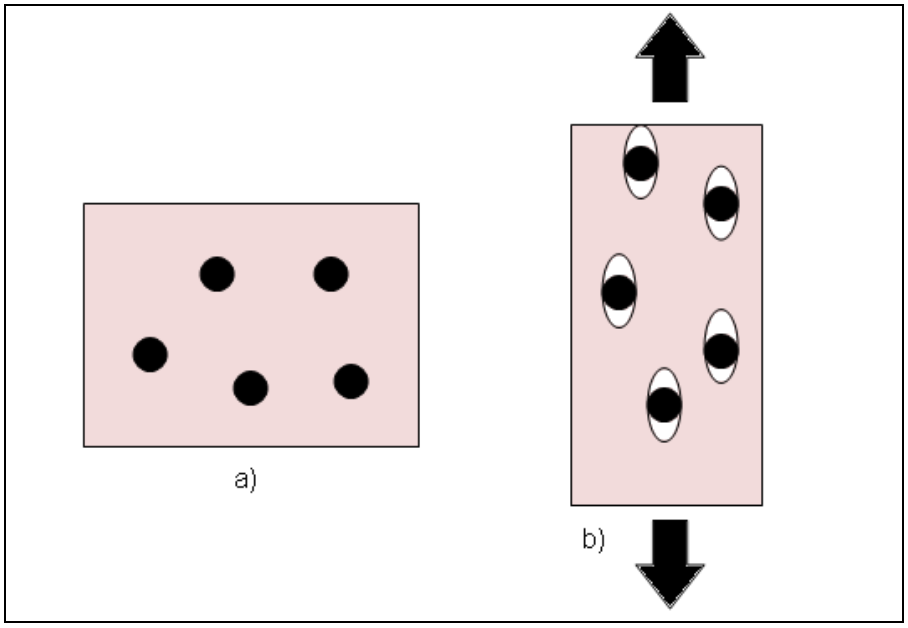

Figure 61. Tension in polymer composites.

4.3 Friction Determination

Two types of friction were determined for all the composites, namely dynamic and static friction following the ASTM D 1894-90 standard. At least 7 measures of friction were performed on each sample and the average of these values are reported. Typically, the error bars for the experiments range from ±0.003 to ±0.007. Thus, the differences observed in the results obtained can be effectively attributed to the different properties of the composites.

Even though the values of static and dynamic friction are not the same, the tendency of the composites is the same for the two types of friction. This is shown in Figure 62; here the dynamic and static friction for LDPE + Al micropowder are plotted as a function of particle wt %. This tendency is seen in all of the composites tested. Therefore, from now on only results of static friction are presented.

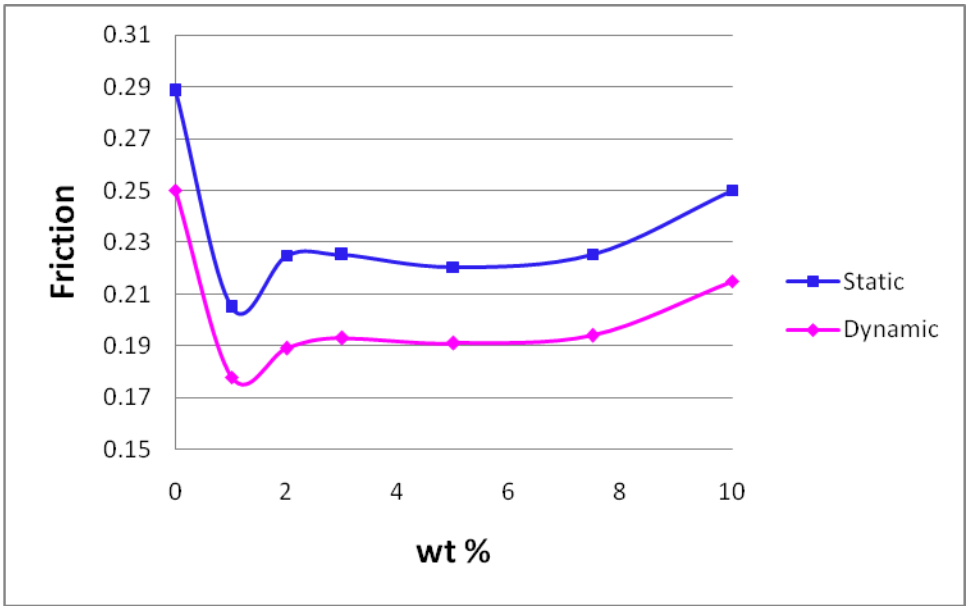

Figure 62. Dynamic and static friction for LDPE + Al microcomposites.

Microcomposites

Figure 63 shows the static friction of LDPE microcomposites against steel as the sliding surface. There is a common trend for all three metals: a reduction of friction to a minimum followed by an increase with concentration. The reduction can be explained by the phenomenon which involves the reduction in real contact area as more particles appear protruding from the surface and less polymer asperities are deformed. Then, after a minimum value, the metal - metal interactions with a higher friction than the metal – polymer ones and begin to dominate, causing a continuous increase in friction values.

Figure 64 shows the static friction of LDPE + primer microcomposites. With the addition of the primer, we still see the initial decrease seen in the case without primer. However, the following increase is less pronounced and for Ni a low friction value is kept constant even at high metal concentration. Apparently, the primer covering the metal particles acts similarly to a lubricating agent.

Figure 65 shows the static friction of Hytrel microcomposites against steel as the sliding surface. As in the case of LDPE there are the same two competitive phenomena: a reduction of contact area and metal - metal contact. In both cases, LDPE and Hytrel, the highest friction observed is the one of Ni; this was expected since according to the literature [70] the contact stainless steel - Ni has higher friction than the other two metals contacting stainless steel.

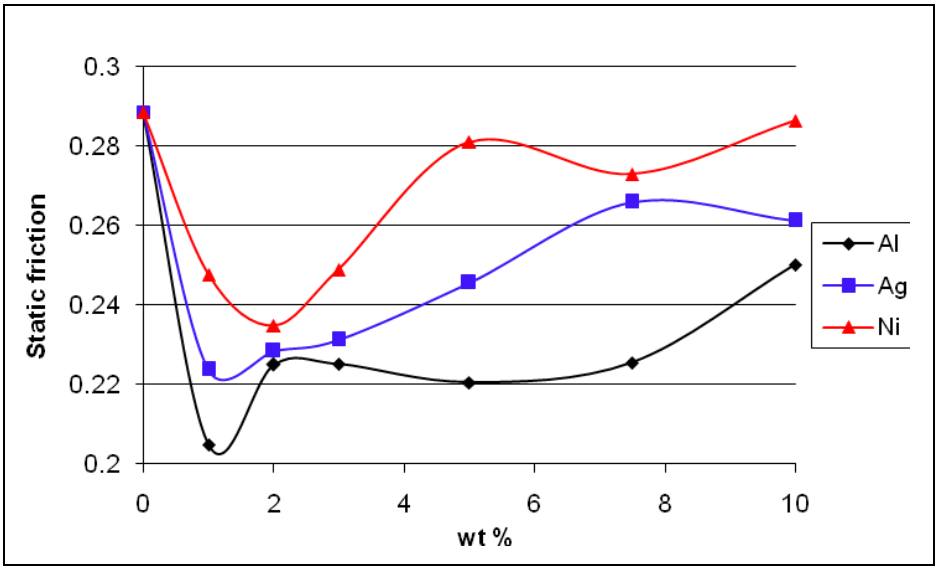

Figure 63. Static friction of LDPE microcomposites.

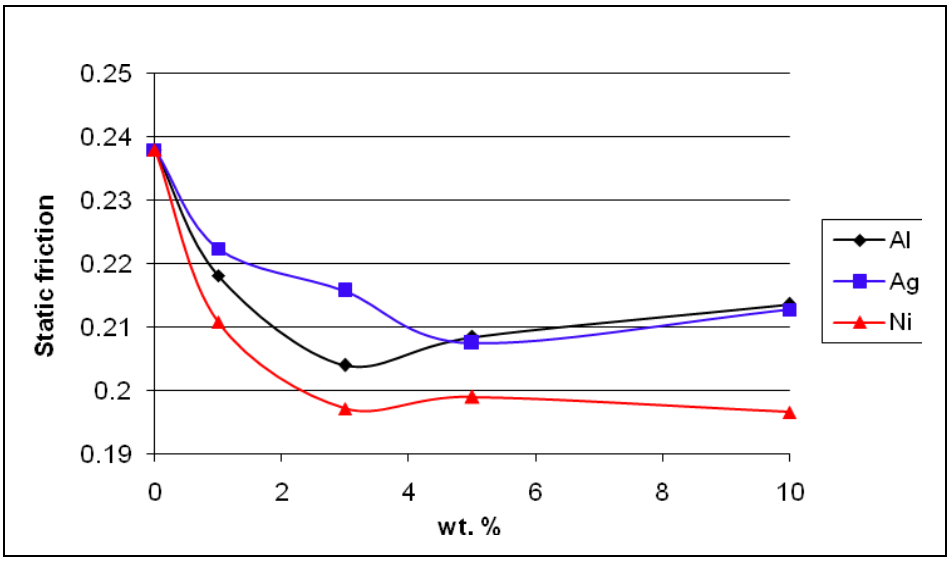

Figure 64. Static friction of LDPE + primer microcomposites.

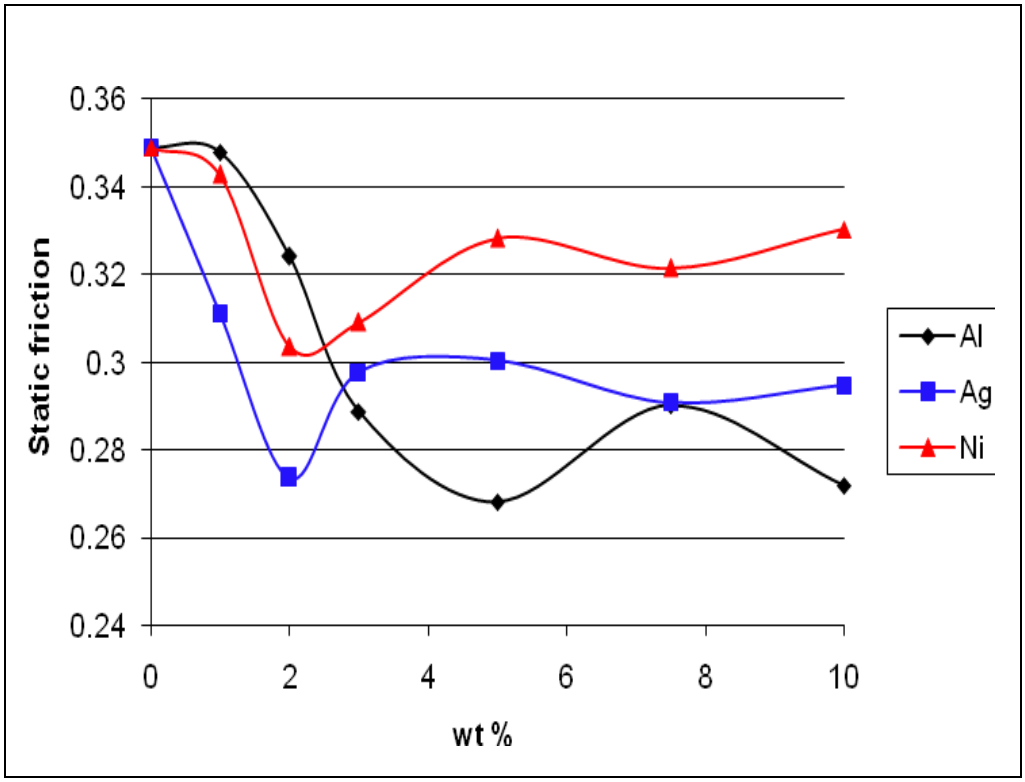

Figure 65. Static friction of Hytrel microcomposites.

Nanocomposites

Figure 66 shows the static friction of LDPE nanocomposites. The same tendency as in the microcomposites is seen. An initial reduction of the friction reaching a minimum value isfollowed by an increase as the concentration is higher. For Ag the same explanation applies, since big micrometric agglomerates are present. However, for Al nanoparticles there is a difference since the nanometric particles are smaller than the asperities of the surface (usually few microns for a non-polished surface). Probably, the particles act as a reinforcement of the asperities reducing the amount of deformation - thus diminishing the real contact area. Later, as the concentration increases, again the metal – metal contact starts dominating and the friction also increases. The case of Hytrel is similar (see Figure 67) and the explanation is the same as for the LDPE nanocomposites.

Microcomposites and Nanocomposites Comparison

Figures 68 and 69 show the static friction of micro and nanocomposites of LDPE + Al and Ag respectively. In the case of Al, the tendency is very similar. Although the friction mechanisms could differ, the final effect on friction is practically the same. In the case of Ag the microcomposites show *lower* friction than the nanocomposite. This can be explained, since the nanoparticles tend to form agglomerates that can be bigger than the ones formed with Ag micropowders - as discussed in section 4.1 in this Chapter.

Figures 70 and 71 show the static friction of micro and nanocomposites or Hytrel + Al and Ag respectively. For Al, the microcomposite has its minimum value at 5 wt % while the nanocomposite shows it at only 3 wt %. However, the lowest friction is reached by the microcomposite at 5 wt %. Again, in the case of Ag the microcomposites show a slightly lower friction than the nanocomposites. The same explanation for LDPE composites applies for Hytrel.

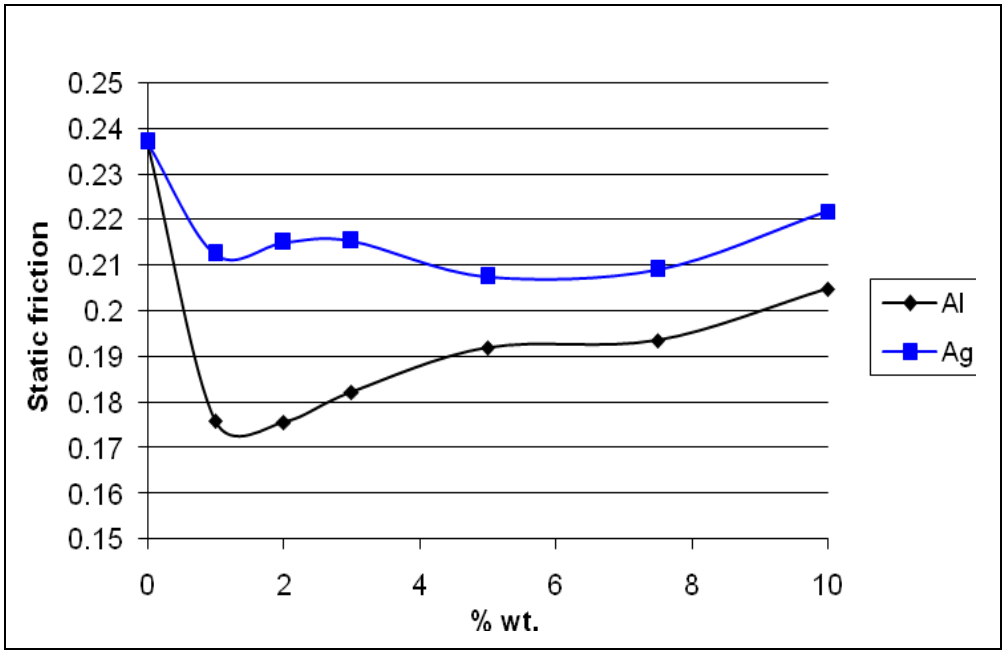

Figure 66. Static Friction of LDPE nanocomposites.

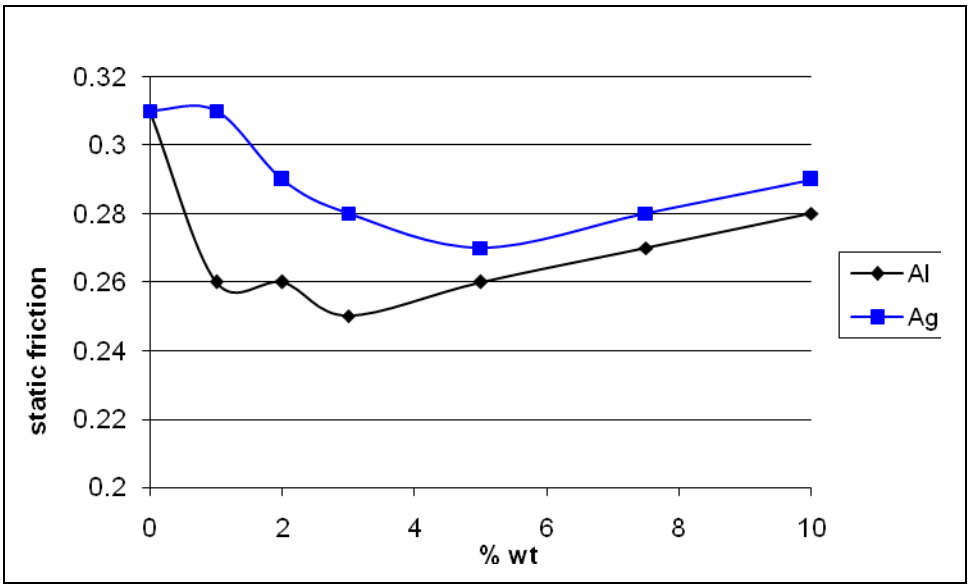

Figure 67. Static Friction of Hytrel nanocomposites.

Summarizing, in general there is a reduction of friction of the composites at low concentrations followed by an increase at higher concentrations. The minimum point will depend on the characteristics of both metallic particles (shape, size, type of metal) and the polymeric matrices (LDPE is branched while Hytrel is a block copolymer). As seen in Figure 4, the responsible for the interaction between the surfaces and hence the friction are the asperities on the material. When we have pure polymer, the asperities are deformed to a certain degree producing a certain value of real contact area. When metallic microparticles are incorporated into the matrix, some of them are sitting in the surface - as proven with SEM. These particles substitute some asperities in the composite surface. Since the metal is harder than the polymer, the contact area for a metallic asperity is smaller than the one for a polymer asperity (considering a similar asperity radius). Thus, there is an effective reduction of real contact area and a consequent reduction of friction occurs since the friction value is directly proportional to the real contact area.

However, as we increase the number of particles in the surface the friction starts increasing after a minimum value. Besides the reduction in contact area, there is other phenomenon

happening simultaneously: the contact between two metals has a higher friction than the one between polymer and metal due to the higher adhesion between two similar materials. There is a critical point (the minimum value of friction) where the higher friction between metals starts to dominate increasing the overall friction of the composite.

The case of polymer with a primer is somehow different. The primer does not affect the deformation of the metallic asperities. However, it covers the surface of the metal particle. The methoxysilane groups are attached to the metal surface and the other side of the primer molecule (organic) is in the outside. This organic part of the primer molecule is the one in contact with the steel surface. Apparently, this layer of primer molecule covering the metal particle act as an apparent lubricant, since we observe a lower friction than the one for polymer without primer at the highest concentrations studied.

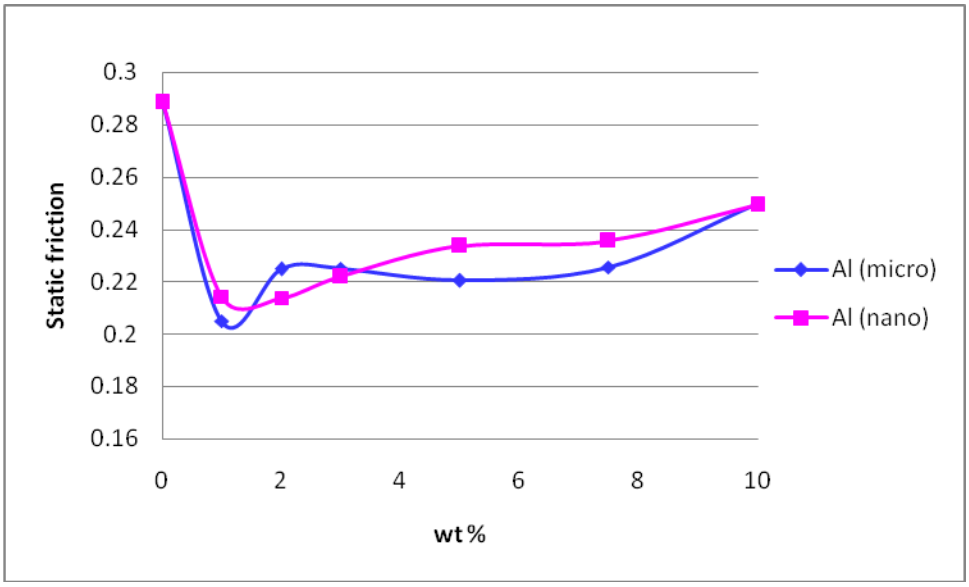

Figure 68. Static friction of LDPE + Al micro and nanocomposites.

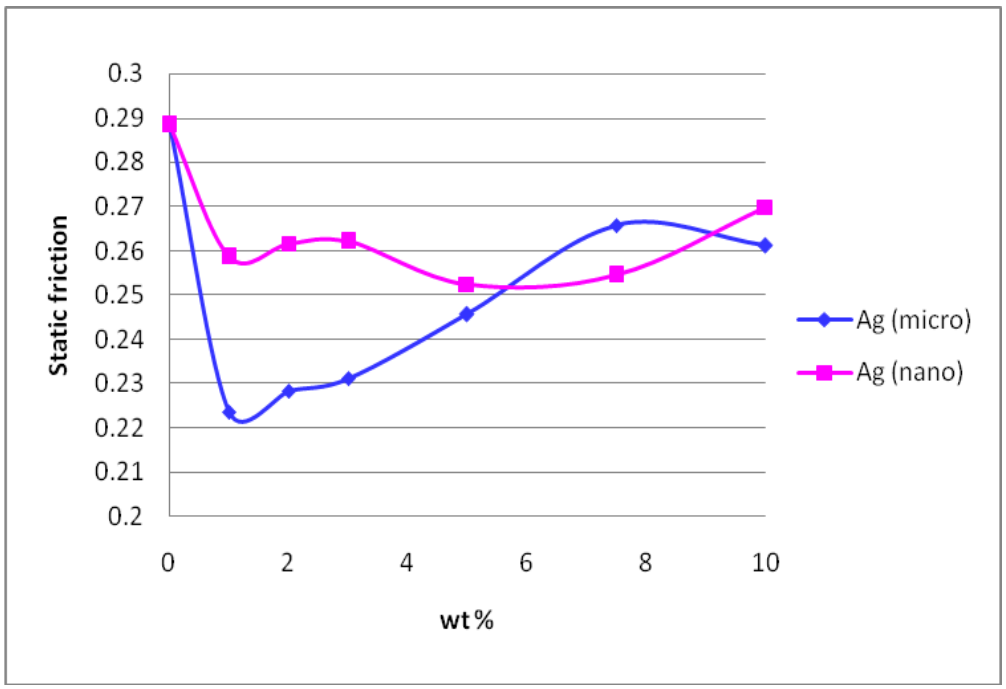

Figure 69. Static friction of LDPE + Ag micro and nanocomposites.

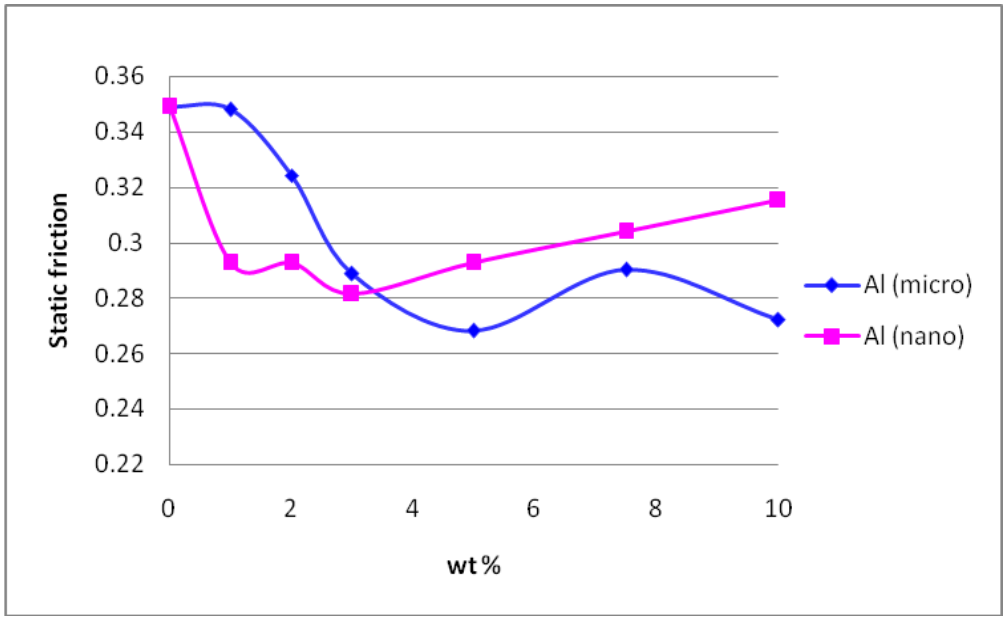

Figure 70. Static friction for Hytrel + Al micro and nanocomposites.

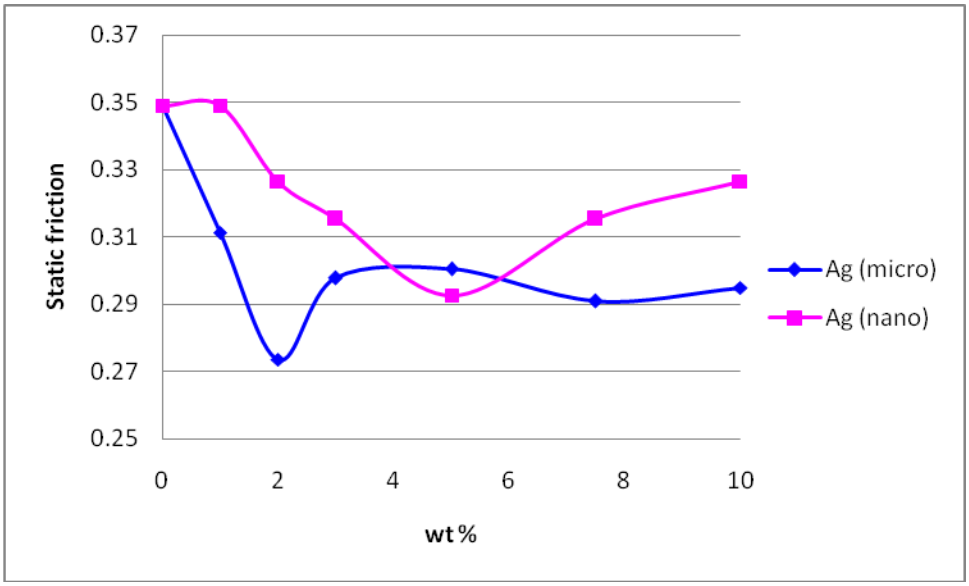

Figure 71. Static friction for Hytrel + Ag micro and nanocomposites.

4.4 Scratch Testing

In scratch testing the sliding distance of the indenter was 5 mm for all composites. The values obtained for penetration and residual depths are an average value from the whole length of the groove. There is an inherent variation of dephts over the length of the scratch. Typically, the error bars on residual depth are around ±3 micrometers while for the penetration depth they are around ±9 micrometers. Thus, the differences observed in the results obtained can be effectively attributed to the different properties of the composites.

Figure 72 show the penetration depth of Hytrel + Ag microcomposites. Although the specimens were tested at different normal loads of the indenter the behavior is very similar for all forces used. This is true for all the materials tested. Only one normal force can be used in order to compare the scratch resistance of the different composites produced. Therefore, from now on, only the curve for 20 N is presented in order to discuss the behavior of the composites.

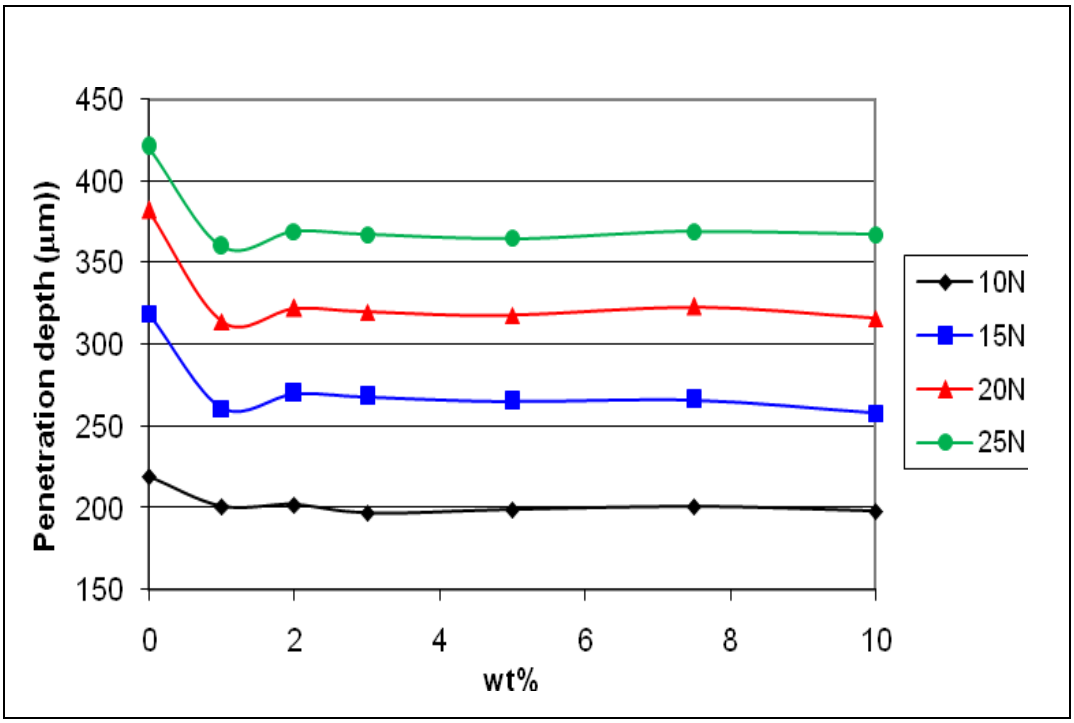

Figure 72. Penetration depth of the Hytrel + Ag microcomposites at several normal loads.

The same way, the residual depth (depth after healing) has been also determined for all specimens. Figure 73 shows the penetration depth R_p and residual depth R_h of LDPE + Ag microcomposites at 10 N of normal load. It is clear that the tendency of Rp and Rh against composition is very similar. This is truo for the other materials too. Furthermore, the difference of the minimum and the maximum value of R_p is several tens of micrometers while for R_h is only few micrometers. The error bars of penetration depth are also a smaller fraction than the total value as discussed above. Thus from this point forward only the penetration depth will be used in order to compare the effect in composition of the scratch resistance of the materials tested.

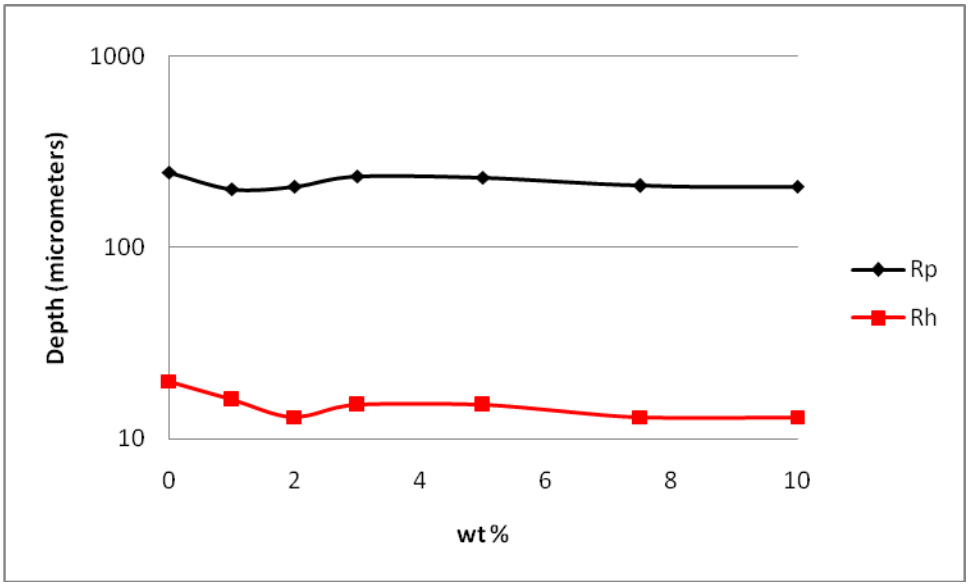

Figure 73. Penetration depth R_p and residual depth R_h of LDPE + Ag microcomposites at 10 N.

Microcomposites

Figure 74 shows the penetration depth for LDPE microcomposites at a normal load of 20 N. The three microcomposites show the same tendency: there is an initial reduction in penetration depth (higher resistance to indenter penetration) reaching a minimum followed by a continuous increase at higher concentrations. The minimum is reached at different concentration for each microcomposite; this can be attributed to the different size of the metallic particles; also in the case of Ag agglomerates formed.

Initially, the metallic particles reinforce the polymeric matrix because they present an extra resistance to the indenter. Therefore, the deformation of the material is lower. This continues to occur as more metallic particles are added to the LDPE until the minimum value is reached. After this value the incorporation of more metallic filler start to weaken the matrix material; the distances between filler particles decrease and the structure of the polymer begins to be disrupted (more of this idea is presented later in this section). However, only at the highest

concentration studied the penetration depth is as high as the one for the neat polymer; below that concentration there is an effective reinforcement effect.

Figure 75 shows the penetration depth for Hytrel microcomposites at 20 N of normal load. As in the case of LDPE there is a reduction in penetration depth as the metal concentration is increased. However, after a minimum value is reached, the penetration depth remains almost constant as the concentration is higher. The initial decrease in penetration depth can be explained the same way as in the LDPE case. After the minimum point, a weakening of the polymer would be expected as in LDPE microcomposites. However, Hytrel as a thermoplastic elastomer is partially crosslinked. The crosslinks prevent to some extent weakening of the polymer when metallic particles get closer together as the concentration is increased. Thus, there are two competitive phenomena: in one hand a weakening as the number of metal particles increases and in the other hand the effect of the crosslinks keeping together the polymer chains.

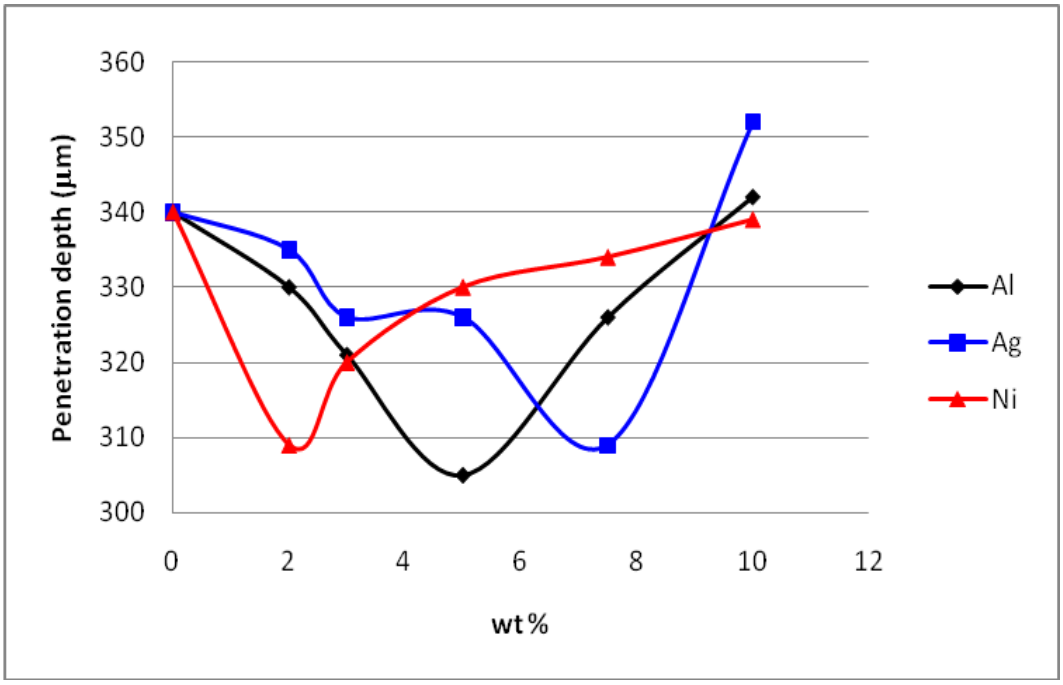

Figure 74. Penetration depth of LDPE microcomposites.

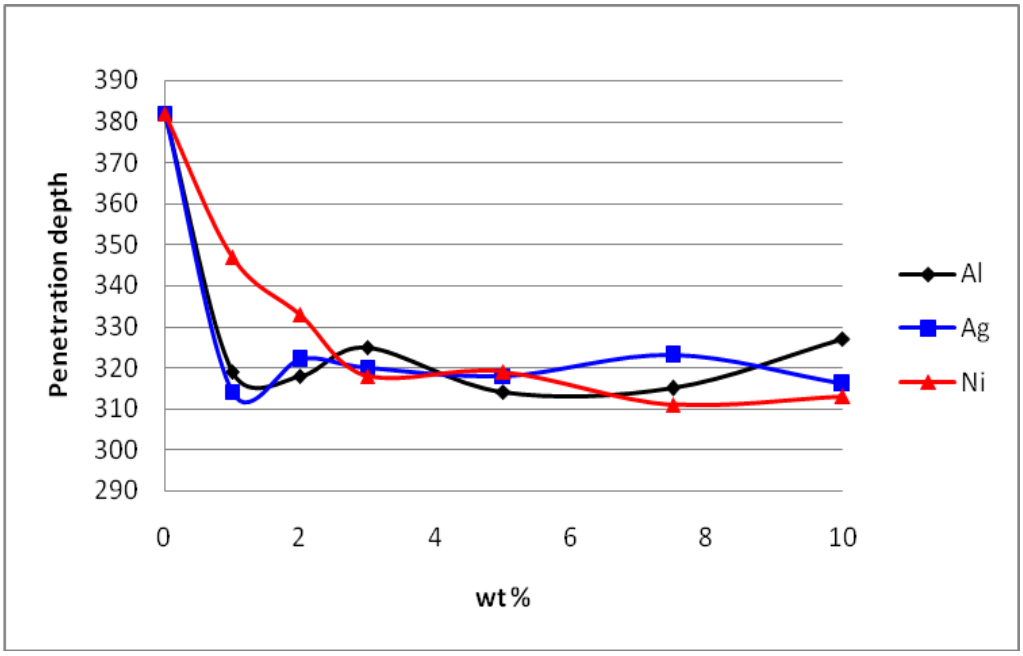

Figure 75. Penetration depth of Hytrel microcomposites.

Nanocomposites

Figure 76 shows the penetration depth of LDPE nanocomposites at 20 N of normal load. For Al there is a sharp decrease in penetration depth at low concentrations followed by a less pronounced continuous decrease as the concentration increases. The initial sharp decrease can be explained the same way as in the microcomposites. The less pronounced continuous reinforcement at higher concentrations occurs because of the much smaller size of the Al particles. At this scale, more particles produce a stronger reinforcement against penetration – in contrast to the microcomposites where a greater number of bigger particles weakens the polymeric matrix. This idea is reinforced by observing the behavior of LDPE + Ag nanocomposites; since Ag nanoparticles tend to form agglomerates, their behavior is closer to that of microcomposites where there is a minimum followed by a continuous increase in penetration depth. However, even the highest concentration studied the LDPE + Ag

nanocomposites still show a significantly lower penetration depth than the one of the neat polymer.

Figure 77 shows the penetration depth of Hytrel nanocomposites at 20 N of normal load. The case of Al is very similar as in LDPE + Al nanocomposites: there is a continuous reinforcement with concentration and the explanation is the same. On the other hand, the case of Ag + Hytrel nanocomposites is a more complex one. There is an initial decrease reaching a minimum value of penetration depth, followed by an increase reaching a maximum and finally there is a continuous decrease at the higher concentrations. The increase in penetration depth after the minimum can be explained because of the agglomerates present with Ag nanoparticles. After the maximum value at around 5 wt % the reinforcement effect can be attributed to the crosslinks present in Hytrel in a similar way they support the polymer matrix in the Hytrel microcomposites.

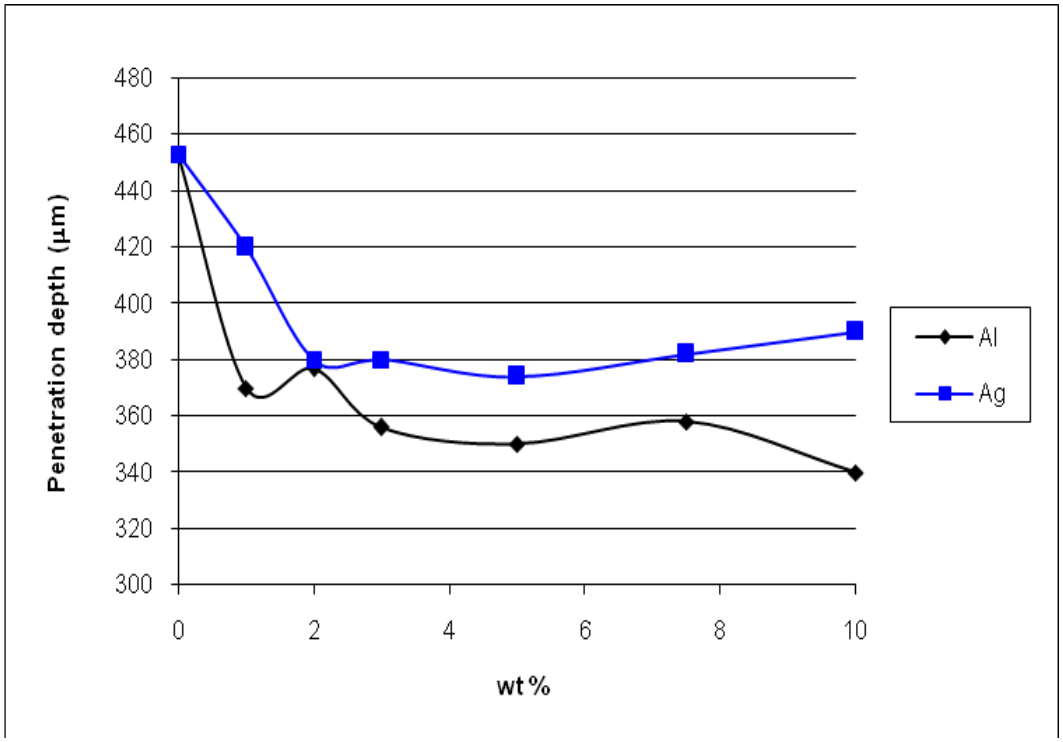

Figure 76. Penetration depth of LDPE nanocomposites at 20 N.

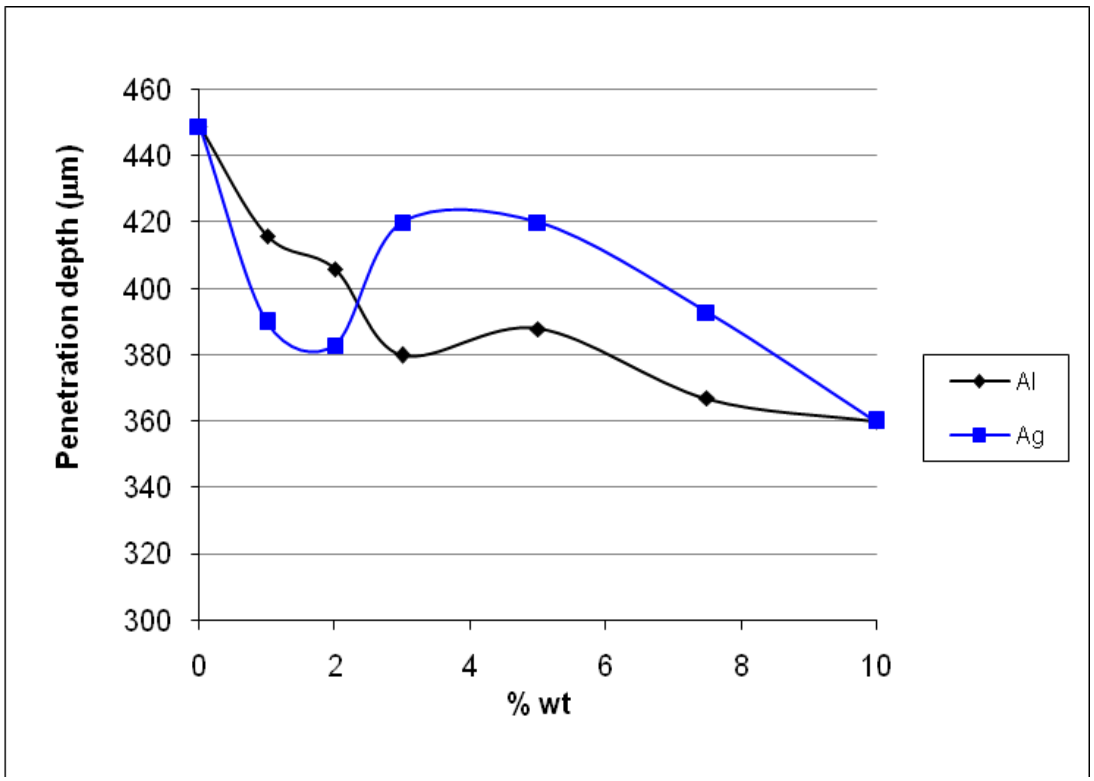

Figure 77. Penetration depth of Hytrel nanocomposites at 20 N.

Microcomposites and Nanocomposites Comparison

Figures 78 and 79 show the penetration depth of Al + LDPE and Ag + LDPE micro and nanocomposites at 20 N of load force, respectively. In both cases the nanoparticles present a stronger reinforcement than the microparticles. However, the difference between the penetration depth of micrometric Al and nanometric Al is larger than for Ag micro and nanoparticles. This is due to the good dispersion of nanometric Al powder while – as already noted - nanometric Ag particles tend to form agglomerates showing a similar trend as the micrometric Ag filler.

Figures 80 and 81 show the penetration depth of Al + Hytrel and Ag + Hytrel micro and nanocomposites at 20 N of load force respectively. In contrast to LDPE, the degree of reinforcement for nano and microparticles is comparable and even better for the latter ones. This means that for Hytrel the particle size is not as important as for LDPE. Hytrel is a block

copolymer with rigid and elastic regions (as discussed in Chapter 3.) as well as a certain degree of crosslinking. The reinforcement is due to the interaction between the particles and the crosslinks as well as the elastic and rigid parts of the polymeric chains – apparently affected little by the particle size.

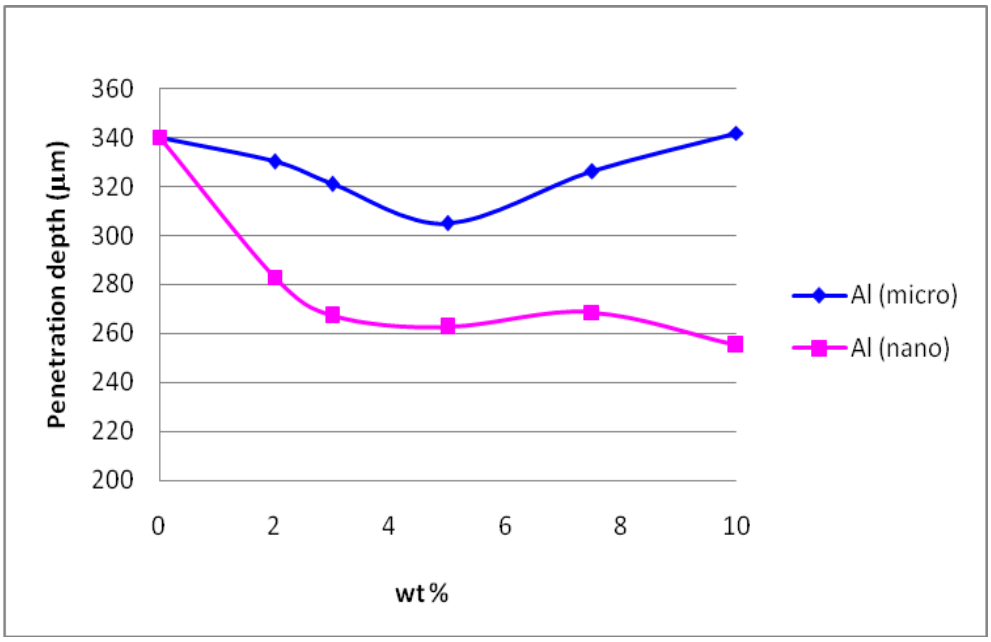

Figure 78. Penetration depth for LDPE + Al micro and nanocomposites.

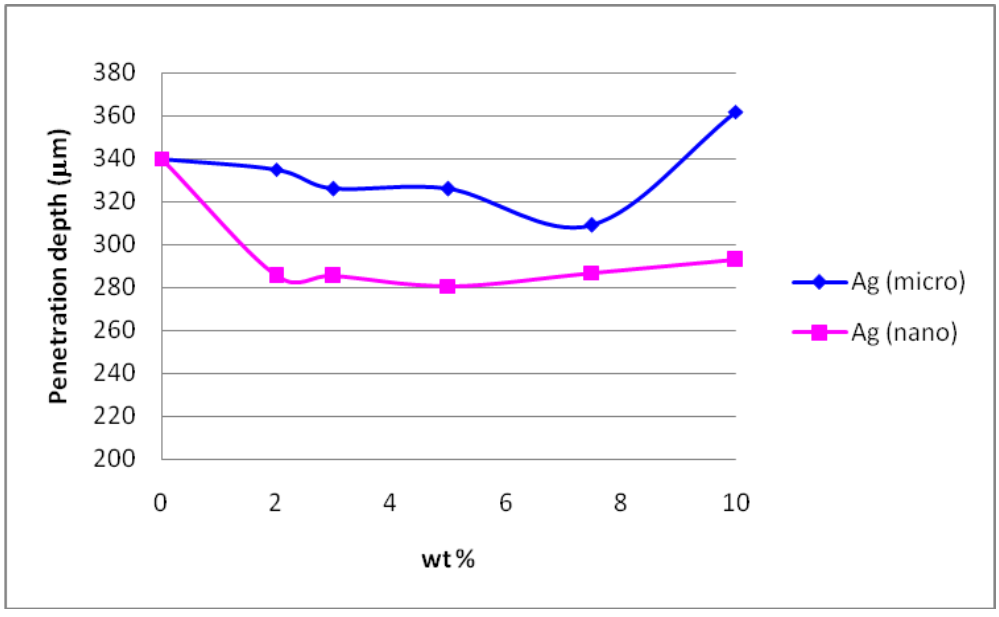

Figure 79. Penetration depth for LDPE + Ag micro and nanocomposites.

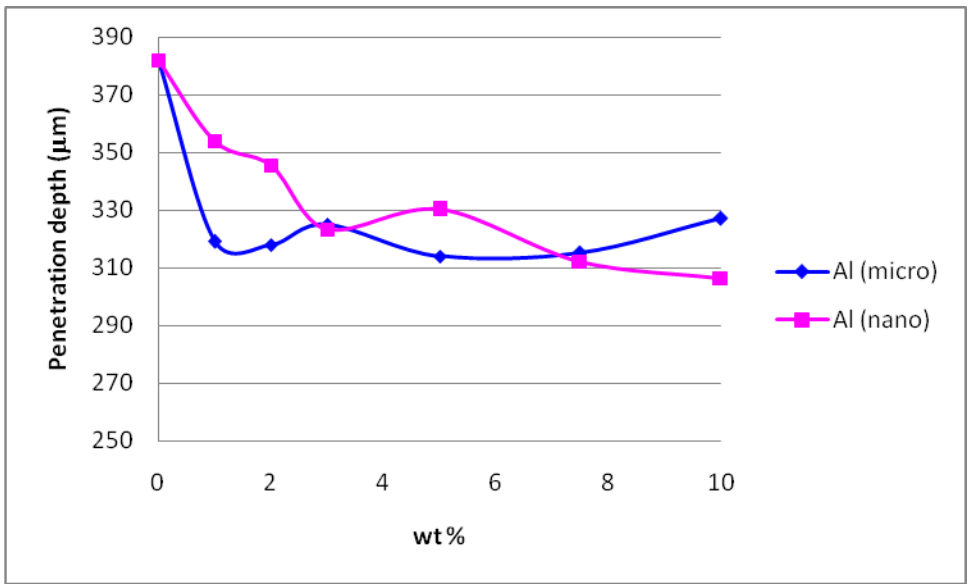

Figure 80. Penetration depth for Hytrel + Al micro and nanocomposites.

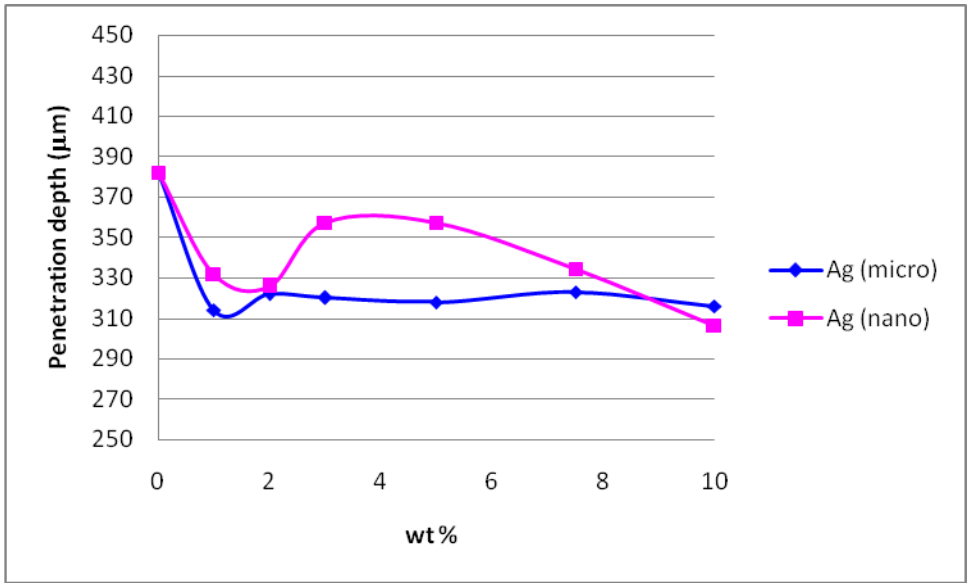

Figure 81. Penetration depth for Hytrel + Ag micro and nanocomposites.

Summarizing, in the scratch tests performed, a conical indenter is moved over the composite specimens at a certain constant load. The center of the tip of the indenter is compressing the material parallel to the direction of the indentation. The sides of the indenter move the material aside of the indenter creating a groove. When the metallic particles are incorporated there is an extra resistance to the compressive forces since the metal particles are

harder than the polymer matrix. This result in reinforcement against scratching and it is represented in Figure 82.

When we increase the concentration of the particles there is weakening of cohesion in the polymeric matrix. In other words, there is a disruption by filler particles of the homogeneous structure of the matrix. Thus, we have two effects acting in opposing directions: reinforcement by metal particles and structure perturbation which weaken the material.

The perturbation phenomena is much more pronounced for the LDPE composites. Hytrel having crosslinks and rigid regions inside the structure can withstand more the disrupting effect while branched chains in LDPE can be more easily separated.

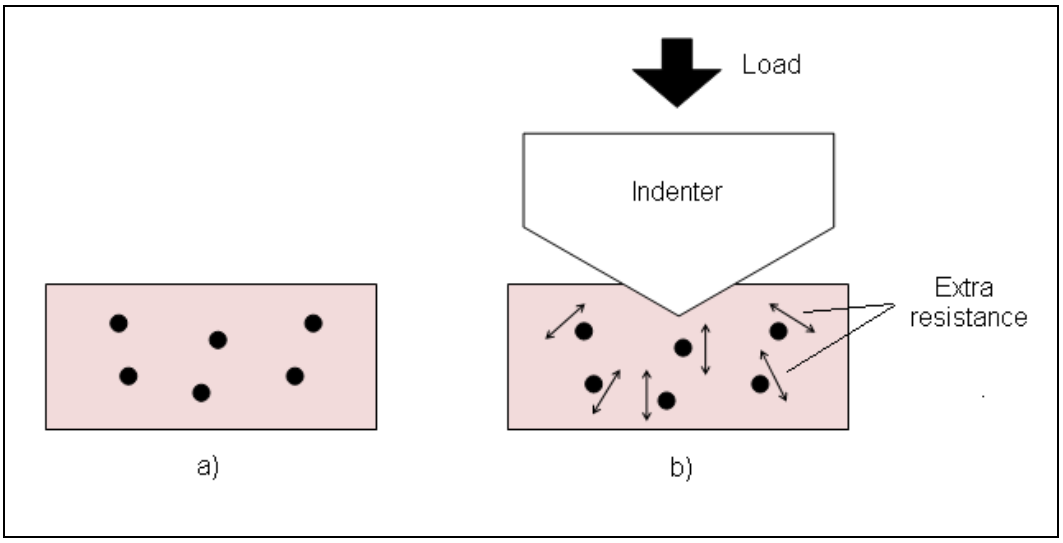

Figure 82. Scratching of polymer composites.

4.5 Pin-On-Disc Wear Determination and Wear Mechanisms

Wear is a phenomenon quite complex that depends on the variables of the system being studied. Current understanding of wear mechanisms in polymers is largely based on work by two groups. The first was founded by Bely [71] and is continued by Mishkyn, Petrokovets and

coworkers in Homel, Belarus [72-74]. The second is the group of Bricoe [75-78]. On this basis as well as on the basis of the present results one can make a list of wear mechanisms.

- *Adhesive wear*. It results from the shear of the friction junctions. This wear process evolves in formation of adhesion junction, its growth and fracture. A distinguishing feature of this wear is that transfer of material from one surface to another occurs due to localized bonding between the contacting solid surfaces.
- *Abrasive wear*. The key aspect of abrasive wear relates to cutting of polughing of the surface by harder particles or asperities. This cutting points may either be embedded in the counterface (two body abrasion), or lose within the contact zone (three body abrasion).
- *Fatigue wear*. Fatigue is known to be a change in the material state due to repeated (cyclic) stressing which results in provressive fracture. Its characteristic feature Is accumulation of irreversible changes , which give rise to generation and development of cracks.

In order to study wear and its mechanisms it is important to have as many variables controlled as possible. This section results on wear of the composites obtained by using a Pin-on-disc tribometer. The ASTM G 99 standard test was applied. Although this standard procedure was first intended to be used for metals, it is possible to use it for plastics as a good approximation [79-81]. SEM pictures of the wear tracks were taken in order to measure the track thickness and to determine a dominant wear mechanism. In order to calculate the wear and wear constants the following equation taken from the ASTM G 99 standard was used:

$$v = 2\pi R[r^2 \sin^{-1}(d/2r) - (d/4)(4(r^2 - d^2)^{1/2}] \quad (4.1)$$

here: v = wear volume loss

R = wear track radius

d = wear track width

r = pin end radius

Eq. 4.2 contains the wear constant K which represents the volume loss v divided by the normal load W and the sliding distance l.

$$K = \frac{v}{lW} \tag{4.2}$$

Since the constant K is normalized with respect to load and wear distance the results presented below to this constant rather than to the volume loss.

According to the standard, fifty different values of width of the wear track were measured in two different sections of the wear track (two different images) and an average of the calculated K values is reported. The standard deviation for the measurements of the width of the wear track is usually about 0.01 mm. This difference leads to a range of the K values of around ± 0.00015 mm^3/Nm. Thus, the differences observed in the results obtained can be effectively attributed to the different properties of the composites.

In the case of the scratch testing discussed in Section 4.4 the groove left by the indenter is caused by deformation of the material. In the case of the pin-on-disc testing there is a detachment and an effective loss of material. This is due to the different wear regime at similar normal loads but significantly higher linear velocity of the pin. The type of wear mechanisms present in different samples can be inferred observing the wear track left by the indenter as well as the wear debris particles detached from the material.

Microcomposites

Figure 83a shows the wear track of LDPE at a normal load of 7 N. It is clear by observing the edges of the groove that deformation is the main wear mechanism. However, by examining the groove at a higher magnification (see Figure 83b) it is clear that also delamination by adhesive wear occurs to some extent.

Figure 84 shows the wear track of LDPE + 10 wt % Al microcomposite at a normal load of 7 N. Figure 84a shows the inside of the wear track; it is clear that the parallel grooves are formed by abrasive wear. Figure 84b shows the wear debris particles of the microcomposite. The wear particles are also formed by adhesive wear delamination similarly to that happening in neat LDPE.

Figure 85 shows the wear track of LDPE + 10 wt % Ag microcomposite at a normal load of 7 N. In this case the dominant mechanism is adhesive wear as seen in Figure 85a. Consequently, the wear debris particles are formed by adhesive delamination as seen in Figure 85b.

Figure 86 shows the wear track of LDPE + 10 wt % Ni microcomposite at a normal load of 7 N. As seen in Figure 86a. The main mechanism is adhesive wear as the parallel grooves suggest. However the wear debris formation is different than in the previous cases; the wear debris stays inside the sear track and starts to roll-up to forms rolls of materials. As shown in Figure 86b these rolls can be several millimeters long.

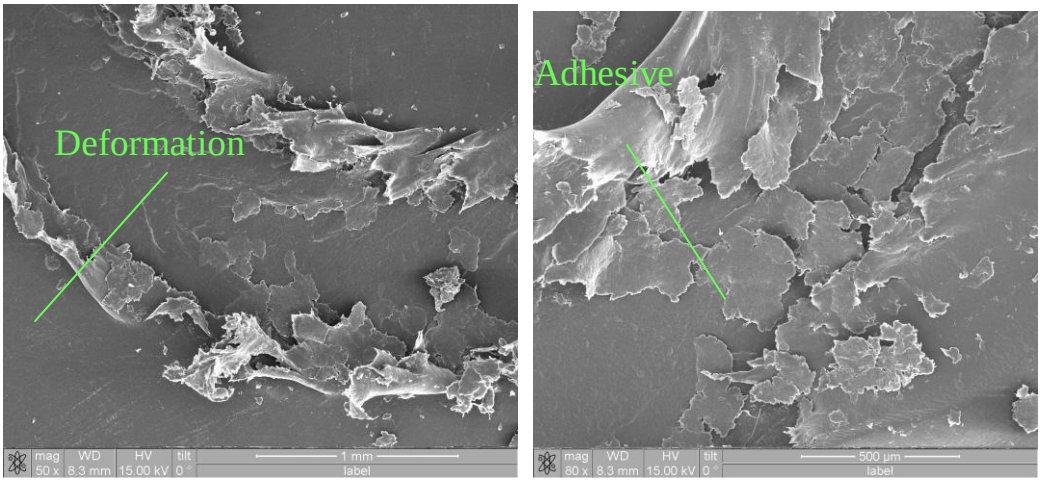

a) b)

Figure 83. a) LDPE wear track against a Si_3N_4 pin. b) The same as a) at a higher magnification at a different point of the wear track.

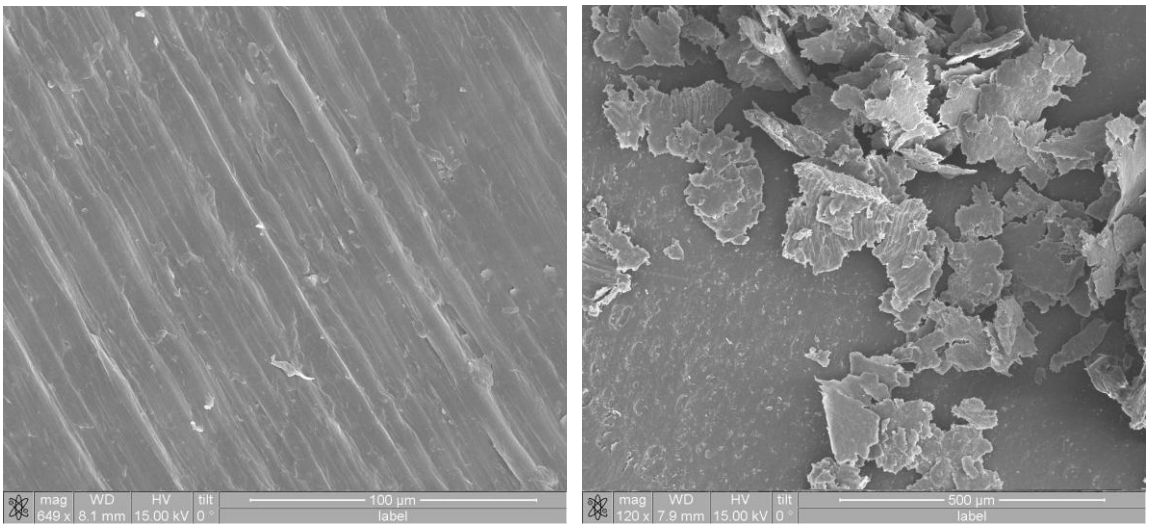

a) b)

Figure 84. a) Wear track of LDPE + 10 wt % Al microcomposite. b) Wear debris particles of the same material.

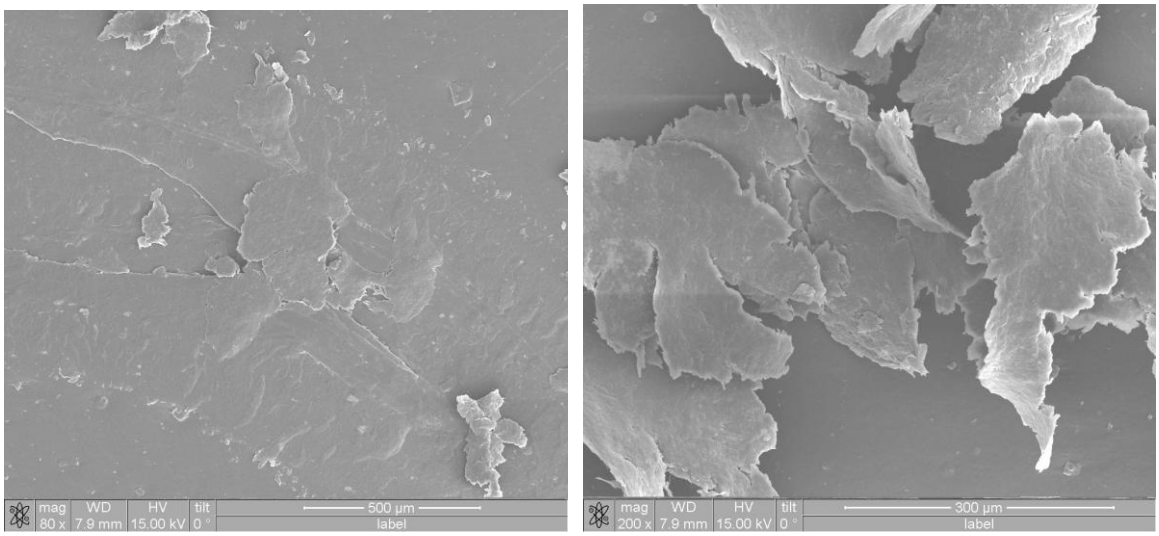

a) b)

Figure 85. a) Wear track of LDPE + 10 wt % Ag microcomposite. b) Wear debris particles of the same material.

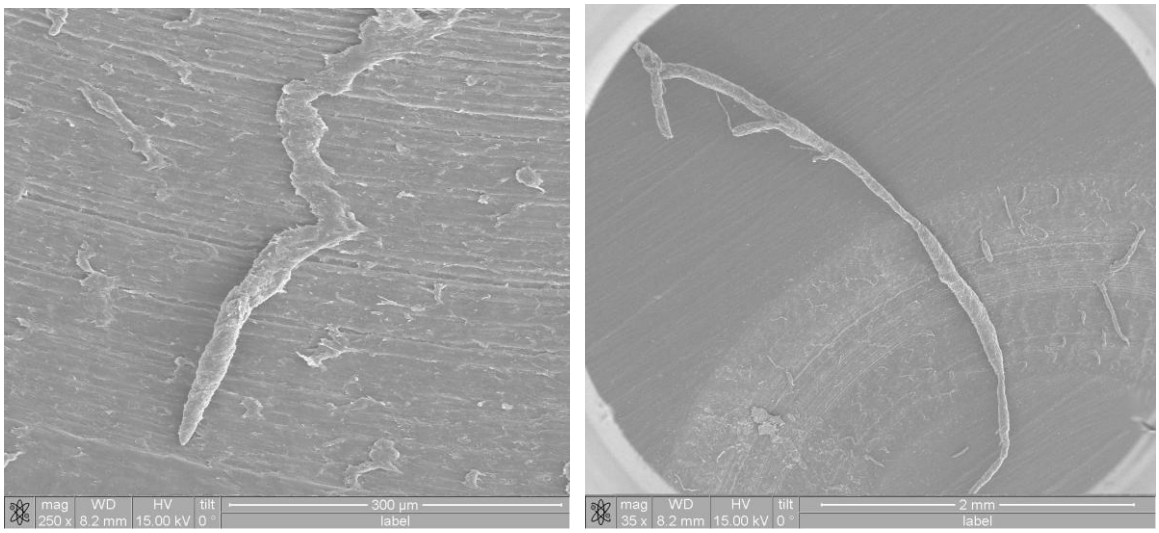

a) b)

Figure 86. a) Wear track of LDPE + 10 wt % Ni microcomposite. b) Wear debris particles of the same material.

Figure 87 shows the wear track of Hytrel at a normal load of 7 N. It is clear that the main wear mechanism is deformation; in contrast to LDPE, no adhesive delamination is observed.

Figure 88 shows the track of Hytrel + 10 wt % Al microcomposite at a normal load of 7 N. It can be seen from Figure 88a that the mechanism is very similar to that of the LDPE + 10 wt % Ni microcomposite. There is formation of grooves parallel to the wear direction due to abrasive wear and the debris forms rolls inside the track as seen in Figure 88b.

Figure 89 shows the track of Hytrel + 10 wt % Ag microcomposite at a normal load of 7 N. From Figure 89a it is clear that adhesive wear is here the dominant mechanism, in contrast to the behavior of Hytrel + 10 wt % Al microcomposite and neat Hytrel. However, the wear debris particles behave in a similar way as in the previous cases, forming rolls of material vusible in Figure 89b.

Figure 90 shows the track of Hytrel + 10 wt % Ni microcomposite at a normal load of 7 N. In this case there is a combination of wear mechanisms that can be seen in Figure 90a; there

is abrasive wear although the parallel grooves are not as apparent as in the case of Hytrel + 10 wt % Al microcomposite. On the other hand there is adhesive wear although not in the same extent as to the case of Hytrel + 10 wt % Ag microcomposite. The wear particles still behave the same way, rolling up as shown in Figure 90b.

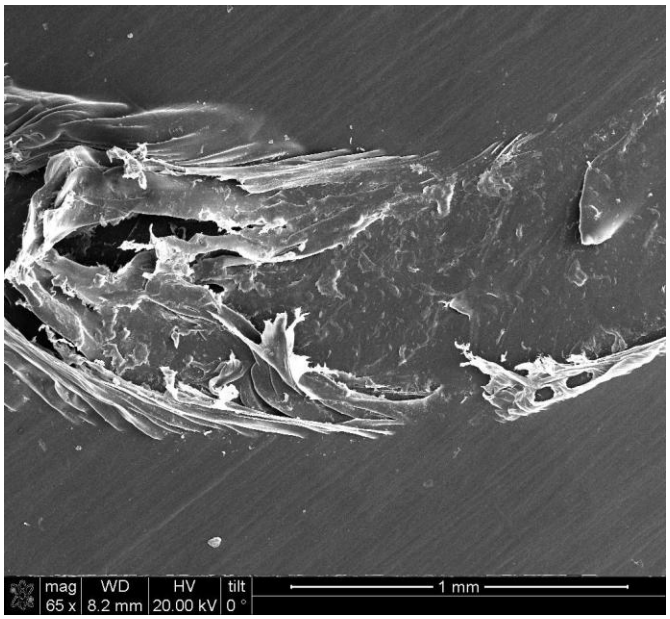

Figure 87. Hytrel wear track against a Si_3N_4 pin at a load of 7 N.

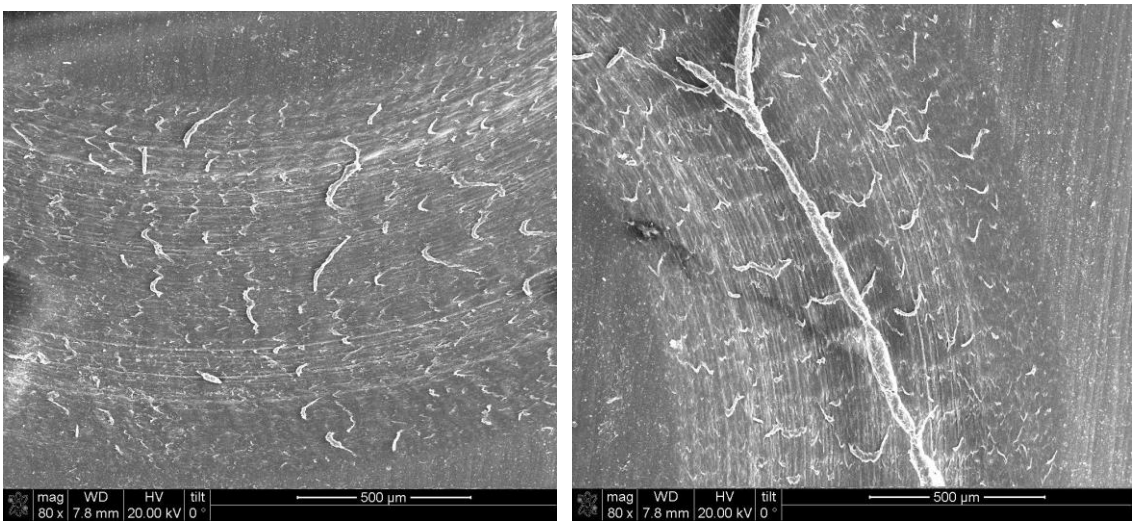

a) b)

Figure 88. a) Wear track of Hytrel + 10 wt % Al microcomposite. b) Wear debris particle of the same material.

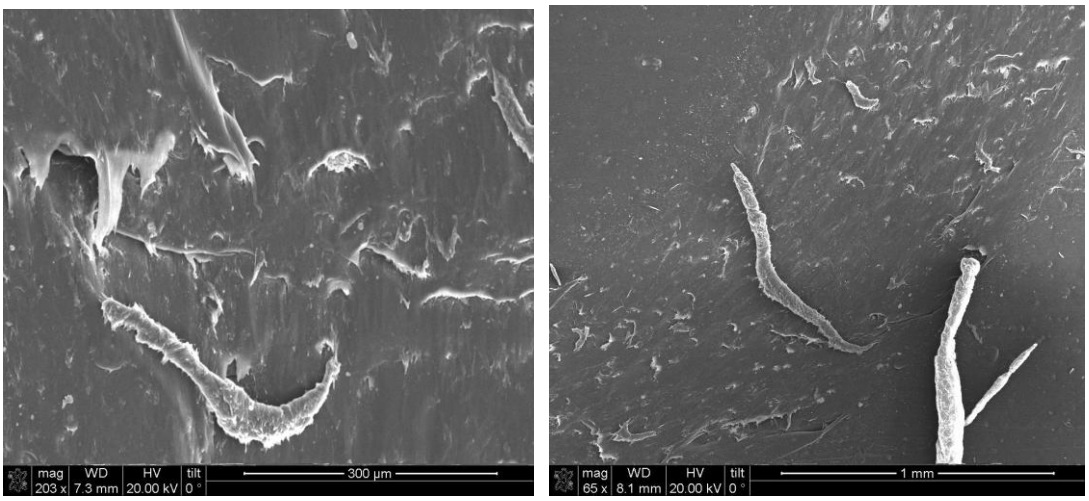

a) b)

Figure 89. a) Wear track of Hytrel + 10 wt % Ag microcomposite. b) Wear debris particles of the same material.

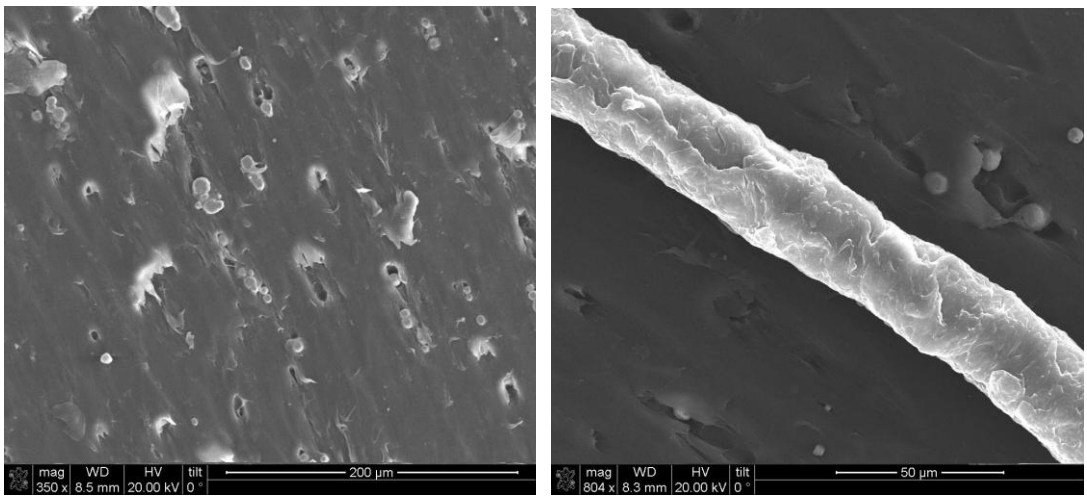

a) b)

Figure 90. a) Wear track of Hytrel + 10 wt % Ni microcomposite. b) Wear debris particle of the same material.

Using Eqs. (4.1) and (4.2), the wear constant *K* was calculated for all the microcomposites. Figure 91 shows the wear constant of LDPE microcomposites at a load of 7 N. It is clear that the lowest *K* is achieved when Al particles are present. Even though the

abrasive wear is more detrimental than adhesion in many cases, in this case is the opposite. A probable reason is that the detached spherical aluminum particles from the composite surface actually roll between the metal and the polymer acting as bearings and thus, the three body abrasion shows reinforcement for wear resistance. By adding Ni particles, the mass loss is the highest. Once the debris rolls start forming, the material is removed continuously and the rate of removal is higher than the pure material by deformation. For Ag the wear loss is similar to that for neat LDPE. Despite the different main wear mechanisms for Ag microcomposites (adhesion) and LDPE (deformation) the rate of material removal is comparable.

Figure 92 shows the wear constant of Hytrel microcomposites at 7 N. It is clear that any kind of metallic particle will increase the wear loss at the conditions tested. In contrast to the LDPE microcomposites there is a negative effect in wear loss for Hytrel microcomposites. The reason is that in all three cases there is formation of rolls as wear debris. We have seen with LDPE + Ni microcomposites that the amount of material removed during a certain time is higher when these rolls are formed than where only deformation of the polymer occurs.

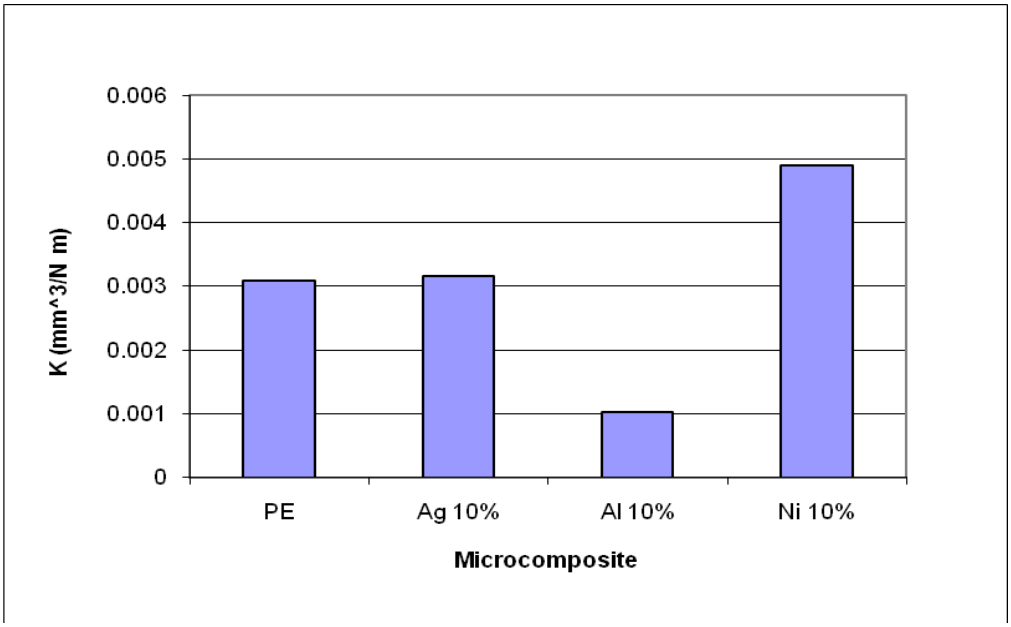

Figure 91. Wear constant *K* for LDPE and LDPE microcomposites at 7 N load.

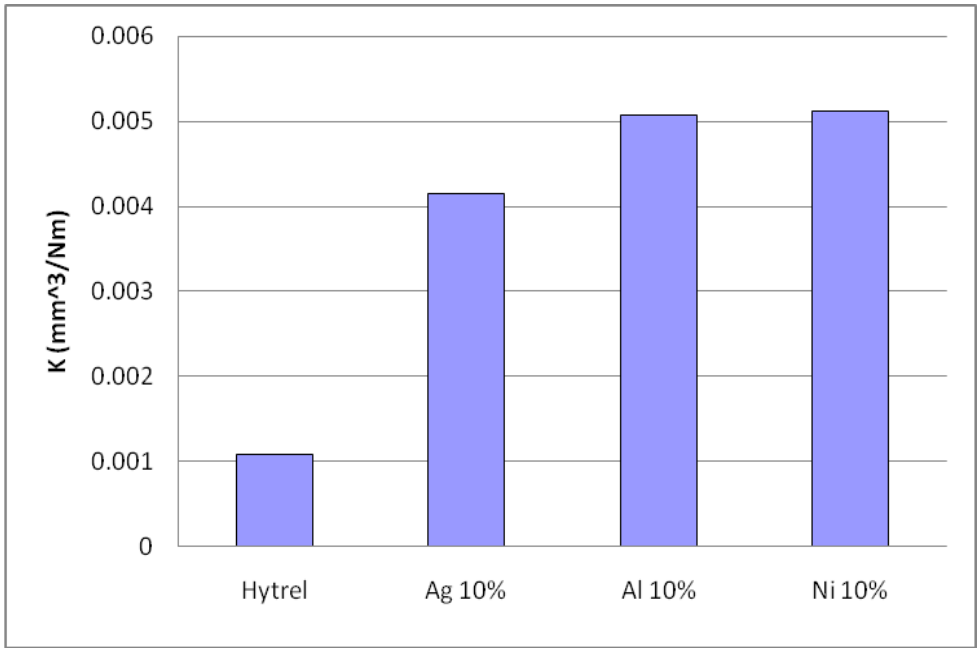

Figure 92. Wear constant *K* for Hytrel and Hytrel microcomposites at 7 N load.

Nanocomposites

Figure 93 shows the wear track of LDPE + 10 wt % Al nanocomposite at a normal load of 7 N. In Figure 93a edges perpendicular to the sliding direction are seen. This is an indication that the dominant wear mechanism is adhesion. The wear debris are small laminate particles.

Figure 94 shows the wear track of LDPE + 10 wt % Ag nanocomposite at a normal load of 7 N. The wear mechanism of this nanocomposite is similar to that of the + 10 wt % Al nanocomposite. Small transversal edges are found inside the wear track and the debris particles are small laminates. The dominant wear mechanism is adhesion.

Figure 95 shows the wear track of Hytrel + 10 wt % Al nanocomposite. As seen in Figure 95a the wear mechanism is mainly adhesive; however, the wear track surface is smoother than in all the previous cases. The wear debris particles again are rolls of material formed inside the wear track.

Figure 96 shows the wear track of Hytrel + 10 wt % Ag nanocomposite. From Figure 96a it is possible to observe that a combination of abrasive and adhesive wear is present. There is a tendency to form grooves along the sliding direction (as shown in Figures 84a and 88a) but also adhesive wear is present since transversal cracks are observable. The debris particles are rolls of material as in previous cases.

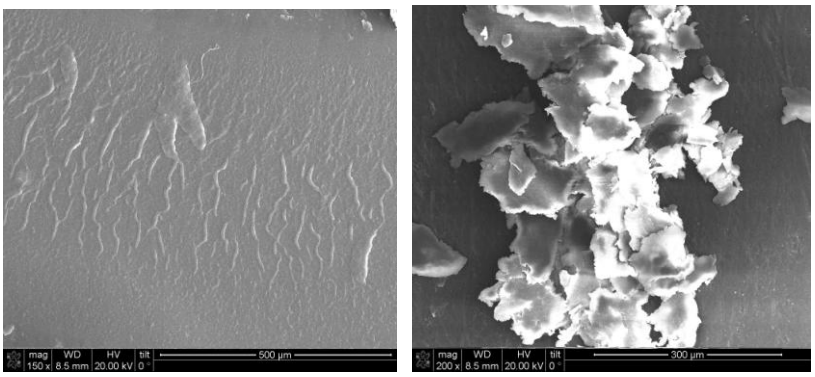

a) b)

Figure 93. a) Wear track of LDPE + 10 wt % Al nanocomposite. b) Wear debris particles of the same material.

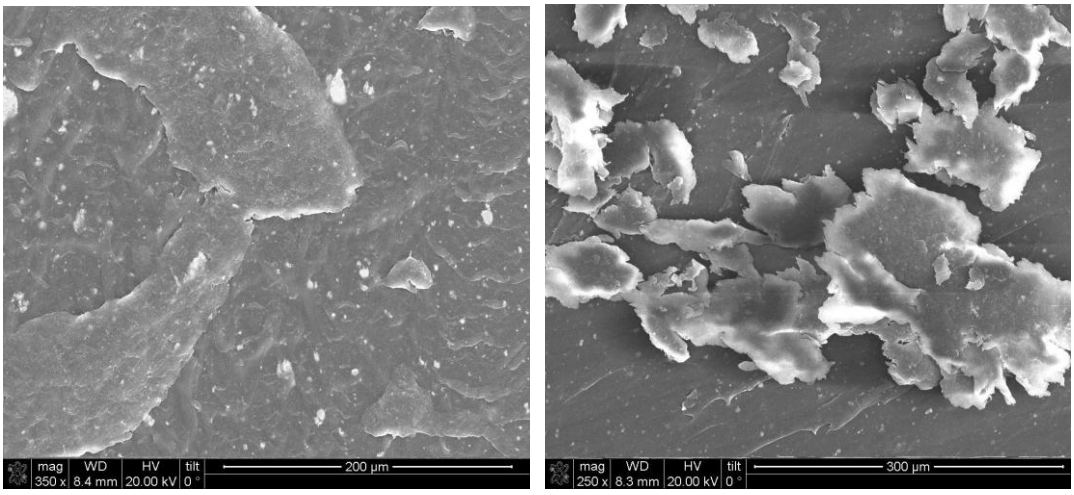

a) b)

Figure 94. a) Wear track of LDPE + 10 wt % Ag nanocomposite. b) Wear debris particles of the same material.

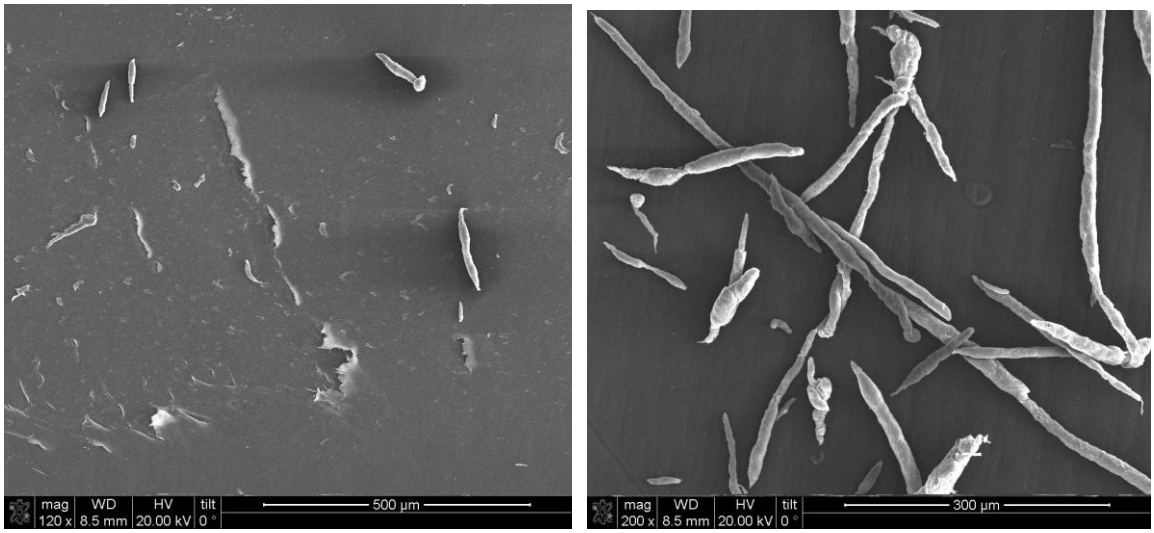

a) b)

Figure 95. a) Wear track of Hytrel + 10 wt % Al nanocomposite. b) Wear debris particles of the same material.

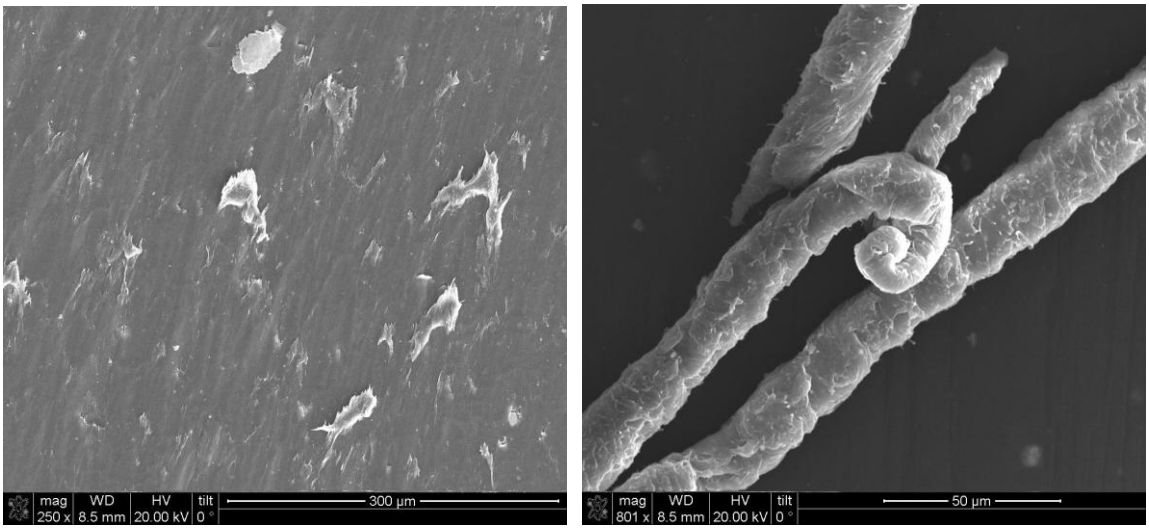

a) b)

Figure 96. a) Wear track of Hytrel + 10 wt % Ag nanocomposite. b) Wear debris particles of the same material.

Figure 97 shows the wear constant of LDPE nanocomposites at a load of 7 N. It is clear that only Al nanoparticles reinforce LDPE against wear. As seen in tensile, friction and scratch tests there is reinforcement of the matrix when Al nanoparticles are added. This reinforcement

of the matrix chains is also observed in pin-on-disc test where shear stresses occur resulting in less wear of the composite. Addition of Ag nanoparticles results in a higher mass loss, however the value is comparable to the neat polymer; this is expected because of micrometric agglomerates can act in similar way as in the Ag microcomposites.

Figure 98 shows the wear constant of Hytrel nanocomposites at a load of 7 N. Addition of Al nanoparticles lower the mass loss, but only slightly. In the case of Ag nanoparticles again the result is a negative one because the micrometric size and thus their behavior as well as rolls formation. On the contrary, when Al nanoparticles are introduced the polymer matrix is reinforced in a similar way than for LDPE. However, the improvement is very little in comparison to the one for LDPE because the high wear from formation of rolls is still present.

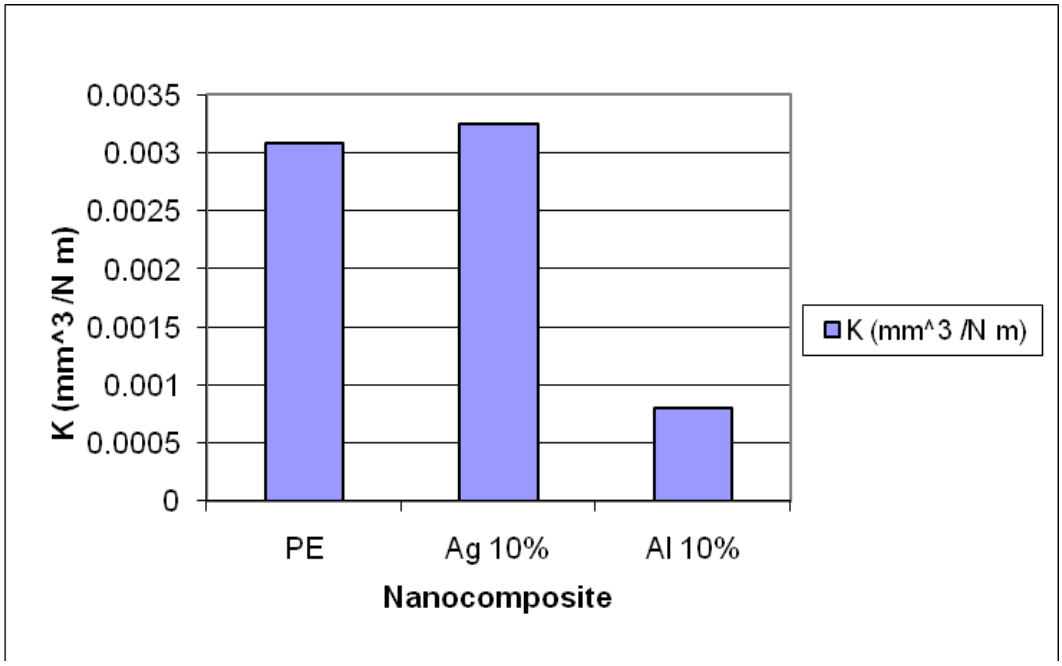

Figure 97. Wear constant *K* of LDPE and LDPE nanocomposites at 7 N.

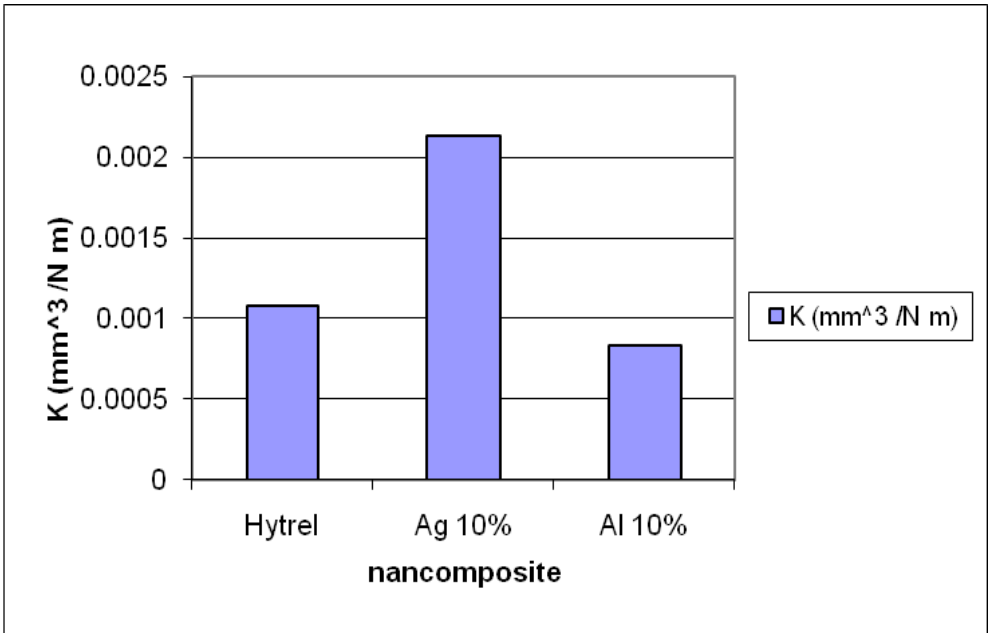

Figure 98. Wear constant *K* of Hytrel and Hytrel nanocomposites at 7 N.

Microcomposites and nanocomposites comparison

Figure 99 shows the wear constant *K* of LDPE micro and nanocomposites at 7 N of normal load. In the case of Ag there is a similar effect in the mass loss for both micro and nanoparticles; this is because nanometric Ag tends to form micrometric agglomerates and thus behaves as micrometric material. In the case of Al there is a considerable improvement in wear resistance for both micro- and nanoparticles although the improvement mechanisms are different (discussed in the previous section).

Figure 100 shows the wear constant *K* of Hytrel micro and nanocomposites at 7 N of normal load. For both Al and Ag microparticles the wear constant is significantly higher than that of the neat Hytrel. On the other hand, Ag and Al nanoparticles are better than the microparticles. In the case of Ag nanoparticles the value of *K* is almost half of the one for Ag microparticles even though nanometric Ag particles tend to form agglomerates which mean that some reinforcement or the matrix is achievable despite the agglomeration. For Al nanoparticles the

value of *K* is almost five times less than the one for Al microparticles and it is lower than the one for pure Hytrel. The reasons for this behavior were explained in the previous section. In this case the reduction of particle size from a micrometric to a nanometric scale has a significant positive effect.

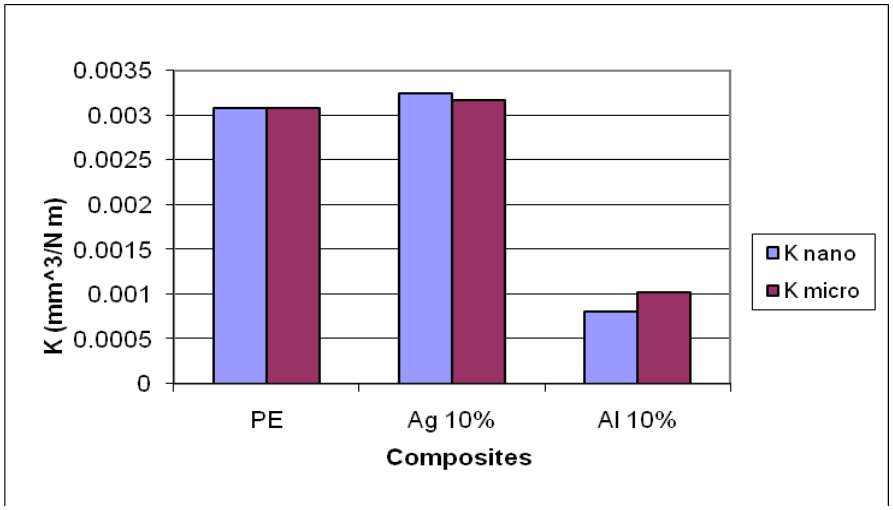

Figure 99. Wear constant *K* of LDPE and LDPE micro and nanocomposites at 7 N.

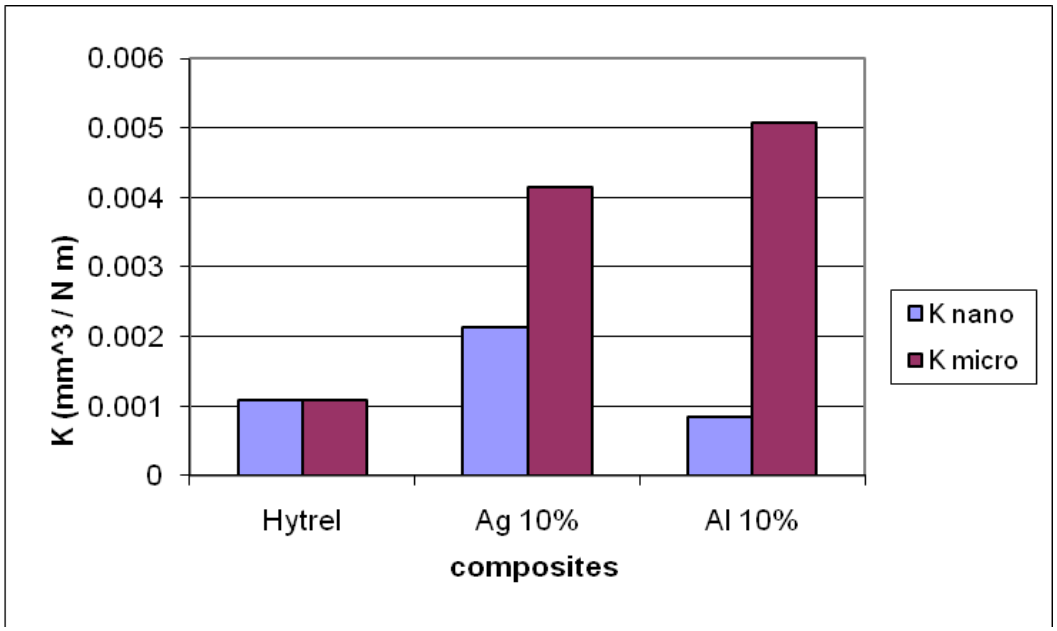

Figure 100. Wear constant *K* of Hytrel and Hytrel micro and nanocomposites at 7 N.

5. CONCLUSIONS

Composites made with a polymeric matrix and a metallic disperse phase were prepared. Low density polyethylene (LDPE) a thermoplastic elastomer Hytrel were the matrices. Al, Ag and Ni powders in the micrometric range were the dispersed phase in microcomposites. Al and Ag powders in the nanometric range were the dispersed phase in nanocomposites.

Scanning electron microscopy (SEM) and focused ion beam (FIB) were the techniques utilized to investigate the morphology of the composites. Since the microcomposites consist of materials with considerable differences in atomic mass, backscattered electron imaging proved to be a suitable technique to determine the position of the particles inside the material. Al and Ni particles are well dispersed throughout the material while Ag tends to form agglomerates. This is true for both microcomposites and nanocomposites. The particles are located on the surface as well as in the bulk. We see how the FIB + SEM technique is useful to elucidate the morphology of hybrids with polymer matrices. Although there can be certain problems during milling, such as buildup heating that provoked cracking. This detrimental phenomena can be overcome by reducing the overlap of the beam which increases the allowed time for cool down to the material being milled.

For the microcomposites, the elastic modulus shows a common trend: an initial decrease in modulus due to disruption of the polymer structure followed by an increase caused by hampering of the chain movement. Only in the case of Hytrel + Al microcomposites it was possible to achieve a higher modulus than the one of the neat polymer. When a primer is added between the metal phase and the polymer phase an improvement in the modulus is observed. Groups OH formed on the sides on the primer molecule can react between the metal and the polymer creating a chemical link between them. This results in improvement of the mechanical properties.

In the case of nanocomposites, the elastic modulus is notably higher than for the microcomposites. For LDPE the same trend (a decrease followed by an increase) is observed; however, the higher reinforcement comes from the fact that having more small particles inside the polymer matrix the disruption is exceeded by the resistance to chain movement.

In general the frictional behavior of all the microcomposites shows similar trends. There is an initial decrease of friction due to a smaller real contact area caused by the inclusion of metallic particles in the surface. Then the friction starts increasing as the filler concentration increases; this happens because there is an increase in the number of metal against metal contacts having higher friction. When a primer is added, the friction values do not increase as much at high metal concentrations. The primer molecules are covering the metallic particles and it act apparently as a lubricant.

For nanocomposites the frictional behavior is similar to that for the microcomposites. The behavior of Ag nanocomposites is comparable to the microcomposites because of the micrometric agglomerates formed. For Al nanocomposites the situation differs somewhat. The nanometric particles reinforce the asperities, lowering the real contact area. Again, after a minimum, the metal against metal contacts start dominating.

The scratch resistance of LDPE microcomposites is the same for all three metals: a decrease of the penetration depth followed by an increase. The initial decrease is due to the extra resistance of the metallic particles against penetration. The increase is caused by a smaller distance between particles disrupting the polymeric matrix weakening it. Hytrel microcomposites do not show the increase but reach a constant value of penetration depth. These differences arise from different polymeric structures; LDPE is a branched polymer while Hytrel is crosslinked to a certain degree.

The nanocomposites of the two polymeric matrices show lower penetration depths than the microcomposites. This is attributed to differences in size of the fillers. Even though Ag tends to form agglomerates, the final result is a lower penetration depth than for micrometric Ag.

The wear mechanisms of the composites were studied by observing the wear tracks on SEM. Although more than one mechanism is present in the samples, there is a dominant in each case. In general, microcomposites tend to suffer more from the abrasive wear mode while for nanocomposites the dominant mechanism is adhesive wear. The debris particles were also observed by SEM. All the LDPE composites (nano and micro except for LDPE + Ni microparticles) wear debris particles are laminates which indicate that the loss of material is due to delamination. For Hytrel the wear debris particles are rolls of material that form continuously inside the wear track which provoke high wear losses; these rolls can be as long as a few millimeters.

The wear constant *K* which is defined as the volume loss per unit length per unit force was determined. For all LDPE composites (micro and nano) only the addition of Al lowers the value of *K* because the spherical particles can act as bearings in the three body abrasion mode. In the case of Hytrel composites only nanometric Al reduces the value of *K* and it is attributed to an effective reinforcement of the matrix. For all other composites there is a negative effect of the filler addition because even there is some reinforcement of the matrix, it is not enough to overcome the high wear losses due to the rapid formation of rolls.

REFERENCE LIST

1. D. Hull and T. W. Clyne. An introduction to composite materials. Second edition, Cambridge university press. Cambridge. 1996
2. D. D. L. Chung. Composite materials: Functional materials for modern technologies. Springer. London. 2003
3. E. K. Sichel, editor. Carbon-black polymer composites. Marcel Dekker, Inc. New York 1982.
4. T. J. Pinnavaia and G. W. Beall. Polymer-clay nanocomposites. Wiley, New York 2000.
5. M Wilson, K Kannangara, G Smith, M Simmons and B Raguse. Nanotechnology, basic science and emerging technologies. Chapman and Hall/CRC.Sydney. 2002
6. Klabunde, K.J. Nanoscale Materials in Chemistry. Wiley, New York 2001.
7. K. I. Winey and R. A. Vaia. *Polymer nanocomposites*. MRS Bulletin. 32 (2007) 314-319
8. L. Shen, J. Li, B. M. Liau, F. Detale and J. H. Chung. *Modeling and analysis of the electrical resistance measurement of carbon fiber polymer-matrix composites.* Composite Science and Technology. 67. (2007). 2513-2520
9. M. Baibarac, M. Lira-Cantu, J. Oro Sol, I Baltog, N. Casan-Pastor, P. Gomez-Romero. *Poly (N-vinyl-carbazole) and carbon nanotubes based composites and their application to rechargeable lithium batteries*. Composites Science and Technology. 67. (2007). 2556-2563
10. J. Shen, W. Huang, L. Wu, Y. Hu and M. Ye. *Thermo-physical properties of epoxy nanocomposites reinforced with amino-functionalized multi-walled carbon nanotubes*. Composites A. 38. (2007) 1331-1336
11. J. Lee and C. Soutis. *A study on the compressive strength on thick carbon fiber-epoxy laminates.* Composites Science and Technology. 67 (2007) 2015- 2026
12. A. M. Shanmugharaj, J. H. Bae, K. Y. Lee, W. H. Noh, S. H. Lee and S. H Ryu. *Physical and chemical characteristics of multiwalled carbon nanotubes functionalized with aminosilane*

and its influence on the properties of natural rubber composites. Composites Science and Technology. 67 (2007) 1813-1822

13. A. Selmi, C. Friebel, I. Doghri and H. Hassis. *Prediction of the elastic properties of single walled carbon nanotube reinforced polymers: A comparative study of several micromechanical models*. Composites Science and Technology. 67 (2007) 2071-2084
14. R. Li, Y. S. Cho, and S. Zhang. *Punching shear behavior of concrete flat plat slab reinforced with carbon fiber reinforced polymer rods*. Composites B. 38 (2007) 712-719
15. F. Croce, S. Sacchetti and B. Scrosati. *Advanced, lithium batteries based on high-performance composite polymer electrolytes*. Journal of Power Sources. 162 (2006). 685-689
16. H. M. J. C. Pitawala, M. A. K. L. Dissanayake and V. A. Seneviratne. *Combined effect of Al_2O_3 nano-fillers and EC plasticizer on ionic conductivity enhancement in the solid polymer electrolyte $(PEO)_9LiTf$*. Solid state ionics. In press (2007)
17. T. Hu, J. Juuti, H. Hantunen and T. Vilkman. *Dielectric properties of BSST/polymer composite*. Journal of the European Ceramic Society. In press (2007)
18. G. Subodh, C. Pavithran, P. Mohanan and M. T. Sebastian. *PTFE/$Sr_2Ce_2Ti_5O_{19}$ polymer ceramic composites for electronic packaging applications*. Journal of the European Ceramic Society. 27 (2007) 3039-3044
19. C. B. Joon, S. M. Lee, S. H. Lee, H. E. Kim and K. W. Lee. *Transverse 1-3 piezoelectric ceramic/polymer composite with multi-layered PZT ceramic blocks*. Sensors and actuators A. 134 (2007) 480-485
20. R. Popielarz and C. K. Chiang. *Polymer composites with the dielectric constant comparable to that of barium titanate ceramics*. Materials Science and Engineering B. 139 (2007) 48-54

21. S. Chandra, S. B. Rai, P. K. Singh, K. Kumar and A. Chandra. *Thermal diffusivity and electrical conductivity in fast ion conducting composites: A correlation.* Solid state ionics. 177. (2006) 1613-1617

22. P. L. Teh, M. Mariatti, H. M. Akil, C. K. Yeoh, K. N. Seetharamu, A. N. R. wagiman and K. S. Beh. *The properties of epoxy resin coated silica filler composites*. Materials letters. 61. (2007) 2156-2158.

23. W. Pompe, H. Worch, E. Epple, W. Friess, M. Gelinsky, P. Greil, U. Hempel, D. Scharnweber and K. Schulte. *Functionally graded materials for biomedical applications*. Materials Science and Engineering A. 362 (2003) 40-60

24. J. Wei, Y. Li and K. T. Lau. *Preparation and characterization of nano apatite/polyamide6 bioactive composite.* Composites B. 38. (2007) 301-305

25. L. M. Mathieu, P.E. Bourban and J. A. E. Manson. *Processing of homogeneous ceramic/polymer blends for bioresorbable composites*. Composites Science and Technology. 66 (2007) 1606-1614

26. E. Rivera-Munoz, J. R. Diaz, J. Rodriguez, W. Brostow, V. M. Castano, *Hydroxyapatite spheres with controlled porosity for eye ball prosthesis: processing and characterization,* Journal of Materials Science Medicine. 12 (2001) 305

27. A. de la Isla, W. Brostow, B. Bujard, M. Estevez, J. R. Rodriguez, S. Vargas, V. M. Castano, *Nanohybrid scratch resistant coatings for teeth and bone viscoelasticity manifested in tribology,* Materials Research Innovations. 7 (2003) 110.

28. A Sáenz, E Rivera, W Brostow, V M Castaño, *Ceramic Biomaterials: An Introductory Overview*, Journal of Materials Education. 21 (1999) 267

29. H. F. Ko, C. Sfeir and P. N Kumta. *In situ synthesis and characterization of porous polymer-ceramic composites as scaffolds for gene delivery.* Materials Science and Engineering C. 27 (2007) 479-483.

30. Z. Yefang, D. W. Hutmacher, S. L. Varawan and L. T. Meng. International Journal of Oral and Maxillofacial Surgery. 36. (2007) 137-145.

31. E. P. Giannelis, R. Krishnamoorti and E. Manias. *Polymer silicate nanocomposites: Model systems for confined polymers and polymer brushes*. Advances in Polymer Science. 138 (1998) 107-148

32. P.C. LeBaron, Z. Wang, T. J. Pinnavaia. *Polymer layered-silicate nanocomposites: an overview*. Applied Clay Science. (1999) 11-29

33. E. P. Giannelis. *Polymer-layered silicate nanocomposites: Synthesis, properties and applications*. Applied Organometallic Chemistry. 12 (1998) 675.

34. R. Xu, E. Manias, A. J. Snyder and J. Runt. *New biomedical poly(urethane urea)-layered silicate nanocomposites*. Macromolecules. 34 (2007) 337-339

35. J. W. Gilman. *Flammability and thermal stability studies of polymer layered-silicate (clay) nanocomposites.* Applied Clay Science. 15 (1999) 31-49

36. J. W. Gilman, C. L Jackson, A. B. Morgan, R. Harris, E. Manias, E. P. Giannelis, M. Guthenow, D. Hilton and S. H. Philips. *Flammability properties of polymer-layered-silicate nanocomposites. Polypropylene and polystyrene composites.* Chemestry of Materials. 12 (2000) 1866-1873

37. S. S. Ray, K. Yamada, M. Okamoto and K. Ueda. *Polylactide layered-sylicate nanocomposite: A novel degradable material*. Nano Letters. 2 (2002) 1093-1096

38. M. Muszynska, H. Wycislik and M. Siekierski. *Composite polymeric electrolytes based on poly(ethylene oxide) matrix and metallic aluminum filler*. Solid State Ionics. 147 (2002) 281-287

39. Y. P. Mamunya, V.V. Davydenko, P. Pissis and E. V. Lebedev. *Electrical and thermal conductivity of polymers filled with metal powders*. European Polymer Journal. 38. (2002) 1887-1897

40. S. W. Kim, Y. W. Yoon, S.J. Lee, G. Y. Kim, Y. B. Kim, Y. Y. Chun and K. S. Lee. *Electromagnetic shielding properties of soft magnetic powder-polymer composite films for the application to suppress noise in the radio frequency range*. Journal of Magnetism and Magnetic Materials. In press. (2007)

41. Z. Brito and G. Sanchez. *Influence of metallic fillers on the thermal and mechanical behaviour in composites of epoxy matrix*. Composite Structures. 48. (2000) 79-81

42. K. Gosh and S. N. Maiti. *Mechanical properties of silver-powder-filled polypropylene composites. Journal of Applied Polymer Science*. 60. (1996) 323-331

43. W. Bare, C. Albano, J. Reyes and N. Dominguez. *Effect of irradiation on the mechanical properties of high-density polyethylene reinforced with metallic fibers*. Surface and Coatings technology. 158-159 (2002) 404-407

44. J Kubat and M. Rigdahl. *Reduction of internal stresses in injection molded parts by metallic fillers*. Polymer Engineering and Science. 16 (1976) 792-798

45. A Punning, M. Kruusmaa and A. Aabloo. *A self-sensing ion conducting polymer metal composite (IPMC) actuator*. Sensors and actuators A. 136 (2007) 656-664

46. D. Kim and K. G. Kim. *Ionic polymer-metal composite actuators exhibiting self-oscillation*. Sensors and actuators A. 137 (2007) 129-133

47. B. K. Fang, M. S. Ju and C. C. K. Lin. *A new approach to develop ionic polymer-metal composites (IPMC) actuator: Fabrication and control for active catheter systems*. Sensors and actuators A. In press (2007)

48. Q. Zhao, C. Wang, Y Liu and S. Wang. *Bacterial adhesion on the metal-polymer composite coatings.* International journals of adhesion and adhesives. 27 (2007) 85-91

49. L. Nicolais and G. Carotenuto, editors. Metal-polymer nanocomposites. Wiley, New Jersey. 2005

50. A. Heilman. Chapter 6 in: L. Nicolais and G. Carotenuto, editors. Metal-polymer nanocomposites. Wiley, New Jersey. 2005

51. S. Barcikowski, B. N. Chichkov. *Nanocomposite manufacturing using ultrashort-pulsed laser ablation in solvents and monomers*. E-MRS fall meeting 2006, *Proceedings*. Warsaw, Poland

52. R. M. Tilaki, A. I. Zad, S. M. Mahdavi, M. Ranjbar and M. Raftari. Synthesis and optical properties of silver nanoparticles/polystyrene nanocomposites. E-MRS Fall Meeting 2006, *Proceedings*. Warsaw

53. I. P. Dostenko, G. Y. Yurkov, V. G. Shevchenko, S. P. Gubin and A. T. Ponomarenko. Study of influence of size, structure and electrophysical properties of iron-containing nanoparticles depending on concentration in the polymer matrix. E-MRS Fall Meeting 2006, *Proceedings*. Warsaw

54. *http://en.wikipedia.org/wiki/Injection_molding*

55. H. R. Allcock, F. W. Lampe and J. E. Mark Contemporary polymer chemistry. Third Edition. Pearson education, Inc.city, NJ. 2003.

56. J. Williams. Engineering Tribology. Cambridge University Press. New York 2005

57. B. Bhushan. Introduction to tribology. Wiley, New York 2002

58. W Brostow, P E Cassidy, H E Hagg, M Jaklewicz and P E Montemartini. *Fluoropolymer addition to an epoxy: phase inversion and tribological properties*. Polymer. 42 (2001) 7971

59. W Brostow and M Jaklewicz, *Friction and scratch resistance of polymer liquid crystals: Effects of magnetic field orientation*, J. Mater. Res. 19 (2004) 1038

60. W Brostow, G Damarla, J Howe, D Pietkiewicz, *Determination of wear of surfaces by scratch testing*. e-Polymers. no. 025 (2004).

61. M. D. Bermudez, W Brostow, F. J. Carrion-Vilches, J. J. Cervantes, G. Damarla, J. M. Perez. *Scratch velocity and wear resistance*. e-Polymers (2005) no.003

62. M. D. Bermudez, W Brostow, F. J. Carrion-Vilches, J. J. Cervantes, D. Pietkiewicz. *Wear of thermoplastics determined by multiple scratching*. e-Polymers. (2005) no.001

63. GG. W. Ehrenstein, G. Riedel and P. Trawiel. Thermal analysis of plastics: theory and practice. Hanser, Cincinnati 2002

64. J. Goldstein, D. Newbury, D. Joy, C Lyman, P Echlin, E Lifshin, L Sawyer and J Michael. Scanning Electron Microscopy and X-Ray Microanalysis. Third edition. Springer. New York. 2003

65. C A Volkert and A M Minor. *Focused ion beam microscopy and micromachining*. MRS Bulletin. 32 (2007) 389.

66. J Mayer, L A Giannuzzi, T Kamino and J Michael. *TEM sample preparation and FIB-induced damage*. MRS Bulletin. 32. (2007) 400

67. J Loos, J K J van Duren, F Morrissey and R A J Hanssen. *The use of the focused ion beam technique to prepare cross-sectional transmission electron microscopy specimen of polymer solar cell deposited on glass*. Polymer. 42 (2002) 7493.

68. J Li, T Malis and S Dionne. Recent advances on FIB – TEM specimen preparations techniques. Mater. Characterization. 57 (2006) 64

69. W Brostow, B P. Gorman and O Olea-Mejia. *Focus ion beam milling and scanning electron microscopy characterization of metal + polymer hybrids.* Mater. Letters, 61 (2007) 1333

70. *http://www.school-for-champions.com/science/frictioncoeff.htm*

71. V A Bely, A. I. Sviridenok, M.I. Petrokovets and V. G. Savkin. Friction and wear in polymer-based materials. Pergamon Press, Oxford, 1982

72. N. K. Myshkin, M. I. Petrokovets, S.A. Chizhik. *Simulation of real contact in tribology*. Tribol Int 31 (1998) 79

73. A. Kovalev, H. Shulga, M Lemieux, N. Myshkin, V. V. Tsukruk. *Nanomechanical probing of layered nanoscale polymer films with atomic force microscopy*. J Mater Res. 19 (2004) 716

74. M. I. Petrokovets. *Effect of temperature on real contact area of tough surfaces*. J Friction Wear. 20 (1999) 1

75. N. K. Myshkin, M. I. Petrokovets, S. A. CHizhik. Basic problems in contact characterization at nanolevel. Tribol Int. 32 (1999) 379

76. B. J. Briscoe. Interfacial friction of polymer composites. General fundamental principles. In: Klaus F, editor. Friction and wear of polymer composites. Elsevier. Amsterdam. 1986

77. B. J. Briscoe. Friction of organic polymers. In: Singer, H. M. Pollok, editors. Fundamental of friction: macroscopic and microscopic processes. Klwver Academic Publishers. Dordrecht. 1992

78. B. J. Briscoe, L. Fiori, E. Pelillo. Nano-indentation of polymeric surfaces. J Phys D: Appl Phys. 31 (1998) 2395

79. M. D. Bermudez, F. J. Carrion-Vilches and C. Martinez-Nicolas. *Wear of liquid crystal - additivated polymers against steel.* J. Appl. Polym. Sci. 74 (1999) 831

80. M. D. Bermudez, F. J. Carrion-Vilches and I. Martinez-Mateo. *Comparative studies of the tribological properties of polyamide 6 filled with molybdenum disulfide and liquid crystalline additives*. J. Appl. Polym. Sci. 81 (2001) 2426

81. M. D. Bermudez, F. J. Carrion-Vilches and P. Iglesias. A study of the wear behavior of polymer-matrix composites containing discontinuous nanocrystalline alloy reinforcements. Tribo. Internat. 40 (2007) 479